PHENOMENOLOGY AND EXPERIMENTAL OBSERVATIONS IN HIGH TEMPERATURE TERNARY INTERDIFFUSION

by

ABBY LEE ELLIOTT
A.A. Indian River Community College, 1997
B.S. University of Central Florida, 2002

A thesis submitted in partial fulfillment of the requirements
for the degree of Master of Science in Materials Science and Engineering
in the Department of Mechanical, Materials, and Aerospace Engineering
in the College of Engineering and Computer Science
at the University of Central Florida
Orlando, Florida

Spring Term
2004

ABSTRACT

A new method to extract composition dependent ternary interdiffusion coefficients from a single diffusion couple experiment is presented. The calculations involve direct determination of interdiffusion fluxes from experimental concentration profiles and local integration and differentiation of Onsager's formalism. This new technique was applied to concentration profiles obtained from selected semi-infinite, single-phase diffusion couple experiments in the Cu-Ni-Zn, Fe-Ni-Al, and Ni-Cr-Al systems. These couples exhibit features such as uphill diffusion and zero flux planes. The interdiffusion coefficients from the new technique along with coefficients reported from other methods are graphed as functions of composition. The coefficients calculated from the new technique are consistent with those determined from Boltzmann-Matano analysis and an alternate analysis based on the concept of average ternary interdiffusion coefficients. The concentration profiles generated from the error function solutions using the calculated interdiffusion coefficients are in good agreement with the experimental profiles including those exhibiting uphill diffusion. The new technique is checked for accuracy and consistency by back-calculating known interdiffusion coefficients; in this exercise, the new method accurately predicts constant diffusivity.

After rigorous verification, the new technique is applied to previously unexamined couples in the Ni-Pt-Al system. With Ni as the dependent component, the main coefficients are shown to be relatively constant and the cross coefficients are negative. The interdiffusion coefficient

representing the contribution of the concentration gradient of Pt to the interdiffusion flux of Al is relatively large for couples whose Al content is low, indicating that Pt has a significant effect on Al when Al concentration is low.

Another important aspect of analyzing diffusional interactions is the movement of single and multi-phase boundaries within a diffusion couple. Phase boundaries for an n-component system are newly classified and boundary movement is analyzed in terms of degrees of freedom. Experimental evidence of a category 2:1 boundary is presented with a solid-to-solid semi-infinite diffusion couple in the Fe-Ni-Al system with two single-phase terminal alloys. The diffusion path for this couple surprisingly passes through the vertex of the equilibrium tie triangle on the phase diagram to exhibit three phase equilibria in a ternary system. Here is shown for the first time experimental verification of this phenomenon.

ACKNOWLEDGMENTS

With all my grateful heart, I thank God, my family, and especially my husband Rick; my achievements are theirs in kind. Deep appreciation is expressed to the AMPAC faculty and staff, my committee members, Dr.'s Desai and Coffey, and of course, my advisor Dr. Sohn, a great professor whose expertise is truly noteworthy. I would also like to thank eTMF, our research group, for all their support and whose friendship I will cherish always.

TABLE OF CONTENTS

LIST OF FIGURES

LIST OF TABLES

LIST OF NOMENCLATURE

$\widetilde{J}_i$	Interdiffusion flux of component *i*
C_i	Concentration of component *i*
$\widetilde{D}_i$	Binary interdiffusion coefficient associated with component *i*
t	Time in seconds
x_0	Matano plane location
$C_i^{-/+}$	Terminal alloy composition of component *i*
λ	The Boltzmann parameter
C_i^0	The composition of component *i* at the Matano plane
$\widetilde{D}_{ij}^n$	Ternary interdiffusion coefficient with *n* as the dependent component
$\overline{\widetilde{D}}_{ij}^n$	Average ternary interdiffusion coefficient
$x^{-/+}$	The terminal positions
x_{ZFP}^i	Location of the zero flux plane of component *i*

1 INTRODUCTION

Interdiffusion processes within multicomponent alloys continue to be a subject of great interest in materials science engineering. In order to better understand diffusional interactions among components in a given system, a mathematical formalism is needed that describes diffusion behavior. To this end, Onsager's formalism[1-3] of Fick's first law, for an *n*-component system, relates the interdiffusion flux of component *i* to (*n*-1) independent concentration gradients. For an *n* component system this formalism yields $(n\text{-}1)^2$ independent interdiffusion coefficients and (*n*-1) independent flux equations. This means that increasing the number of elements in a given system greatly increases the difficulty of the problem of how to solve for the interdiffusion coefficients. As such, the scope of the current analysis is limited to the case of ternary diffusion. In Onsager's Formalism, the interdiffusion fluxes and concentration gradients are readily calculated. The interdiffusion coefficients are the unknowns for which we wish to solve. Therefore, Onsager's Formalism is a system of two equations and four unknowns; an additional two equations are needed to solve for the four interdiffusion coefficients. One method for overcoming this discrepancy is the extension of the Boltzmann-Matano method. For the ternary case, this method requires two couples whose diffusion paths intersect on the ternary isothermal phase diagram and the method yields coefficients only at one composition corresponding to the intersection point. Other methods, such as that proposed by Dayananda and Sohn,[4] may be utilized to calculate average ternary interdiffusion coefficients over a composition range using

only one couple. However, this method requires an assumption of constant diffusivity over a wide range of compositions.

The main objective of this thesis is to present a method for calculating concentration dependent interdiffusion coefficients from a single isothermal ternary diffusion couple. Bouchet and Mevrel[5] have developed a numerical method for calculating composition dependent ternary interdiffusion coefficients from a single couple using a finite difference scheme with computer algorithms. Their results show that the method is accurate in the case of computer generated concentration data, yet no coefficients for real, experimental diffusion couples have been reported. The method presented in this thesis uses a similar approach to the Dayananda and Sohn method,[4] and thus it may be regarded as an extension of this method for the case of concentration dependent diffusivity. Interdiffusion fluxes are calculated directly from the experimental concentration profiles. Local integration and differentiation of Onsager's formalism are implemented to determine a discrete set of interdiffusion coefficients for a myriad of compositions. The analysis is applied to selected single-phase isothermal diffusion couples in the Cu-Ni-Zn,[6] Fe-Ni-Al,[7] and Ni-Cr-Al[8,9] systems and main and cross interdiffusion coefficients are calculated over short compositional ranges. Calculations from both the Boltzmann-Matano method and the Dayananda and Sohn method verify the determined coefficients. As further verification, error function solutions based on the calculated coefficients for these systems are compared with the experimental concentration profiles. Concentration profiles are also generated using given interdiffusion coefficients and then the coefficients are back calculated for comparison. This exercise demonstrates the accuracy and consistency of the new technique.

Once verified, the new method is used to determine interdiffusion coefficients for previously unexamined Ni-Pt-Al couples.

Another important aspect of analyzing diffusional interactions is the movement of interphase boundaries within a diffusion couple. In this thesis is outlined a classification of phase boundaries for binary and ternary isothermal systems as constructed by Morral.[10] This classification of boundary types has been modified and extended to include an additional boundary type for a ternary system. The movement of the phase boundaries is discussed in terms of degrees of freedom via Gibb's phase rule. Experimental evidence of a category 2:1 boundary is presented with a solid-to-solid semi-infinite diffusion couple in the Fe-Ni-Al system with two single-phase terminal alloys. The diffusion path for this couple surprisingly passes through the vertex of the equilibrium tie triangle on the phase diagram to exhibit three phase equilibria in a ternary system and here is shown for the first time experimental verification of this phenomenon.

2 PHENOMENOLOGY OF MULTICOMPONENT DIFFUSION

2.1 Quantifying Diffusion

Given two alloys of varying composition in contact with one another at high temperatures, it behooves us to be able to understand and predict how the components will interact with one another, that the system may be modified to better suit our needs. If we can predict the final concentration profiles that will develop after diffusion takes place, then we may predict which phases will develop. This would be advantageous since certain phases are more or less desirable than others due to their physical properties. Another advantage to predicting diffusional interactions is to be able to develop a slow diffusing system, so that undesirable interactions may not occur, for instance, between a substrate and bond coat. This is the heart of the study of diffusion. In order to better understand such interactions among components in a given system, a mathematical formalism is needed that models diffusion behavior. To this end, Onsager's formalism[1-3] of Fick's first law, for an *n*-component system, relates the interdiffusion flux of component *i* to (*n*-1) independent concentration gradients. In this context, an *n* component system is defined as two alloys bonded together to form a diffusion couple, each with at most *n* elements. When this couple is exposed to high temperatures, diffusion takes place, after which, a cross-section of the couple is examined so that the concentration profile of each element may be plotted with respect to distance. There are (*n*-1) independent concentration gradients in an *n*-

component system because the concentrations sum to one. There are also (*n*-1) independent interdiffusion fluxes because the fluxes sum to zero. The interdiffusion flux is defined as the number of atoms to pass through a given cross-sectional area per unit area per unit time. Onsager's formalism relates this flux to the gradients of the concentration profiles for an *n*-component system.

2.1.1 Fick's Laws and Onsager's Formalism

Consider a binary concentration profile and the need for a mathematical formalism, that is, an equation(s) that models diffusion behavior. In 1855 Adolf Fick applied Fourier's heat conduction equation to diffusion, and in the realm of diffusion, this equation came to be known as Fick's first law that describes unidimensional diffusion behavior in a binary system.[11-13]

$$\tilde{J}_i(x,t) = -\tilde{D}_i \cdot \frac{\partial C_i(x,t)}{\partial x} \qquad (1)$$

$\tilde{J}_i$ is the interdiffusion flux of component *i*, C_i is the concentration of component *i*, *x* is distance, *t* is time, and $\tilde{D}_i$ is the binary interdiffusion coefficient corresponding to component *i*. $\tilde{D}_i$ is said to measure the diffusivity of *i*; often when these equations are used, constant diffusivity is assumed, meaning this interdiffusion coefficient is treated as a constant. The tildes in the above equation indicate interdiffusion, also known as chemical diffusion, meaning a laboratory fixed frame of reference is used. Without tildes, intrinsic diffusion is meant, wherein

a lattice fixed frame of reference is used. In the laboratory fixed frame, C_i varies with time *t* at a location *x* according to the continuity equation.[12-14]

$$\left(\frac{\partial C_i}{\partial t}\right)_x = -\left(\frac{\partial \tilde{J}_i}{\partial x}\right)_t \tag{2}$$

Equation 2 can be used with Equation 1 to generate Fick's second law[12-14]

$$\frac{\partial C_i}{\partial t} = \frac{\partial}{\partial x}\left(\tilde{D}_i \frac{\partial C_i}{\partial x}\right) \tag{3}$$

Onsager's formalism of Fick's law extends Fick's first law to describe unidimensional interdiffusion in an *n*-component system using (*n*-1) independent concentration gradients.

$$\tilde{J}_i = -\sum_{j=1}^{n-1} \tilde{D}_{ij}^{n} \frac{\partial C_j}{\partial x} \qquad (n = 1, 2, \ldots n-1) \tag{4}$$

Going back to the need for an equation that models the concentration profiles, when Equation 3 is extended for the case of *n*=3, assuming constant diffusivity, the solution for *C*(*x*) is a linear combination of error functions as will be seen in the next section.

2.1.2 Error Function Solutions Assuming Constant Diffusivity

Assuming constant diffusivity, Fick's second law was extended, much the same as Fick's first law was extended by Onsager, for the case of n=3[15] to yield an ordinary differential equation that may be solved for the concentrations given appropriate boundary conditions. Using boundary conditions C_i^+ and C_i^- for the terminal alloy compositions, Fujita and Gosting[15] rigorously solved for concentrations C_1 and C_2 for the ternary case. These equations have been modified[4,16-19] for clarity. Two equations may be employed for one concentration profile: one for the left-hand side of the Matano plane and one for the right-hand side. The Matano plane is located at the point where mass balance is achieved. It is denoted x_0 and is defined by[12-14]

$$\int_{C_i^-}^{C_i^+} (x - x_0)\, dC_i = 0 . \qquad (5)$$

The definition of the Matano plane as stated by Equation 5 is shown schematically in Figure 1. The concentration profile shown for some element is typical for a binary system. The Matano plane is where area A equals area B.

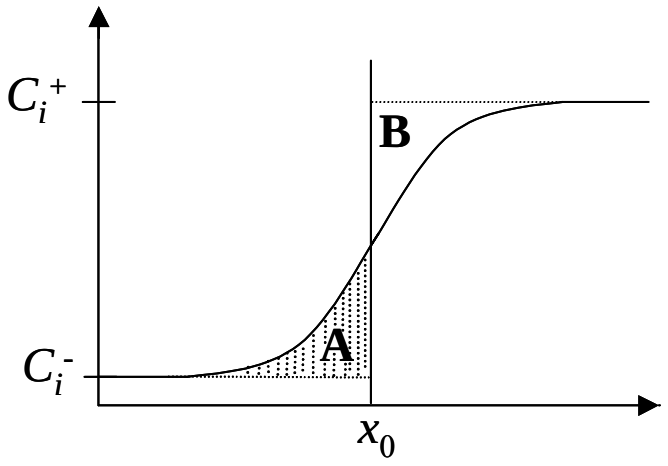

Figure 1. A schematic concentration profile illustrating the definition of the Matano plane x_0: where area A equals area B.

Below are explicitly stated the error function solutions for C_1 and C_2 for the right-hand side of the Matano plane. Note that the 1 and 2 in the subscripts are representative of elements; if 1 represents Ni then C_1 is the concentration profile of Ni. Since the concentrations of all the elements add to one, one of the components is dependent on all the others. This is why for a ternary 1-2-3 system, only C_1 and C_2 are calculated.

$$C_1 = a \cdot erf\left(\frac{\lambda}{2\sqrt{u}}\right) + b \cdot erf\left(\frac{\lambda}{2\sqrt{v}}\right) + c \tag{6}$$

$$C_2 = d \cdot erf\left(\frac{\lambda}{2\sqrt{u}}\right) + e \cdot erf\left(\frac{\lambda}{2\sqrt{v}}\right) + f \tag{7}$$

where *a*, *b*, *c*, *d*, *e*, *f*, *u*, and *v* are given by

$$a = \frac{1}{\widetilde{D}}\left\{\left[\widetilde{D}_{12}^3\left(C_2^+ - C_2^0\right)\right] - \left[\widetilde{D}_{22}^3 - \widetilde{D}_{11}^3 - \widetilde{D}\right] \cdot \left[\frac{C_1^+ - C_1^0}{2}\right]\right\} \tag{8}$$

$$b = \frac{1}{\widetilde{D}}\left\{\left[\widetilde{D}_{12}^{3}\left(C_2^0 - C_2^+\right)\right] - \left[\widetilde{D}_{22}^{3} - \widetilde{D}_{11}^{3} + \widetilde{D}\right]\cdot\left[\frac{C_1^0 - C_1^+}{2}\right]\right\} \tag{9}$$

$$c = C_1^0 \tag{10}$$

$$d = \frac{1}{\widetilde{D}}\left\{\left[\widetilde{D}_{21}^{3}\left(C_1^+ - C_1^0\right)\right] - \left[\widetilde{D}_{11}^{3} - \widetilde{D}_{22}^{3} - \widetilde{D}\right]\cdot\left[\frac{C_2^+ - C_2^0}{2}\right]\right\} \tag{11}$$

$$e = \frac{1}{\widetilde{D}}\left\{\left[\widetilde{D}_{21}^{3}\left(C_1^0 - C_1^+\right)\right] - \left[\widetilde{D}_{11}^{3} - \widetilde{D}_{22}^{3} + \widetilde{D}\right]\cdot\left[\frac{C_2^0 - C_2^+}{2}\right]\right\} \tag{12}$$

$$f = C_2^0 \tag{13}$$

$$u = \frac{1}{2}\left(\widetilde{D}_{11}^{3} + \widetilde{D}_{22}^{3} + \widetilde{D}\right) \tag{14}$$

$$v = \frac{1}{2}\left(\widetilde{D}_{11}^{3} + \widetilde{D}_{22}^{3} - \widetilde{D}\right) \tag{15}$$

where

$$\widetilde{D} = \sqrt{\left(\widetilde{D}_{11}^{3} - \widetilde{D}_{22}^{3}\right)^2 + 4\cdot\widetilde{D}_{12}^{3}\cdot\widetilde{D}_{21}^{3}} \tag{16}$$

In the above equations, x_0 is the Matano plane location, λ is the Boltzmann parameter $\left(x - x_0\right)/\sqrt{t}$, C_i^0 is the composition of component *i* at the Matano plane, and the $\widetilde{D}_{ij}^{k}$'s are the ternary interdiffusion coefficients with *k* being the dependent component. The equations for the left-hand side of the Matano plane may be calculated by simply replacing C_i^+ with C_i^-. Because of the square roots involved, the following conditions must be satisfied in order to make use of Equations 6 and 7.

$$\widetilde{D}_{11}^{3} \cdot \widetilde{D}_{22}^{3} - \widetilde{D}_{12}^{3} \cdot \widetilde{D}_{21}^{3} \geq 0 \tag{17}$$

$$\left(\widetilde{D}_{11}^{3} - \widetilde{D}_{22}^{3}\right)^{2} + 4 \cdot \widetilde{D}_{12}^{3} \cdot \widetilde{D}_{21}^{3} \geq 0 \tag{18}$$

$$\widetilde{D}_{11}^{3} + \widetilde{D}_{22}^{3} \geq 0 \tag{19}$$

With Equations 6-16 and the appropriate $\widetilde{D}_{ij}$ values, one may generate concentration profiles. These equations can serve to verify calculated $\widetilde{D}_{ij}$ values.

2.1.3 Relations Among Ternary Interdiffusion Coefficients

For a ternary, 3-component system, one of the three elements is dependent on the other two since the concentrations of the three elements add to one. The interdiffusion coefficients for a ternary system are denoted $\widetilde{D}_{ij}^{k}$, where *k* is the dependent component. The choice of the dependent component influences the values of the $\widetilde{D}_{ij}$'s, that is $\widetilde{D}_{11}^{2} \neq \widetilde{D}_{11}^{3}$. In order to translate a set of $\widetilde{D}_{ij}$'s with 3 being the dependent component to the set of $\widetilde{D}_{ij}$'s with 2 being the dependent component, the following relations have been established.[20-23]

$$\widetilde{D}_{11}^{2} = \widetilde{D}_{11}^{3} - \widetilde{D}_{12}^{3} \tag{20}$$

$$\widetilde{D}_{13}^{2} = -\widetilde{D}_{12}^{3} \tag{21}$$

$$\widetilde{D}_{31}^{2} = \widetilde{D}_{22}^{3} + \widetilde{D}_{12}^{3} - \widetilde{D}_{11}^{3} - \widetilde{D}_{21}^{3} \tag{22}$$

$$\widetilde{D}_{33}^{2} = \widetilde{D}_{22}^{3} + \widetilde{D}_{12}^{3} \tag{23}$$

If the interdiffusion coefficients corresponding to component 1 as the dependent variable, i.e., the $\widetilde{D}_{ij}^{1}$'s, need to be calculated, then "1" may be switched with "2" in the above equations.

2.2 Calculation of the Interdiffusion Flux

In 1957, Kirkaldy published the following relation that the Boltzmann-Matano analysis may be used to solve for interdiffusion coefficients in an *n*-component system.[24]

$$\int_{C_i^0}^{C_i} \lambda dC_i = -2\sum_{k=1}^{n-1} D_{ik} \frac{dC_k}{d\lambda} \tag{24}$$

The short derivation of Equation 24 was said to follow a procedure used for binary systems, extended to an *n*-component system. Of course, to make use of this equation for Boltzmann-Matano analysis, it would be necessary to have a common intersection between the diffusion paths of all (*n*-1) components on the phase diagram, a quite painstaking, if not impossible, measure for higher order systems, though quite possible for ternary systems. This method for calculating interdiffusion coefficients via Equation 24 was thereafter commonly referred to as an "extension of the Boltzmann-Matano analysis" for an *n*-component system.[20,25] Though Onsager's Formalism of Fick's First Law was well-known by this time, none of the publications made this simple substitution into Equation 24 to formalize an equation for the interdiffusion flux containing no diffusion coefficients. It was not until 1979 that Dayananda and Kim

published a derivation in the likeness of Kirkaldy's only taking it that one crucial step further, substituting in Onsager's Formalism to achieve[26]

$$\widetilde{J}_i(x) = \frac{1}{2t}\int_{C_i^- or C_i^+}^{C_i(x)} (x - x_0)\,dC_i \qquad (25)$$

where *t* is time, x_0 is the Matano plane location, and C_i^- and C_i^+ are the terminal alloy compositions. Now the interdiffusion flux for an *n*-component system may be easily calculated without the need of interdiffusion coefficients. It is a bit perplexing why the earlier authors did not take the final step to achieve Equation 25; perhaps the flux was not of great interest at that time and Dayananda and Kim did publish Equation 25 in light of their interest in zero flux planes. This point is laboured because Equation 25 is so functional and broadly used today.[4,5,6,19,23,26-30]

2.3 Determination of Interdiffusion Coefficients in Ternary Systems

Onsager's formalism[1-3] of Fick's first law, for an *n*-component system, relates the interdiffusion flux of component *i* to (*n*-1) concentration gradients, as stated in Equation 4. For an *n* component system this formalism yields $(n\text{-}1)^2$ interdiffusion coefficients and (*n*-1) independent interdiffusion flux equations. This means that for the case of quaternary and higher order systems, the difficulty in calculating interdiffusion coefficients grows exponentially. As such, the scope of the current analysis is limited to the case of ternary diffusion. In Onsager's Formalism, the interdiffusion fluxes and concentration gradients are readily calculated. The

sought interdiffusion coefficients are unknown. Therefore, Onsager's Formalism is a system of two equations, Equations 26 and 27, and four unknowns; an additional two equations are needed to solve for the four interdiffusion coefficients.

$$\tilde{J}_1 = -\tilde{D}_{11}^3 \frac{\partial C_1}{\partial x} - \tilde{D}_{12}^3 \frac{\partial C_2}{\partial x} \tag{26}$$

$$\tilde{J}_2 = -\tilde{D}_{21}^3 \frac{\partial C_1}{\partial x} - \tilde{D}_{22}^3 \frac{\partial C_2}{\partial x} \tag{27}$$

One method for overcoming this discrepancy for the ternary case is the Boltzmann-Matano method;[24] another is the Dayananda and Sohn method.[4] A new technique is proposed in this thesis that holds an edge over these established methods.

2.3.1 The Boltzmann-Matano Method

The Boltzmann-Matano method may be employed to calculate ternary interdiffusion coefficients.[24] This method requires two diffusion couples whose diffusion paths intersect on the ternary isotherm. The ternary isotherm is the phase diagram for a three-component system where temperature is held constant. A point on the ternary isotherm corresponds to an alloy composition; in Figure 2, the boxes connected by a diffusion path represent two alloys joined to form a diffusion couple. The diffusion path is mapped out by translating the concentration profiles from the couple onto the isotherm. Because of the current lack of predictability of diffusion, there is no guarantee that two given couples will have paths that intersect as shown in Figure 2.

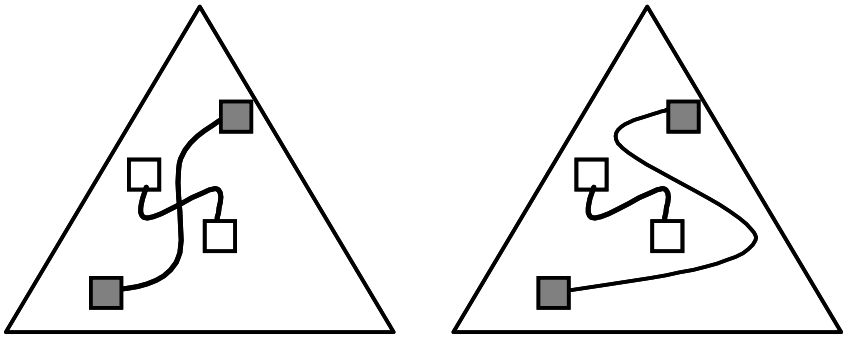

Figure 2. Alternative paths ternary diffusion couples may take, one where the paths intersect and another where the paths do not intersect.

Consequently, several experimental couples may have to be made before finding two whose paths intersect. The possibility of having to create several couples is a major drawback of the Boltzmann-Matano method as these experiments are costly and time consuming. Given two couples whose paths intersect, the interdiffusion coefficients are calculated by using Equations 26 and 27 twice each, once for each couple, yielding four equations and four unknowns. The calculated coefficients are only valid at the point of compositional intersection, another drawback of this method. Overall, the Boltzmann-Matano method is a proven method for calculating ternary interdiffusion coefficients; however, the experimental investment is great and the return is small.

2.3.2 The Dayananda and Sohn Method

The Dayananda and Sohn[4] method, which will hereby be referred to as the DAYSO method, may be utilized to calculate ternary interdiffusion coefficients from a single diffusion couple. This method adopts the idea of *average* interdiffusion coefficients, which means instead of considering one point on the profile at a time, large ranges of the concentration profile are used.

Recall the problem of having two equations (Equations 26 and 27) and four unknowns (the interdiffusion coefficients). There is another equation available that may help in this dilemma: Equation 25. Unfortunately, Equation 25 does not suffice as the additional two equations (one for *i*=1 and one for *i*=2) needed to solve for the interdiffusion coefficients because it does not contain $\widetilde{D}_{ij}$'s. However, the DAYSO method uses a clever manipulation of Onsager's formalism so that Equation 25 is made useful.

In order to make use of Equation 25, Onsager's formalism is first multiplied by $(x - x_0)$, and then integrated as follows.

$$\widetilde{J}_i(x - x_0) = -\widetilde{D}_{i1}^3(x - x_0)\frac{\partial C_1}{\partial x} - \widetilde{D}_{i2}^3(x - x_0)\frac{\partial C_2}{\partial x} \qquad (i = 1, 2)$$

$$\rightarrow \int_{x_1}^{x_2} \widetilde{J}_i(x - x_0)dx = -\overline{\widetilde{D}}_{i1}^3 \int_{x_1}^{x_2} (x - x_0)dC_1 - \overline{\widetilde{D}}_{i2}^3 \int_{x_1}^{x_2} (x - x_0)dC_2$$

$$\xleftarrow{\text{Eq.[25]}} \int_{x_1}^{x_2} \widetilde{J}_i(x - x_0)dx = 2t\left\{\overline{\widetilde{D}}_{i1}^3\left[\widetilde{J}_1(x_1) - \widetilde{J}_1(x_2)\right] + \overline{\widetilde{D}}_{i2}^3\left[\widetilde{J}_2(x_1) - \widetilde{J}_2(x_2)\right]\right\} \qquad (28)$$

Equation 28 is actually two equations, one for *i*=1 and another for *i*=2, and so these are the first two of four equations needed to solve for the four $\overline{\widetilde{D}}_{ij}$'s. Notice that $\overline{\widetilde{D}}_{ij}$ must be constant over the range $[x_1, x_2]$ in Equation 28, and so when using this equation (and hence this method), $\overline{\widetilde{D}}_{ij}$ is considered the *average* interdiffusion coefficient over $[x_1, x_2]$, hence the notation $\overline{\widetilde{D}}_{ij}$ that includes a bar over the coefficient. For the second two equations, consider again Equations 26 and 27, suppose *i*=1, 2 and integrate.

$$\int_{x_1}^{x_2} \widetilde{J}_i dx = -\int_{C_1(x_1)}^{C_1(x_2)} \widetilde{D}_{i1}^{3} dC_1 - \int_{C_2(x_1)}^{C_2(x_2)} \widetilde{D}_{i2}^{3} dC_2 \qquad (i = 1, 2)$$

$$\Leftrightarrow \int_{x_1}^{x_2} \widetilde{J}_i dx = \overline{\widetilde{D}}_{i1}^{3}\left[C_1(x_1) - C_1(x_2)\right] + \overline{\widetilde{D}}_{i2}^{3}\left[C_2(x_1) - C_2(x_2)\right] \qquad (29)$$

And so Equation 29 gives the other two equations necessary to solve for the four coefficients.

Note the limits of integration in Equations 28 and 29. The concentration and interdiffusion flux profiles are integrated from x_1 to x_2 so the resultant coefficients from the DAYSO method are deemed *average* ternary interdiffusion coefficients: they are an "average" of all the coefficients that exist from $C_i(x_1)$ to $C_i(x_2)$. Another way of stating this is to say that the DAYSO method assumes constant diffusivity from $C_i(x_1)$ to $C_i(x_2)$. The publication that introduces the DAYSO method and that reports interdiffusion coefficient data from the method uses limits of integration from the terminal alloy to the Matano plane, from $C_i^{+/-}$ to C_i^0. As compared to the classic Boltzmann-Matano method, the experimental investment for the DAYSO method is at least half and the return double.

2.4 Phase Boundary Classification

Morral et al. have classified phase boundaries for binary systems in the following manner for the purpose of computer simulation.[10] The Type 0 boundary occurs when both components of the couple are of the same phase, and the diffusion path does not exit this phase, i.e., (α+β)|(α+β). |

represents a stationary boundary, > represents rightward boundary movement, < represents leftward boundary movement, and <> represents a boundary that may move either to the right or to the left. The Type I boundary occurs when one of the components contains one more phase than the other and the diffusion path crosses from one region of the phase diagram into another, i.e., α>(α+β). The Type II boundary indicates the change of single phase, i.e. α <> β, and the diffusion path travels through three regions of the phase diagram, such as from α to (α+β) to β as shown in Figure 3.

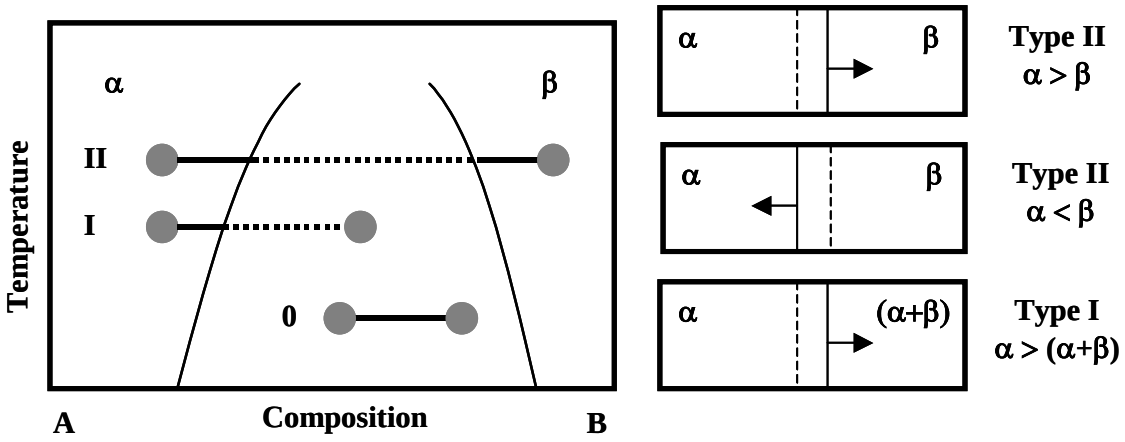

Figure 3. Diffusion paths and examples of moving boundaries for an isothermal binary system.

Each of the two elements in the binary system can contribute to at most one phase, thus the maximum number of phases in a multiphase region is two. This limits the number of boundary types in a binary system. This classification can be annexed to describe the boundaries that may occur in an isothermal ternary system.

Whereas in a binary system the multi-phase regions consist of exactly two phases, a ternary isotherm may contain multi-phase regions of either two or *three* phases. This yields the

possibility of a Type III boundary such as $(\alpha+\beta)> \gamma$ where the diffusion path travels from the $(\alpha + \beta)$ phase region to the equilibrium tie triangle $(\alpha + \beta + \gamma)$, exiting out the vertex of the triangle to the γ phase region. In this thesis, this boundary is classified and experimentally observed for the first time.

3 DEVELOPMENT OF ANALYSIS FOR A NEW TECHNIQUE FOR CALCULATING COMPOSITION DEPENDENT TERNARY INTERDIFFUSION COEFFICIENTS

The focus of this thesis is the development of a new technique for calculating composition dependent ternary interdiffusion coefficients, presented in Section 3.5. In the course of developing and implementing this new technique, the results delineated in the first four sections of this chapter have been achieved.

3.1 An Alternative form of the Interdiffusion Flux Equation

Recall Equation 25, the equation for calculating the interdiffusion flux directly from the concentration profiles. For numerical analysis purposes, Microsoft® Excel, MathCAD, and Matlab have been employed for various calculations. As such, certain considerations must be made to minimize uncertainty in the calculations. In order to directly implement Equation 25 into mathematical software, the software must invert the concentration profile, since the integral is with respect to the vertical axis, *C*. It must be inverted because integration is taken with respect to the horizontal axis. This leads to two problems: one, when a profile is being inverted by means of computer software, a degree of accuracy may be lost, and two, the concentration profile may not be an invertible function. For example, if the concentration profile exhibits uphill diffusion, it is not an invertible function.

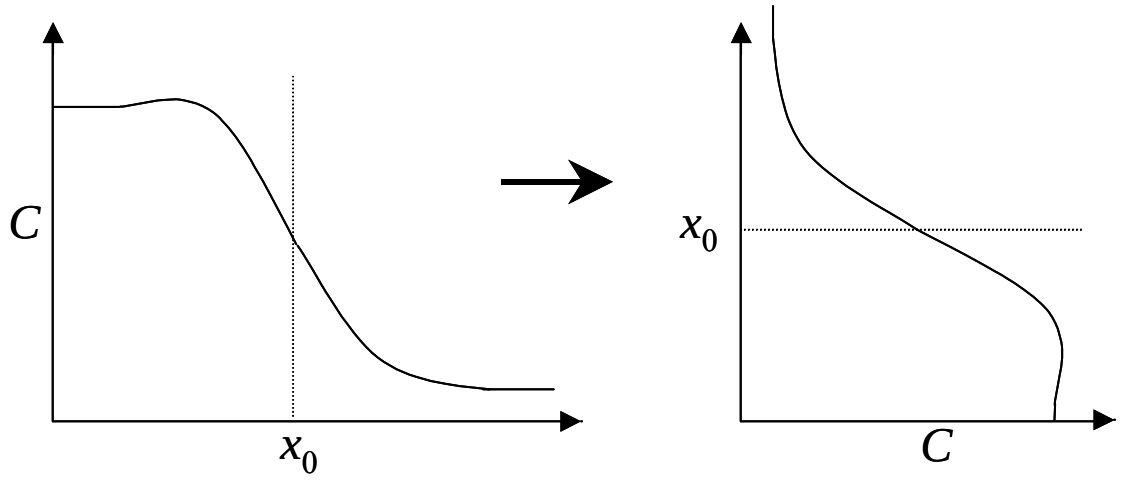

Figure 4. Schematic demonstration of how uphill diffusion hinders the interdiffusion flux calculation of Equation 25.

Figure 4 demonstrates a concentration profile with uphill diffusion. In order to perform the integral in Equation 25, by the rules of calculus, one must first invert, or "flip", the function as shown in Figure 4. Once inverted so that the concentration is the horizontal axis, it is clear that this inverted profile is not a function (recall the vertical line test: one point on the horizontal axis is only allowed to correspond to at most one point on the vertical axis). Since the profile in Figure 4 is not a function, it cannot be integrated. How mathematical software would handle this profile is questionable at best. In order to tackle this issue, the interdiffusion flux equation must be rewritten so that it does not need to be inverted.

Here is introduced the term x^-, referring to the leftmost position, the end location value. Introduction of the x^- term is not unreasonable, considering that the experimental data from which interdiffusion coefficients are calculated is a finite set of data that certainly has two limiting values. For instance, if the experimental data is given at points 0, 1, ...300μm, then x^- is 0 μm and so $C_i\left(x^-\right)$ is simply C_i^-.

Exactly what is the interdiffusion flux? Refer to Figure 5. To calculate the interdiffusion flux at some distance x_1, the area of the shaded region is calculated and this corresponds precisely to the value of the interdiffusion flux at x_1 multiplied by $2t$. Suppose the area of the shaded region is A_1, then the value of the interdiffusion flux at x_1 is $A_1/2t$. Note that the area A_1 is equivalent to the integral $\int_{C^-}^{C(x_1)} (x_1 - x_0)\, dC$ from Equation 25. Alternatively, this area may be calculated as shown in Figure 6. First the area of the rectangle $\left(x_0 - x^-\right)\left(C^- - C(x_1)\right)$ is calculated (Figure 6a), then the integral $\int_{x^-}^{x_1} C dx$ is subtracted away (Figure 6b). Now too much negative area remains, so the rectangle area $(x_1 - x^-)(C(x_1))$ is added (Figure 6d), leaving the sought area as shown. Combining these calculations, simplifying, and dividing by $2t$, the interdiffusion flux may be expressed by

$$\tilde{J}(x) = \frac{1}{2t}\left[(x_0 - x^-)C^- - \int_{x-}^{x} C dx + (x - x_0)C(x) \right]. \qquad (30)$$

Equation 30 does not require an inverse function; it is a straightforward calculation. It shall be noted that Roper and Whittle have made a similar mathematical observation without the determination of the interdiffusion flux.[25] Equation 30 may be employed without difficulty or question in MathCAD or Matlab to calculate the interdiffusion flux.

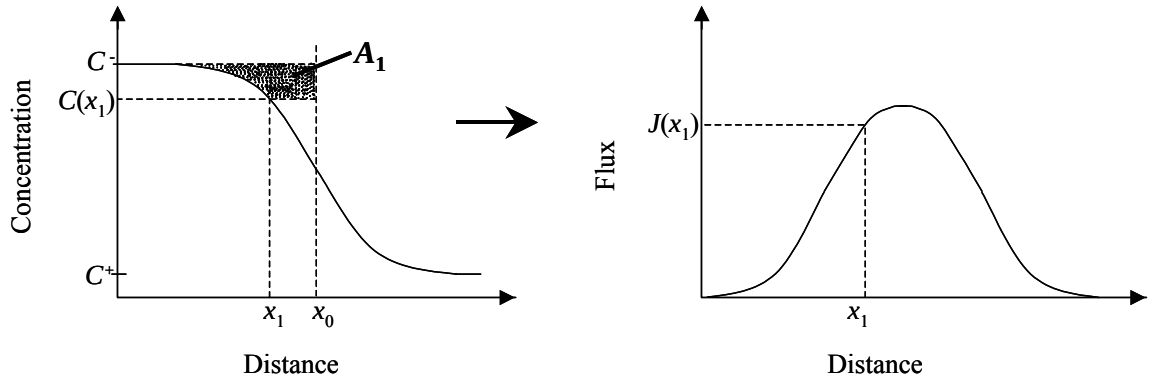

Figure 5. Qualitative evaluation of the interdiffusion flux. The shaded region corresponds to the value of the interdiffusion flux multiplied by a constant.

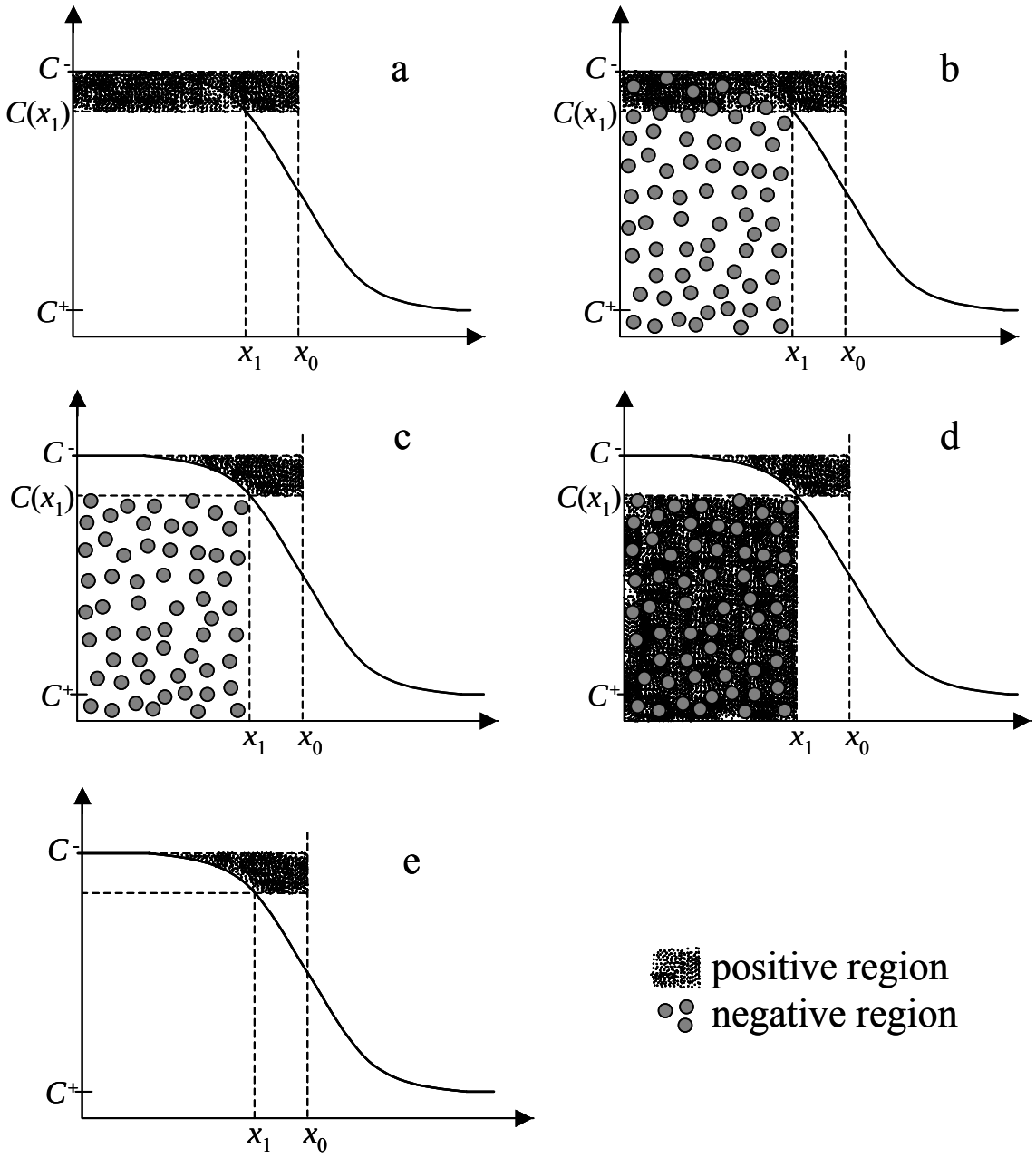

Figure 6. Interdiffusion flux calculation shown graphically. 6a. The rectangular region is calculated. 6b. From this, the integral is subtracted. 6c. Cancellation of the positive and negative areas. 6d. The addition of the rectangular region. 6e. The final area is calculated.

3.2 Matano Plane Location

Previously, a likeness of the following equation was invoked to find the Matano plane location.[20,25,31,32] However, noting the integral, similar problems arise as discussed in the previous section.

$$\int_{C_i^-}^{C_i^+} x dC_i = 0 \tag{31}$$

Here is presented an alternative equation to calculate the Matano plane location. It may be deduced from Figure 1 that the area of A is $\int_{x-}^{x_0} C dx - \left(x_0 - x^-\right)C^-$ and the area of B is $\left(x^+ - x_0\right)C^+ - \int_{x_0}^{x+} C dx$. The Matano plane is defined as the plane such that areas A and B are equal. Then to find the Matano plane location, it is only a matter of setting the aforementioned areas equal to each other and simplifying.

$$\left(x_0 - x^-\right)C^- - \int_{x-}^{x_0} C dx = \int_{x_0}^{x+} C dx - \left(x^+ - x_0\right)C^+$$

$$\Leftrightarrow \left(x_0 - x^-\right)C^- + \left(x^+ - x_0\right)C^+ = \int_{x_0}^{x+} C dx + \int_{x-}^{x_0} C dx$$

$$\Leftrightarrow x_0 C^- - x^- C^- + x^+ C^+ - x_0 C^+ = \int_{x-}^{x+} C dx$$

$$\Leftrightarrow x_0 = \frac{\int_{x-}^{x+} C dx + x^- C^- - x^+ C^+}{C^- - C^+} \tag{32}$$

Typically, concentration profile data is given starting at 0μm and so x^- is 0μm, which simplifies Equation 32 to

$$x_0 = \frac{\int_{0}^{x+} C dx - x^+ C^+}{C^- - C^+}. \tag{33}$$

The concentration profiles do not have to be inverted using Equation 33; it is implemented with extreme ease for calculating the Matano plane location.

3.3 The Derivative of the Interdiffusion Flux

One of the calculations necessary to implement the new technique for calculating ternary interdiffusion coefficients is the derivative of the interdiffusion flux. One way of performing this calculation is to evaluate the interdiffusion flux, and then take the derivative as demonstrated in the following equation:

$$\frac{\partial \tilde{J}}{\partial x} = \frac{\partial}{\partial x}\left\{\frac{1}{2t}\left[(x_0 - x^-)C^- - \int_{x-}^{x} C dx + (x - x_0)C(x)\right]\right\} \tag{34}$$

Instead of performing this rather indirect calculation, which is a manipulation of a manipulation of the concentration, a more direct, and hence more accurate, way of calculating $\frac{\partial \tilde{J}}{\partial x}$ would be to manipulate the concentration profile directly. Taking the derivative Equation 25 and using the Fundamental Theorem of Calculus, the following simplification may be made:

$$\tilde{J}(x) = \frac{1}{2t}\int_{C^-}^{C(x)} (x - x_0)\, dC \Rightarrow$$

$$\frac{\partial \tilde{J}}{\partial x} = \frac{\partial}{\partial x}\left[\frac{1}{2t}\int_{C^-}^{C(x)} (x - x_0)\, dC\right] \Leftrightarrow$$

$$\frac{\partial \tilde{J}}{\partial x} = \frac{1}{2t}\left(\frac{\partial}{\partial x}\int_{C^-}^{C(x)} x\, dC - \frac{\partial}{\partial x}\int_{C^-}^{C(x)} x_0 dC\right) \Leftrightarrow$$

$$\frac{\partial \tilde{J}}{\partial x} = \frac{1}{2t}\left(\frac{\partial C}{\partial x}x - \frac{\partial C}{\partial x}x_0\right) \Leftrightarrow$$

$$\frac{\partial \tilde{J}}{\partial x} = \frac{1}{2t}(x - x_0)\frac{\partial C}{\partial x} \qquad (35)$$

Using the alternate interdiffusion flux equation, Equation 30, the same results are achieved.

$$\tilde{J}(x) = \frac{1}{2t}\left[(x_0 - x^-)C^- - \int_{x-}^{x} C dx + (x - x_0)C(x)\right] \Rightarrow$$

$$\frac{\partial \tilde{J}}{\partial x} = \frac{\partial}{\partial x}\left\{\frac{1}{2t}\left[(x_0 - x^-)C^- - \int_{x-}^{x} C dx + (x - x_0)C(x)\right]\right\} \Leftrightarrow$$

$$\frac{\partial \tilde{J}}{\partial x} = \frac{1}{2t}\left\{\frac{\partial}{\partial x}\left[(x_0 - x^-)C^-\right] - \frac{\partial}{\partial x}\left(\int_{x-}^{x} C dx\right) + \frac{\partial}{\partial x}\left[(x - x_0)C(x)\right]\right\} \Leftrightarrow$$

$$\frac{\partial \tilde{J}}{\partial x} = \frac{1}{2t}\left[0 - C(x) + x\frac{\partial C}{\partial x} + C(x) - x_0\frac{\partial C}{\partial x}\right] \Leftrightarrow$$

$$\frac{\partial \tilde{J}}{\partial x} = \frac{1}{2t}(x - x_0)\frac{\partial C}{\partial x} \qquad (35)$$

Given that Equation 35 is reminiscent of the continuity equation, it was later found that it may be derived from the continuity equation, making use of the Boltzmann parameter. And so Equation 35 is used to calculate the derivative of the interdiffusion flux since it is a direct manipulation of the concentration profile.

3.4 A New Interpretation of Ternary Interdiffusion Coefficients

In the article *The Trouble with Diffusion*,[33] DeHoff points out some flaws associated with the mathematical formalisms and interpretations involving interdiffusion coefficients. Indeed, mathematically modeling diffusion has proved to be a challenging problem that brings to light many issues associated with the traditional models. One central issue is the inconsistency that arises due to the generally accepted meaning of the interdiffusion coefficients. For instance, given an isothermal ternary diffusion couple, $\tilde{D}_{ij}$ corresponds to the contribution of the gradient of component *j* to the interdiffusion flux of component *i*,[33] so if component 3 is taken to be the dependent component then $\tilde{D}_{22}^{3}$ represents the contribution of the concentration gradient of component 2 to the interdiffusion flux of component 2. Suppose instead, for this same system,

component 1 is taken as the dependent component and $\widetilde{D}_{22}^{1}$ is calculated, which also represents the contribution of the gradient to the interdiffusion flux of component 2. Then according to the meaning of the interdiffusion coefficient, it should be that $\widetilde{D}_{22}^{3} = \widetilde{D}_{22}^{1}$. Recall from Section 2.1.3, the equations relating ternary interdiffusion coefficients with different components held as independent. For the above described coefficients, $\widetilde{D}_{22}^{3} = \widetilde{D}_{22}^{1} - \widetilde{D}_{23}^{1}$. These equations are widely accepted and implemented,[20-23] and thus lead to the contradiction $\widetilde{D}_{22}^{3} = \widetilde{D}_{22}^{1} - \widetilde{D}_{23}^{1} \neq \widetilde{D}_{22}^{1}$, unless the cross interdiffusion coefficient is zero, which is not true for a myriad of cases.[34] This contradiction completely obscures the traditional interpretation of the interdiffusion coefficients.

Recall Equations 6 and 7, the error function solutions to Onsager's Formalism for a ternary system, as stated by Fujita and Gosting.[15] These equations are accepted and frequently used for interdiffusion coefficient analyses.[4,5,16-19] Though the error function solutions assume constant diffusivity, they serve well for analysis and verification of interdiffusion coefficients. Given a ternary system, assume the concentration profiles may be modeled with insignificant error using the error function solutions. Recall Onsager's Formalism for the ternary system and the derivative of the interdiffusion flux as shown below, to the left. Assume the frame of reference is shifted so that the Matano plane is located at $x_0 = 0$. Then the two equations may be combined as follows.

$$\left.\begin{aligned} \widetilde{J}_1(x) &= -\widetilde{D}_{11}\frac{\partial C_1}{\partial x} - \widetilde{D}_{12}\frac{\partial C_2}{\partial x} \\ \frac{\partial \widetilde{J}_1}{\partial x} &= \frac{x}{2t}\frac{\partial C_1}{\partial x} \end{aligned}\right\} \Rightarrow -\widetilde{D}_{11}\frac{\partial^2 C_1}{\partial x^2} - \widetilde{D}_{12}\frac{\partial^2 C_2}{\partial x^2} = \frac{x}{2t}\frac{\partial C_1}{\partial x} \qquad (36)$$

$$\left.\begin{aligned}\widetilde{J}_2(x) &= -\widetilde{D}_{21}\frac{\partial C_1}{\partial x} - \widetilde{D}_{22}\frac{\partial C_2}{\partial x} \\ \frac{\partial \widetilde{J}_2}{\partial x} &= \frac{x}{2t}\frac{\partial C_2}{\partial x}\end{aligned}\right\} \Rightarrow -\widetilde{D}_{21}\frac{\partial^2 C_1}{\partial x^2} - \widetilde{D}_{22}\frac{\partial^2 C_2}{\partial x^2} = \frac{x}{2t}\frac{\partial C_2}{\partial x} \qquad (37)$$

Next is a manipulation of Equation 36. Equation 37 may be neglected for now. To use Equation 36, the first and second partial derivatives of C_1 and the second partial derivative of C_2 must be calculated. To do that, recall that the derivative of an error function.

$$\frac{\partial}{\partial z} erf(z) = \frac{2}{\sqrt{\pi}}\exp\left(-z^2\right)$$

Let

$$z = \frac{x}{2\sqrt{t}\sqrt{u}}$$

Then

$$\frac{\partial z}{\partial x} = \frac{1}{2\sqrt{t}\sqrt{u}}$$

$$\Leftrightarrow \partial z = \frac{1}{2\sqrt{t}\sqrt{u}}\partial x$$

$$\frac{\partial}{\partial z} erf(z) = \frac{2}{\sqrt{\pi}}\exp\left(-z^2\right)$$

$$\Leftrightarrow \frac{\partial}{\partial x}\left(2\sqrt{t}\sqrt{u}\right)erf\left(\frac{x}{2\sqrt{t}\sqrt{u}}\right)=\frac{2}{\sqrt{\pi}}\exp\left[-\left(\frac{x}{2\sqrt{t}\sqrt{u}}\right)^2\right]$$

$$\Leftrightarrow \frac{\partial}{\partial x}erf\left(\frac{x}{2\sqrt{t}\sqrt{u}}\right)=\frac{1}{\sqrt{t}\sqrt{u}\sqrt{\pi}}\exp\left[-\left(\frac{x}{2\sqrt{t}\sqrt{u}}\right)^2\right] \tag{38}$$

$$\Rightarrow \frac{\partial^2}{\partial x^2}erf\left(\frac{x}{2\sqrt{t}\sqrt{u}}\right)=\frac{1}{\sqrt{t}\sqrt{u}\sqrt{\pi}}\exp\left[-\left(\frac{x}{2\sqrt{t}\sqrt{u}}\right)^2\right]\left\{-2\left(\frac{x}{2\sqrt{t}\sqrt{u}}\right)\left(\frac{1}{2\sqrt{t}\sqrt{u}}\right)\right\}$$

$$\Leftrightarrow \frac{\partial^2}{\partial x^2}erf\left(\frac{x}{2\sqrt{t}\sqrt{u}}\right)=\frac{-x}{2tu\sqrt{t}\sqrt{u}\sqrt{\pi}}\exp\left[-\left(\frac{x}{2\sqrt{t}\sqrt{u}}\right)^2\right] \tag{39}$$

Now that the first and second partial derivatives of the error functions are calculated, the first and second partial derivatives of the concentration may be calculated.

$$\frac{\partial C_1}{\partial x}=\frac{\partial}{\partial x}\left[a\cdot erf\left(\frac{x}{2\sqrt{t}\sqrt{u}}\right)+b\cdot erf\left(\frac{x}{2\sqrt{t}\sqrt{v}}\right)+c\right]$$

$$\Leftrightarrow \frac{\partial C_1}{\partial x}=a\cdot\frac{\partial}{\partial x}erf\left(\frac{x}{2\sqrt{t}\sqrt{u}}\right)+b\cdot\frac{\partial}{\partial x}erf\left(\frac{x}{2\sqrt{t}\sqrt{v}}\right)+\frac{\partial}{\partial x}c$$

Then from Equation 38, the above equation becomes:

$$\Leftrightarrow \frac{\partial C_1}{\partial x}=\frac{a}{\sqrt{t}\sqrt{u}\sqrt{\pi}}\exp\left[-\left(\frac{x}{2\sqrt{t}\sqrt{u}}\right)^2\right]+\frac{b}{\sqrt{t}\sqrt{v}\sqrt{\pi}}\exp\left[-\left(\frac{x}{2\sqrt{t}\sqrt{v}}\right)^2\right] \tag{40}$$

The second derivative of the concentration may be calculated as follows:

$$\frac{\partial^2 C_1}{\partial x^2} = \frac{\partial^2}{\partial x^2}\left[a \cdot erf\left(\frac{x}{2\sqrt{t}\sqrt{u}}\right) + b \cdot erf\left(\frac{x}{2\sqrt{t}\sqrt{v}}\right) + c \right]$$

$$\Leftrightarrow \frac{\partial^2 C_1}{\partial x^2} = a \cdot \frac{\partial^2}{\partial x^2} erf\left(\frac{x}{2\sqrt{t}\sqrt{u}}\right) + b \cdot \frac{\partial^2}{\partial x^2} erf\left(\frac{x}{2\sqrt{t}\sqrt{v}}\right) + \frac{\partial^2}{\partial x^2} c$$

Using Equation 39

$$\Leftrightarrow \frac{\partial^2 C_1}{\partial x^2} = a \cdot \frac{-x}{2tu\sqrt{t}\sqrt{u}\sqrt{\pi}} \exp - \left(\frac{x}{2\sqrt{t}\sqrt{u}}\right)^2 + b \cdot \frac{-x}{2tv\sqrt{t}\sqrt{v}\sqrt{\pi}} \exp - \left(\frac{x}{2\sqrt{t}\sqrt{v}}\right)^2 \qquad (41)$$

Similarly, the first and second derivatives of the concentration of component 2 are

$$\frac{\partial C_2}{\partial x} = \frac{d}{\sqrt{t}\sqrt{u}\sqrt{\pi}} \exp\left[-\left(\frac{x}{2\sqrt{t}\sqrt{u}}\right)^2 \right] + \frac{e}{\sqrt{t}\sqrt{v}\sqrt{\pi}} \exp\left[-\left(\frac{x}{2\sqrt{t}\sqrt{v}}\right)^2 \right] \qquad (42)$$

$$\frac{\partial^2 C_2}{\partial x^2} = d \cdot \frac{-x}{2tu\sqrt{t}\sqrt{u}\sqrt{\pi}} \exp - \left(\frac{x}{2\sqrt{t}\sqrt{u}}\right)^2 + e \cdot \frac{-x}{2tv\sqrt{t}\sqrt{v}\sqrt{\pi}} \exp - \left(\frac{x}{2\sqrt{t}\sqrt{v}}\right)^2 \qquad (43)$$

Plugging Equations 40-43 into Equation 36:

$$-\tilde{D}_{11} \frac{\partial^2 C_1}{\partial x^2} - \tilde{D}_{12} \frac{\partial^2 C_2}{\partial x^2} = \frac{x}{2t} \frac{\partial C_1}{\partial x}$$

$$\Leftrightarrow -\widetilde{D}_{11}\left[a\cdot\frac{-x}{2tu\sqrt{t}\sqrt{u}\sqrt{\pi}}\exp-\left(\frac{x}{2\sqrt{t}\sqrt{u}}\right)^2+b\cdot\frac{-x}{2tv\sqrt{t}\sqrt{v}\sqrt{\pi}}\exp-\left(\frac{x}{2\sqrt{t}\sqrt{v}}\right)^2\right]$$

$$-\widetilde{D}_{12}\left[d\cdot\frac{-x}{2tu\sqrt{t}\sqrt{u}\sqrt{\pi}}\exp-\left(\frac{x}{2\sqrt{t}\sqrt{u}}\right)^2+e\cdot\frac{-x}{2tv\sqrt{t}\sqrt{v}\sqrt{\pi}}\exp-\left(\frac{x}{2\sqrt{t}\sqrt{v}}\right)^2\right]$$

$$=\frac{x}{2t}\left[\frac{a}{\sqrt{t}\sqrt{u}\sqrt{\pi}}\exp\left[-\left(\frac{x}{2\sqrt{t}\sqrt{u}}\right)^2\right]+\frac{b}{\sqrt{t}\sqrt{v}\sqrt{\pi}}\exp\left[-\left(\frac{x}{2\sqrt{t}\sqrt{v}}\right)^2\right]\right]$$

$$\Rightarrow -\widetilde{D}_{11}a\cdot\frac{-x}{2tu\sqrt{t}\sqrt{u}\sqrt{\pi}}-\widetilde{D}_{12}d\cdot\frac{-x}{2tu\sqrt{t}\sqrt{u}\sqrt{\pi}}=\frac{x}{2t}\frac{a}{\sqrt{t}\sqrt{u}\sqrt{\pi}}$$

$$\Leftrightarrow \widetilde{D}_{11}a\cdot\frac{1}{u}+\widetilde{D}_{12}d\cdot\frac{1}{u}=a \qquad (44)$$

and

$$\Rightarrow -\widetilde{D}_{11}b\cdot\frac{-x}{2tv\sqrt{t}\sqrt{v}\sqrt{\pi}}-\widetilde{D}_{12}e\cdot\frac{-x}{2tv\sqrt{t}\sqrt{v}\sqrt{\pi}}=\frac{x}{2t}\frac{b}{\sqrt{t}\sqrt{v}\sqrt{\pi}}$$

$$\Leftrightarrow \widetilde{D}_{11}b\cdot\frac{1}{v}+\widetilde{D}_{12}e\cdot\frac{1}{v}=b \qquad (45)$$

Using Equations 44 and 45 to solve for the interdiffusion coefficients:

$$\widetilde{D}_{11}a\cdot\frac{1}{u}+\widetilde{D}_{12}d\cdot\frac{1}{u}=a$$

$$\Leftrightarrow \widetilde{D}_{11}=\frac{au-\widetilde{D}_{12}d}{a}$$

$$\widetilde{D}_{11}b\cdot\frac{1}{v}+\widetilde{D}_{12}e\cdot\frac{1}{v}=b$$

$$\Leftrightarrow \frac{au - \widetilde{D}_{12} d}{a} b + \widetilde{D}_{12} e = bv$$

$$\Leftrightarrow \widetilde{D}_{12} = \frac{abv - abu}{ae - bd} \tag{46}$$

$$\Rightarrow \widetilde{D}_{11} = \frac{aeu - bdv}{ae - bd} \tag{47}$$

Similarly, using Equation 37

$$\widetilde{D}_{22} = \frac{aev - bdu}{ae - bd} \tag{48}$$

$$\widetilde{D}_{21} = \frac{deu - dev}{ae - bd} \tag{49}$$

Equations 46-49 may be easily verified by plugging them into the error function solution constant equations. In order to compare the four interdiffusion coefficients, to seek out the dominant influence that defines each of the four coefficients, the commonalities they all four share are disregarded. To this end, little emphasis should be placed on *u* and *v*, since they appear in the same manner for all equations. Also notice that all of the four coefficients have the same denominator and so this too yields no knowledge of the uniqueness of each coefficient. From Equations 6 and 7, *a* and *b* are terms of concentration 1, and *d* and *e* are terms of concentration 2. Table 1 summarizes the unique factors of the interdiffusion coefficients. From Table 1, it is revealed that $\widetilde{D}_{11}$ is influenced by both concentration 1 and concentration 2, while $\widetilde{D}_{12}$ is influenced by concentration 1 only. The previous statement is in direct opposition to the current interpretation of these coefficients that assumes the opposite. Traditionally, $\widetilde{D}_{11}$ is said to be

influenced by concentration 1 only and $\widetilde{D}_{12}$ is influenced by both concentration 1 and 2. In effect, the interpretation proposed in this thesis is this: $\widetilde{D}_{11}$ should be defined as the interdiffusion coefficient reflecting the influence of concentrations 1 and 2 on the interdiffusion flux of component 1 and $\widetilde{D}_{12}$ as the interdiffusion coefficient reflecting the influence of concentration 1 on the interdiffusion flux of component 1. Then, $\widetilde{D}_{21}$ is the interdiffusion coefficient reflecting the influence of concentration 2 on the interdiffusion flux of component 2 and $\widetilde{D}_{22}$ is the interdiffusion coefficient reflecting the influence of concentrations 1 and 2 on the interdiffusion flux of component 2.

Table 1. Analysis of the factors that influence the interdiffusion coefficients.

Interdiffusion Coefficients	Unique Factors	Corresponding Influence
$\widetilde{D}_{11} = \frac{aeu - bdv}{ae - bd}$	a, b d, e	Concentration 1 Concentration 2
$\widetilde{D}_{12} = \frac{abv - abu}{ae - bd}$	a, b	Concentration 1
$\widetilde{D}_{21} = \frac{deu - dev}{ae - bd}$	d, e	Concentration 2
$\widetilde{D}_{22} = \frac{aev - bdu}{ae - bd}$	a, b d, e	Concentration 1 Concentration 2

In summary, a new interpretation of the interdiffusion coefficients is established based on the error function solutions of Onsager's Formalism. This interpretation is in direct opposition to the currently accepted interpretation of the coefficients. As further verification, the inconsistency

mentioned earlier in this section, highlighted by DeHoff,[33] does not exist with the new definition. The traditional definition of the coefficients states that the contribution of the concentration gradient of component 2 to the interdiffusion flux of component 2 ($\widetilde{D}_{22}^{3}$) is not equal to the contribution of the concentration gradient of component 2 to the interdiffusion flux of component 2 ($\widetilde{D}_{22}^{1}$). The new definition does not have this inconsistency; it states that the contribution of the concentration gradient of component 1 to the interdiffusion flux of component 1 is equal but opposite to the contribution of the concentration gradient of component 1 to the interdiffusion flux of component 1 when the dependent variable is changed from 3 to 2. This latter statement is the literal translation of Equation 21, $\widetilde{D}_{13}^{2} = -\widetilde{D}_{12}^{3}$. The change in sign stems from the fact that the concentration gradients add to zero so that two of the gradients have the same sign and the third has an opposite sign. Thus, the proposed interpretation irons out some of the wrinkles associated with the traditional interpretation.

3.5 Determination of Composition Dependent Ternary Interdiffusion Coefficients from a Single Diffusion Couple

Here is presented a method for calculating concentration dependent interdiffusion coefficients from a single isothermal ternary diffusion couple. This method uses a similar approach to the DAYSO method, and thus it may be regarded as an extension of this method for the case of concentration dependent diffusivity. Equation 28, which was used in the DAYSO method, suffices as two of the four equations used in the new technique with one subtle alteration. The DAYSO method typically integrates over a large range of compositions, such as from the

terminal alloy to the Matano plane; the new technique integrates over a small range of compositions. The second equation is the differential with respect to *x* of Onsager's Formalism, substituting in Equation 35.

$$\frac{\partial \tilde{J}_i}{\partial x} = -\tilde{D}_{i1}^3 \frac{\partial^2 C_1}{\partial x^2} - \tilde{D}_{i2}^3 \frac{\partial^2 C_2}{\partial x^2} \quad (i = 1,2) \Leftrightarrow$$

$$\frac{1}{2t}(x - x_0)\frac{\partial C}{\partial x} = -\tilde{D}_{i1}^3 \frac{\partial^2 C_1}{\partial x^2} - \tilde{D}_{i2}^3 \frac{\partial^2 C_2}{\partial x^2} \tag{50}$$

Equations 28 and 50 are the four equations (i= 1, 2) necessary to calculate the four ternary interdiffusion coefficients. The reason the presented method is considered concentration dependent and the DAYSO method is not is because Equations 28 and 50 are carried out over a small concentration range for the new technique. Differentiation is taken at the median value of the integration limits. For example, if the interdiffusion coefficients are to be calculated at *x*= 125μm, then Equation 28 is integrated over $[x_1 = 124\mu m, x_2 = 126\mu m]$ and the differentiation of Equation 50 is taken at *x*= 125μm. Thus, the coefficients are technically not continuous functions of composition, but rather a dense set of discrete values. The DAYSO method on the other hand, is designed so that the equations cover a wide range of the profile, such as from $C_i^{-/+}$ to C_i^0. For example, the results from the new technique are compared with the DAYSO method for ternary diffusion couples in Chapter 6. The DAYSO method yields 2 sets of interdiffusion coefficients, one set for each side of the Matano plane; the new technique yields anywhere from 50 to 90 sets of interdiffusion coefficients, one set for each small increment of the concentration profile.

For Equations 28 and 50, interdiffusion fluxes are calculated directly from the experimental concentration profiles via Equation 30; the Matano plane location is calculated via Equation 33; the derivative of the interdiffusion flux is calculated via Equation 35. Small concentration gradients yield unmanageably large coefficients using this new technique. This is due to the division by the concentration gradient within the calculations. However, this makes sense since concentration profiles that exhibit small gradients overall are associated with relatively fast diffusion and thus large interdiffusion coefficients. Consequently, the calculations are taken over the portion of the profile where the slope is significant, disregarding the terminal ends of the concentration profile.

4 A NEW SYSTEM FOR CLASSIFYING PHASE BOUNDARIES

In the study of phase boundaries, it is useful to classify the different types of boundaries that may occur for a particular system. Recall Moral et al.[10] classifies phase boundaries as Type I, Type II, etc. This becomes tedious for an *n*-component system where a Type VIII or Type X boundary must be introduced, and the classification becomes obscured. An alternative is proposed here where the boundary types are according to how many phases are added and how many are subtracted upon crossing the phase boundary. The notation for this classification is n:m, meaning, n phase(s) are added and m phase(s) are subtracted when crossing the phase boundary. For example, a boundary between an α phase and a β phase, denoted $\alpha<>\beta$, is a 1:1 boundary, indicating the addition of the β and the subtraction of the α phase going from left to right across the boundary. The $\alpha>(\alpha+\beta)$ phase boundary falls into the 1:0 category where one phase is introduced and none subtracted when crossing the boundary from left to right. Analogously, one phase is subtracted and none introduced going from right to left; thus the 0:1 category is equivalent to the 1:0 category. In general n:m is the same as m:n. The more components a given system has, the more possibilities for different types of boundaries. Here is outlined this classification system along with experimental evidence of a unique boundary type where the diffusion path on the ternary phase diagram exits through the vertex of the equilibrium tie triangle.

4.1 Phase Boundaries in Binary Systems

Consider an isothermal binary diffusion couple; the two types of phase boundaries that may develop are illustrated in Figure 7.

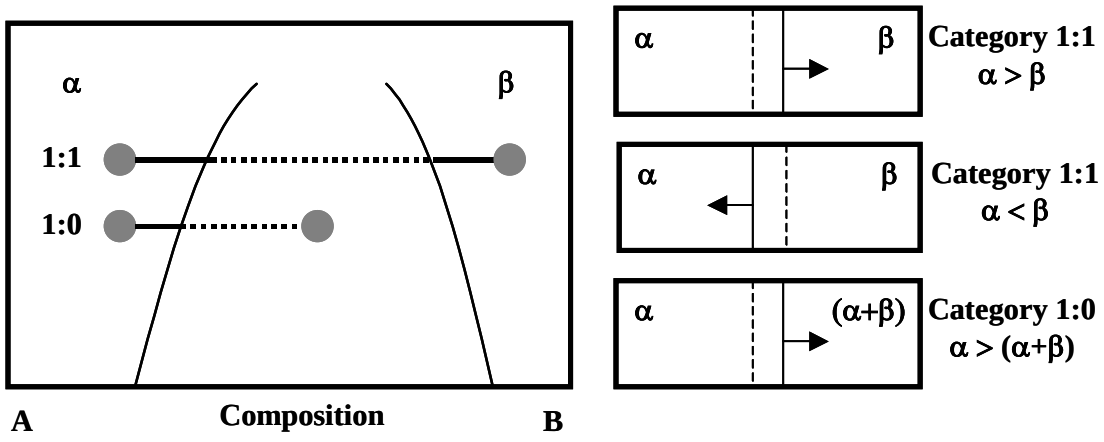

Figure 7. Diffusion paths and examples of moving boundaries for a binary isothermal system.

Morral et al. have classified binary phase boundaries for the purpose of computer simulation[10], and have labeled the categories Type I and Type II. In order to more easily extend this classification to higher order systems, the categories can be denoted by n:m, where n phase(s) are added and m phase(s) are subtracted when crossing the phase boundary. The Category 1:0 boundary joins two regions, one region having one more phase than the other. An example is $\alpha > (\alpha + \beta)$, where > indicates a boundary moving to the right with time; i.e., the α phase will grow at the expense of the (α+β) phase as the system goes toward equilibrium. Leftward boundary movement is indicated by < , a stationary boundary is indicated by |, and a boundary that may move right or left is indicated by < >. Such movement can be predicted by Gibb's phase rule. For an isothermal, isobaric binary diffusion couple, Gibbs phase rule is F = 2-P, where F is the degrees of freedom and P is the number of phases. Consider the 1:0 category boundary, $\alpha > (\alpha +$

β). For the multiphase region there is no degree of freedom since F=2-2=0 and for the single-phase region there is one degree of freedom, F=2-1=1. Thus, the α phase grows at the expense of the α + β phase, and the boundary moves accordingly: α > (α + β). Zero degrees of freedom means that the composition of the phase(s) may not change if equilibrium is to be maintained and so a region with a non-zero degree of freedom will expend a region with zero degrees of freedom. The Category 1:1 boundary indicates the addition of one phase and the subtraction of another across the boundary, for example, α < > β. The diffusion path travels through three regions of the phase diagram, from α to (α + β) to β as shown in Figure 7. Since each α and β have one degree of freedom the boundary may travel in either direction. For a given region in the phase diagram, each of the two elements in the binary system can contribute to at most one phase, thus the maximum number of phases in a multiphase region is two. Since a binary phase diagram only contains single- and two-phase regions, the types of boundaries that may occur according this classification scheme are few. The number of components in a system is the limiting factor for the number of boundary types that may occur. The more components, the more possible boundary types. For a ternary system, the n:m classification system yields an additional boundary type, discussed below.

4.2 Phase Boundaries in Ternary Systems

Figure 8 demonstrates the category 1:0 and 1:1 boundaries that may occur in a ternary system.

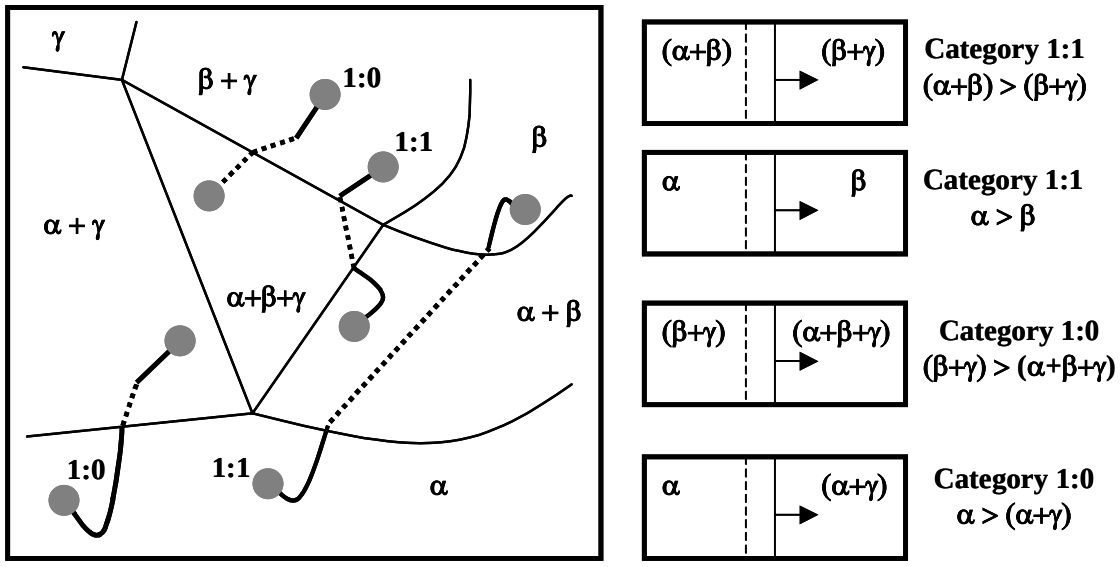

Figure 8. Diffusion paths and examples of Category 1:0 and 1:1 moving boundaries for a ternary isothermal system.

These boundaries may be planar or non-planar and the multiphase layers may be striated in appearance or contain precipitates of various sizes and shapes, such as columnar or circular precipitates. Applying Gibbs phase rule to a ternary isothermal, isobaric diffusion couple, F= 3-P. Then for a single-phase region F=2 degrees of freedom and for a two-phase region F=1 degree of freedom. Thus, the single and two-phase regions have the freedom to grow at the expense of another region. The three phase region has F=0 degrees of freedom, so it may be expended by another region. With this in mind, the Category 1:0 boundaries are of the kind $\alpha <> (\alpha+\gamma)$ and $(\alpha+\beta) > (\alpha+\beta+\gamma)$ and the Category 1:1 boundaries are of the kind $\alpha <> \beta$ and $(\alpha+\beta) <> (\alpha+\gamma)$. A multi-phase region in a ternary system may have at most three phases, and so the above listed boundaries exhaust the list of category 1:0 and 1:1 boundaries that may occur in a ternary system.

An additional type is needed to define the boundary classification system for ternary diffusion couples. Whereas in a binary system a multi-phase region consists of exactly two phases, a ternary isotherm may contain a multi-phase region of either two or *three* phases. A three-phase region yields the possibility of a category 2:1 boundary. The category 2:1 boundary indicates two phases are being introduced and one subtracted across the phase boundary. For example, α < > (β+γ) is a 2:1 boundary.

In an isothermal ternary phase diagram, the equilibrium tie triangle is the triangular shape three-phase region. The diffusion path for the 2:1 boundary is rather unique in that it exits out the vertex of the equilibrium tie triangle. An example of such a path is illustrated in Figure 9. This classification system can easily be extended for an *n*-component system.

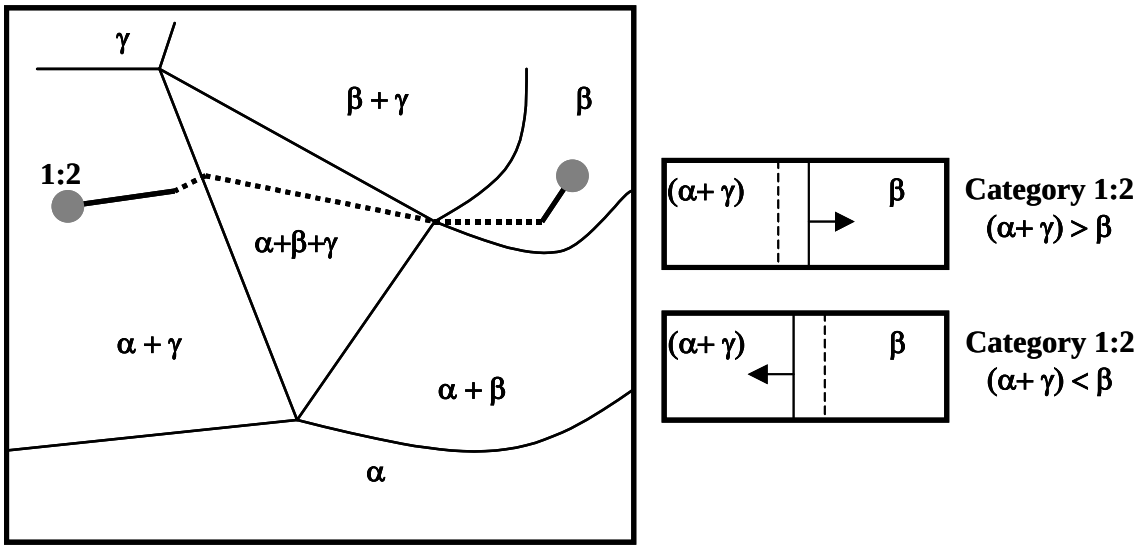

Figure 9. Diffusion path for the Category 1:2 moving boundary in an isothermal ternary system.

5 EXPERIMENTAL PROCEDURES

The preparation of the alloys and couples used in this study are outlined in literature[6-9] and summarized here. The Cu-Ni-Zn alloy ingots[6] were prepared from high purity elements by induction melting in an alumina crucible under argon atmosphere, then cold rolled and homogenized in a quartz tube for a week at 900°C. The alloys were cut into discs of 1 cm thickness, 1 cm in diameter and polished through 0.05-micron alumina. Al_2O_3 particles served as inert markers. The discs were clamped together with Kovar steel jigs, which have a low coefficient of thermal expansion. The assembled couple was placed in a quartz tube, flushed several times with hydrogen, evacuated to low pressure, and sealed to form a capsule. The couple was annealed at 775°C in a Lindberg three-zone tube furnace. The temperature gradient in the capsule was kept within 1°C. After the anneal, the capsules were quenched to retain the high temperature structure of the diffusion zone. The couples were then mounted, sectioned for cross-sectional examination, polished, and etched. A JEOL scanning electron microscope (SEM) equipped with an energy dispersive X-ray analyzer was used to obtain the concentration profiles using an EDAX system with standard ZAF corrections (atomic number (Z), absorption (A), and fluorescence (F)). The Fe-Ni-Al alloys[7] were produced in a similar manner, but were not cold rolled and were annealed at 1004°C for two days. The concentration data was obtained with a microprobe instead of an EDAX system, though the principles in the data collection are the same for both procedures.

The Ni-Cr-Al alloys[8] were arc melted and drop cast in a cylindrical die. The alloys were annealed for 100 hours at 1150°C then sectioned and polished. The disks were bonded by heating them under a 10 m torr vacuum. The diffusion couples were encapsulated in a quartz tube and heated for 100 hours at 1100°C ±2°C and quenched. After being polished and etched, the cut cross sectional areas were examined via standard electron probe microanalysis (EPMA) procedures.

Dr. Hayashi of Iowa State University generously donated the concentration profiles for the Ni-Pt-Al diffusion couples used in this study. They alloys were prepared by arc melting high purity elements into ingots which were then homogenized at 1200°C for 6 hours, then again at 1150°C for 24 hours in an argon atmosphere. Samples of 1.5 mm thickness were cut, polished, washed, and clamped together with an Si_3N_4 clamp. The clamped diffusion couples were sealed in a quartz capsule under an argon atmosphere, heated to 1200°C, held for 30 minutes in order to establish good bonding, and furnace cooled. The bonded diffusion couple was removed from the clamp and encapsulated in an evacuated quartz tube flushed with argon. The couples were annealed at 1150°C for 50 hours.

The concentration profiles obtained from the above procedures were exported to Excel, Matlab, and MathCAD in order to employ the new technique presented in this thesis. The data from the Cu-Ni-Zn, Fe-Ni-Al, and Ni-Cr-Al couples were previously smoothened. The data from the Ni-Pt-Al system was given as raw data and was smoothed using Matlab as demonstrated in Appendix A. Though MathCAD and Excel were used for some of the intermediate calculations, Matlab was used for the final calculations and the creation of all figures.

The alloys for the γ vs. β Fe-Ni-Al couple discussed in Section 6.3 were prepared with high purity elements by induction melting in alumina crucibles under argon atmosphere and were chill-cast in a vacuum by drawing the melt into quartz tubes to obtain rods. The alloy rods were encapsulated in an evacuated quartz tube flushed with hydrogen then homogenized at 1000°C for 5 days in a three-zone tube furnace. The alloys were quenched, polished, and checked for homogeneity using optical microscopy (OM), SEM, energy dispersive spectroscopy (EDS), and EPMA. From these homogenized rods, discs were prepared and held together with a Kovar steel jig to form a couple. Alumina particles at the interface served as inert markers. The clamped couple was then sealed inside an evacuated, hydrogen flushed quartz tube, annealed at 1000°C in a tube furnace for 48 hours. The temperature was controlled within 1.0°C. The couple was then quenched, sectioned, and etched. The diffusion structures were observed by OM and SEM. The surface was repolished and analyzed by point-to-point counting techniques with an EPMA JEOL Superprobe 733 microprobe with pure Fe, Ni, and Al as standards. The K_α characteristic X-rays for each element were collected using a wavelength dispersive spectrometer (WDS) at an accelerating voltage of 15KV and a sample current of 20nA. Appropriate ZAF corrections were employed to obtain the concentrations of Fe, Ni, and Al. The raw microprobe data along with the smoothed spline data is given in Appendix A. The compositions, phases, and anneal temperatures and times for all diffusion couples used in this study are summarized in Table 2.

Table 2. A summary of the phases, compositions, anneal times and temperatures of all diffusion couples used in this study.

Composition	Phase	Anneal Temperature	Anneal Time (hours)	Composition (at.%)
α_5 vs. α_{12} [6]	α	775°C	48	$\boldsymbol{\alpha_5}$ Cu-44.70Ni-25.20Zn $\boldsymbol{\alpha_{12}}$ Cu-19.39Ni
β_5 vs. β_9 [7]	β	1000°C	48	$\boldsymbol{\beta_5}$ Fe-46.00Ni-34.04Al $\boldsymbol{\beta_9}$ Fe-24.23Ni-36.58Al
Alloy 1 vs. Alloy 3 [8,9]	γ	1100°C	100	**1** Ni-7.98Cr-7.78Al **3** Ni-11.65Cr-7.26Al
Alloy 2 vs. Alloy 4 [8,9]	γ	1100°C	100	**2** Ni-9.63Cr-6.24Al **4** Ni-9.45Cr-9.48Al
Alloy 10 vs. Alloy 13	γ'	1150°C	50	**10** Ni-16.9Pt-24.1Al **13** Ni-23.9Pt-27.1Al
Alloy 11 vs. Alloy 16	γ	1150°C	50	**11** Ni-17.1Pt-11.7Al **16** Ni-23.9Pt-4.72Al
Alloy 12 vs. Alloy 15	γ	1150°C	50	**12** Ni-17.4Pt-6.45Al **15** Ni-24.2Pt-9.45Al
γ vs. β	γ β	1000°C	48	$\boldsymbol{\gamma}$ Fe-28.1Ni $\boldsymbol{\beta}$ Fe-11.9Ni-25.6Al

6 RESULTS AND DISCUSSION

6.1 Application of the New Technique for Determining Composition Dependent Ternary Interdiffusion Coefficients to Selected Couples

The present analysis was applied to concentration profiles obtained from diffusion couples selected from literature.[6-9] These semi-infinite couples are single-phase, substitutional alloys from the Cu-Ni-Zn, Fe-Ni-Al, and Ni-Cr-Al systems. These couples exhibit features such as uphill diffusion and zero flux planes (ZFPs).[6,26,27,35,36] The experimental concentration profiles for these couples are shown in Figures 10-13. The interdiffusion fluxes associated with these profiles have been previously reported along with consequential discussions on diffusional interactions.[4] These couples have published interdiffusion coefficients from the DAYSO and Boltzmann-Matano methods and so they serve to verify the results of the new technique. Once verified and checked for consistency, the new technique was applied to previously unexamined couples from the Ni-Pt-Al system.

Figures 14-21 show the interdiffusion coefficients as a function of composition. The interdiffusion profiles were plotted with respect to the concentration of the influencing element. That is, $\widetilde{D}_{11}$ and $\widetilde{D}_{21}$, which reflect the influence of the concentration gradient of component 1,

are plotted with respect to the concentration of component 1 and $\widetilde{D}_{12}$ and $\widetilde{D}_{22}$, which reflect the influence of the concentration gradient of component 2, are plotted with respect to the concentration of component 2. According to Onsager's Formalism for the ternary case, Equations 26 and 27, if the concentration gradient of component *i* is zero and concentration gradient of component *j* is non-zero, then the interdiffusion coefficients $\widetilde{D}_{ij}$ and $\widetilde{D}_{jj}$ may be calculated at this particular composition. These calculations are displayed in Figures 16, 18, and 20 as points. These values are shown to be in good agreement with the interdiffusion coefficients calculated by the new technique. Small concentration gradients yield unmanageably large coefficients using the method proposed in this paper. This is due to the division by the concentration gradient within the calculations; however, this makes sense since concentration profiles that exhibit small gradients overall are associated with relatively faster diffusion and large interdiffusion coefficients. Consequently, the calculations are taken over the portion of the profile where the slope is significant, ignoring the termini of the profile with semi-infinite boundary conditions. This is partially the reason why some of the interdiffusion profiles shown tend to be slightly radical towards the ends.

Figures 10, 14, and 15 represent the Cu-Ni-Zn couple α_5 vs. α_{12}. Note that the left hand side of the Matano plane in Figure 10 actually corresponds to the right-hand side of the Matano plane in Figures 14 and 15. This is because the Ni and Zn concentration profiles are decreasing. Figure 14 shows that the cross coefficient $\widetilde{D}^{\mathrm{Cu}}_{\mathrm{ZnNi}}$ is larger in magnitude than the main coefficient $\widetilde{D}^{\mathrm{Cu}}_{\mathrm{NiNi}}$ and this difference becomes more significant as the composition approaches the zero flux plane of Ni that occurs at approximately 41 at.% Ni, to the extreme right of the profile (not shown). As

observed from the concentration profiles in Figure 10, Zn is the fast diffuser in the system; this is accurately reflected in the large $\widetilde{D}^{Cu}_{ZnZn}$ reported in Figure 15.

Figures 11, 16, and 17 show the β_5 vs. β_9 concentration and interdiffusion coefficient profiles. As with α_5 vs. α_{12}, Figure 16 is relatively reversed to Figure 11, and Figure 17 has the Matano plane on the far right due to the extreme uphill diffusion of Al. $\widetilde{D}^{Fe}_{AlNi}$ is large, reflecting the influence of Ni on Al, which has a significant amount of uphill diffusion. For the Alloy 1 vs. Alloy 3 and Alloy 2 vs. Alloy 4 couples, the uphill diffusion in Figures 12 and 13 are reflected in the large and positive cross coefficients $\widetilde{D}^{Ni}_{AlCr}$ for 1 vs. 3 and $\widetilde{D}^{Ni}_{CrAl}$ for 2 vs. 4. These observations are consistent with previous findings.[4,34,37,38] These two couples also exhibit the phenomenon expressed earlier where the interdiffusion coefficients calculated by this method may go to extremes towards the ends of the profiles.

Dayananda and Sohn previously calculated average ternary interdiffusion coefficients for these four couples and their calculations are reported in Figures 14-21. The DAYSO method results are shown to be comparable and consistent with the results reported in this paper from the new technique. Boltzmann-Matano analysis may be used on Alloy 1 vs. Alloy 3 and Alloy 2 vs. Alloy 4 as their diffusion paths intersect on the ternary isotherm at the composition 82.6at.%Ni-9.7at.%Cr-7.7at.%Al. The results are shown in Figures 18-21 and are comparable to the calculated results. The Boltzmann-Matano analysis numbers for α_5 vs. α_{12} and β_5 vs. β_9 in Figures 14-17 are those previously reported.[34] Each method carries with it an associated error: the Boltzmann-Matano method is sensitive to the angle at which the diffusion paths intersect; the DAYSO method holds error within the integral calculations; the proposed method has error

associated with integration of very small areas and with accuracy in second derivative calculations. Method of differentiation and integration may also lead to variations in the reported results. Data acquisition and the curve fitting of the raw data also yield error for each method; slight alterations in the curve fitting may have a significant effect on the coefficients. Given a particular diffusion couple, the mass balance plane is shifted slightly for each element, which leads to irregularities in the flux; this shift is due to discrepancies in curve fitting and also attributes to error. These errors may result in a difference in excess of 100%, particularly for the cross-interdiffusion coefficients. However, the difference is well under an order of magnitude. Given the above delineated issues, the inconsistencies reported between the methods are all well within the expected margin of error.

The Boltzmann-Matano method yields interdiffusion coefficients at one concentration from at least two diffusion couple experiments; the DAYSO method yields average interdiffusion coefficients on either side of the Matano plane from one diffusion couple. The method presented in this paper yields interdiffusion coefficients at each small increment of the concentration profile. The advantage to this method is a practical one in that it has the capability of providing a method for building a database of coefficients. In this manner the ternary isotherm may be mapped out in terms of interdiffusion coefficients that one may be able to predict coefficients given an unexamined couple. This method also provides an additional consistency check for the other methods.

The error function solutions to Onsager's Formalism for a ternary system, as stated by Fujita and Gosting,[15] are used frequently for interdiffusion coefficient analyses[4,16-19] as a mathematical

model for the profiles. Though the solutions assume constant diffusivity over a wide range of the concentration profile, they serve well for analysis and verification of interdiffusion coefficients. The coefficients calculated from the new technique were averaged (the arithmetic mean) over each side of the Matano plane then plugged into the error function solutions, Equations 6 and 7. These averaged coefficients are compared to the interdiffusion coefficients reported by Dayananda and Sohn in Table 3. The profiles generated from the averaged coefficients in error function solutions, referred to as "Calculated" in the figures, were compared to the experimental profiles. The results are shown in Figures 10-13. The calculated profiles are shown to be good agreement with the experimental profiles, which exhibit diffusion phenomenon such as ZFPs and uphill diffusion.

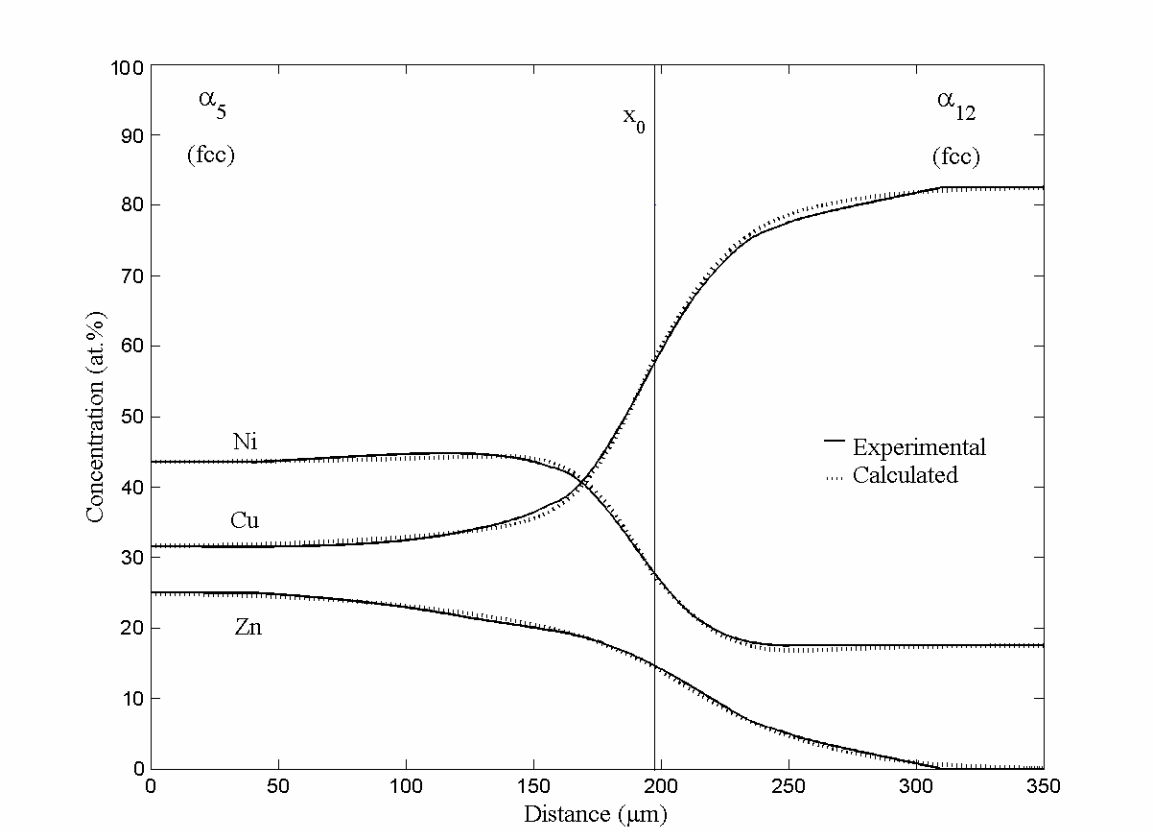

Figure 10. Concentration vs. Distance for the Cu-Ni-Zn diffusion couple α_5 vs. α_{12}; x_0 denotes the Matano plane location. Calculated interdiffusion coefficients are plugged into error function solutions and compared with the original experimental data.

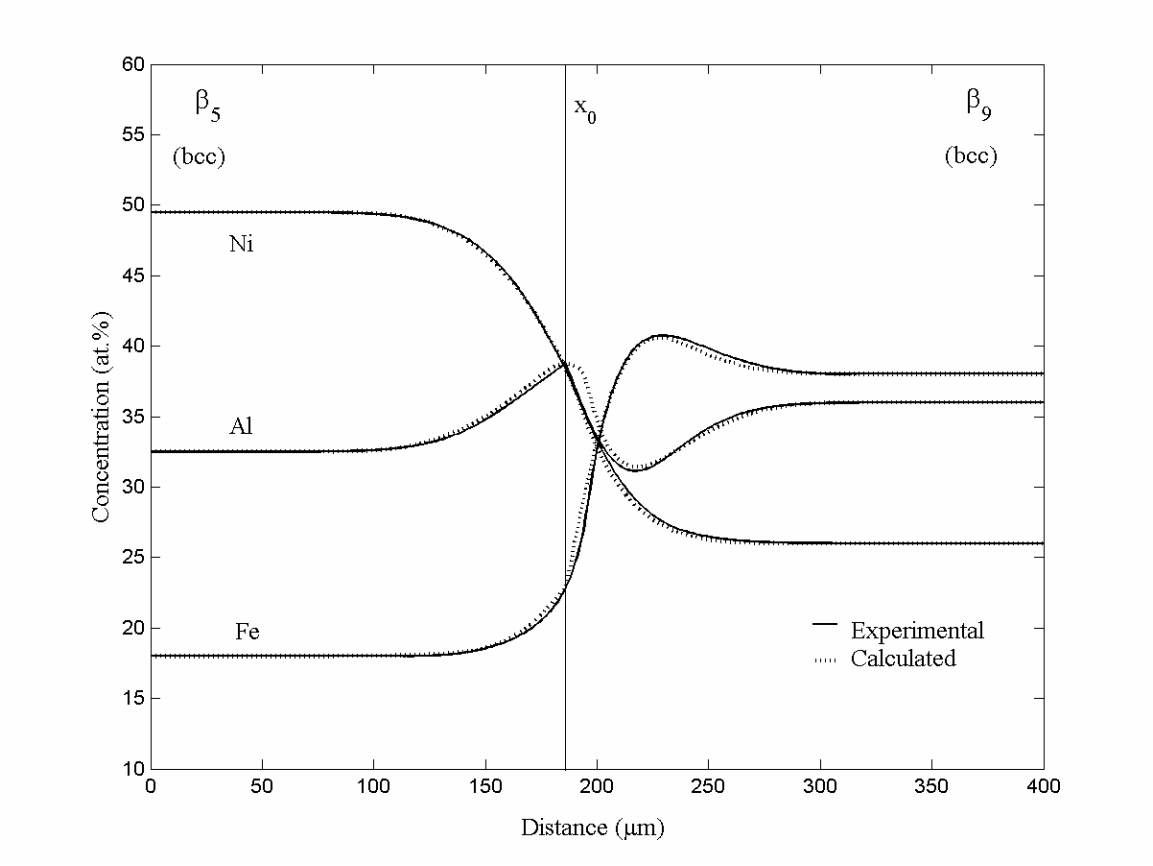

Figure 11. Concentration vs. Distance for the Fe-Ni-Al diffusion couple β_5 vs. β_9; x_0 denotes the Matano plane location. Calculated interdiffusion coefficients are plugged into error function solutions and compared with the original experimental data.

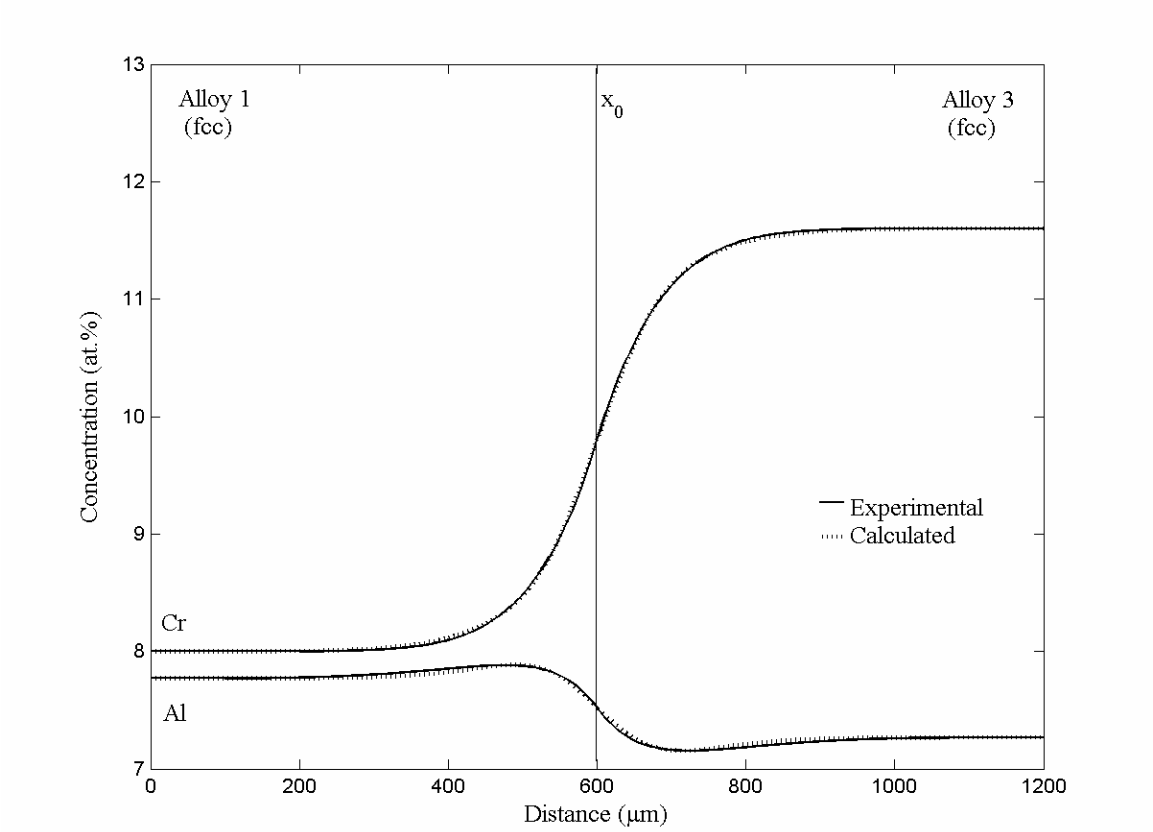

Figure 12. Concentration vs. Distance for the Ni-Cr-Al diffusion couple 1 vs. 3; x_0 denotes the Matano plane location. Calculated interdiffusion coefficients are plugged into error function solutions and compared with the original experimental data.

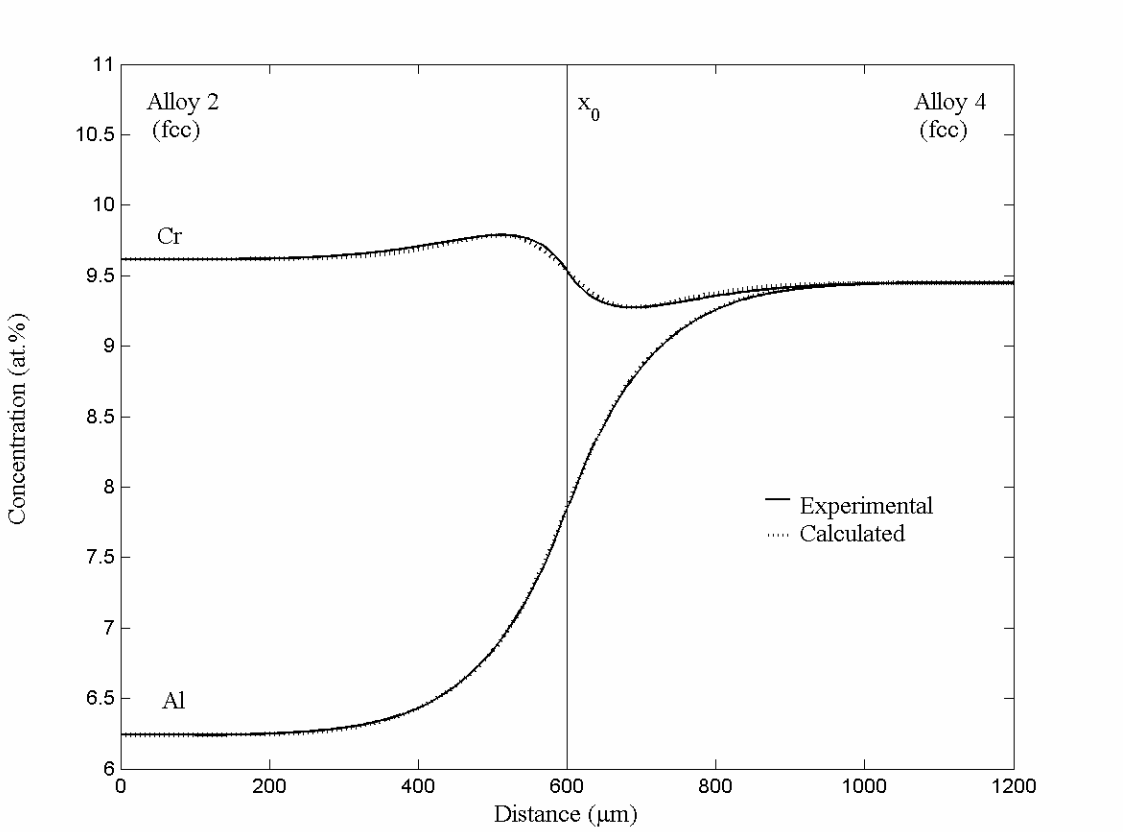

Figure 13. Concentration vs. Distance for the Ni-Cr-Al diffusion couple 2 vs. 4; x_0 denotes the Matano plane location. Calculated interdiffusion coefficients are plugged into error function solutions and compared with the original experimental data.

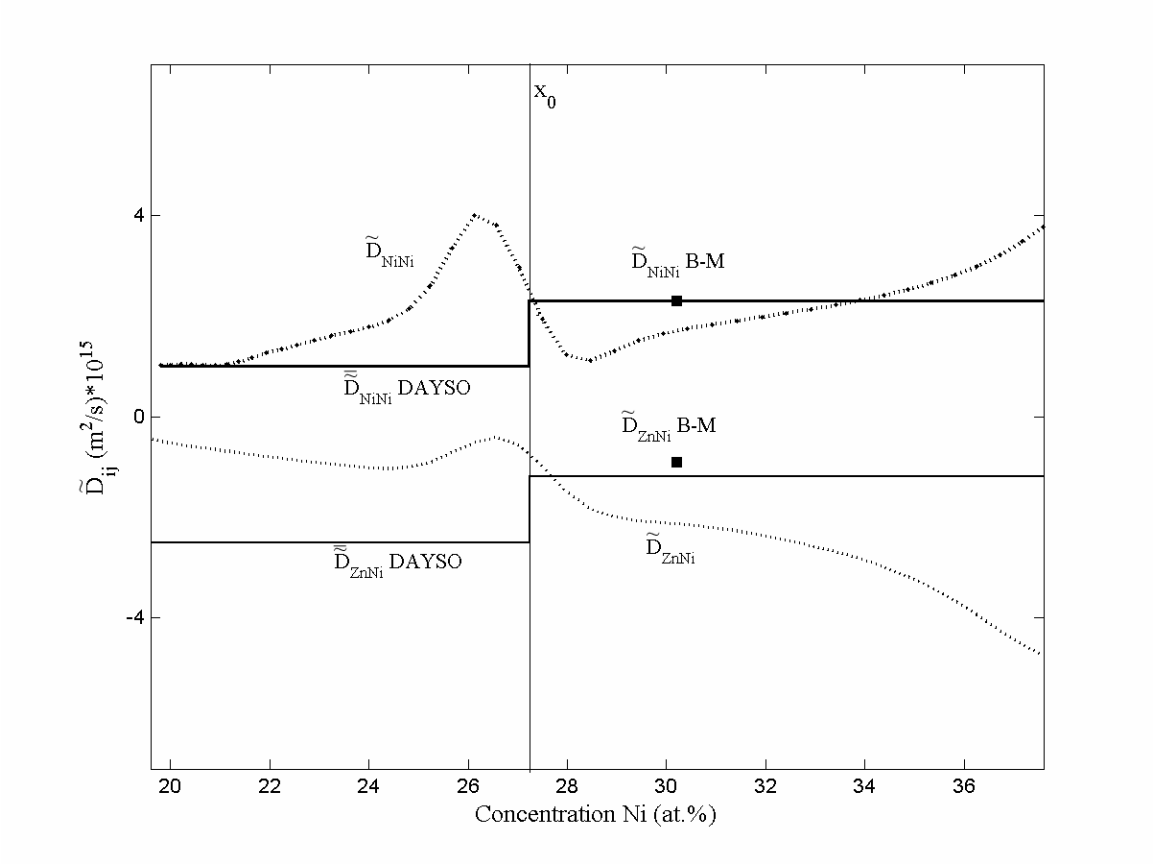

Figure 14. $\widetilde{D}_{NiNi}$ and $\widetilde{D}_{ZnNi}$ vs. Ni Concentration for the Cu-Ni-Zn diffusion couple α_5 vs. α_{12}. The interdiffusion coefficients from the new technique are compared with those reported by Dayananda and Sohn[4] and with Boltzmann-Matano analysis results.[34]

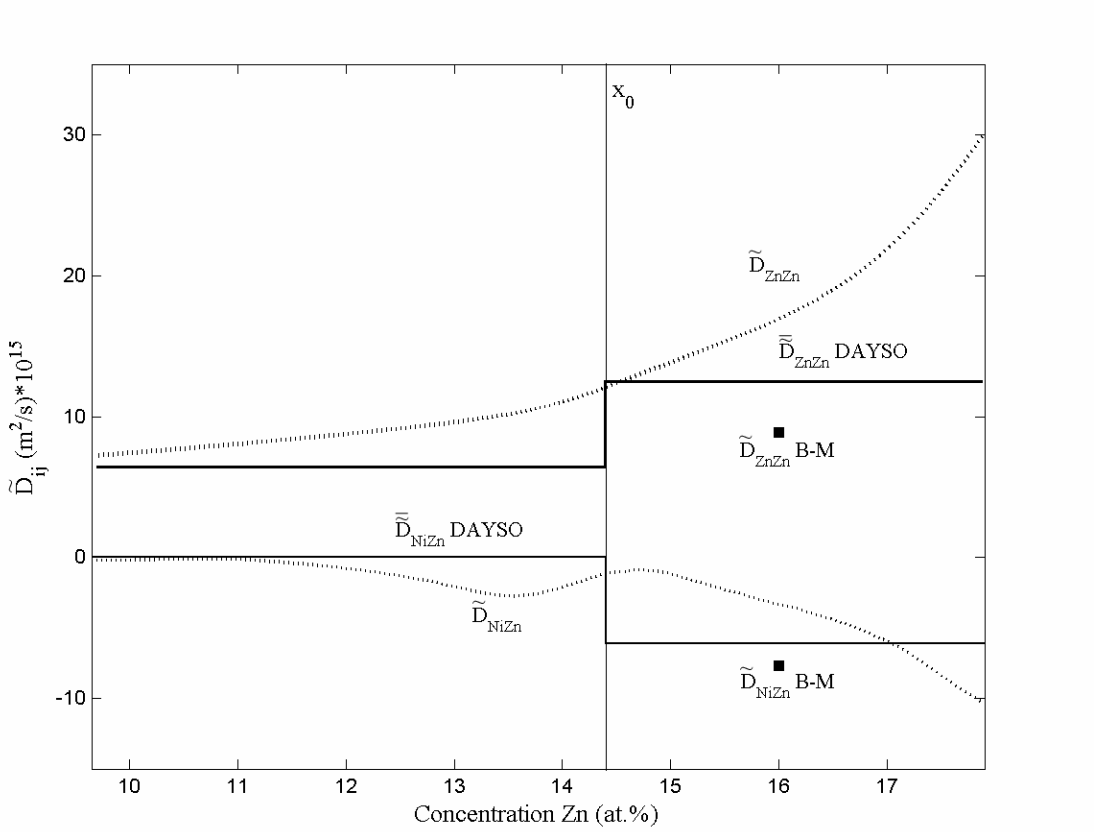

Figure 15. $\widetilde{D}_{NiZn}$ and $\widetilde{D}_{ZnZn}$ vs. Zn Concentration for the Cu-Ni-Zn diffusion couple α_5 vs. α_{12}. The interdiffusion coefficients from the new technique are compared with those reported by Dayananda and Sohn[4] and with Boltzmann-Matano analysis results.[34]

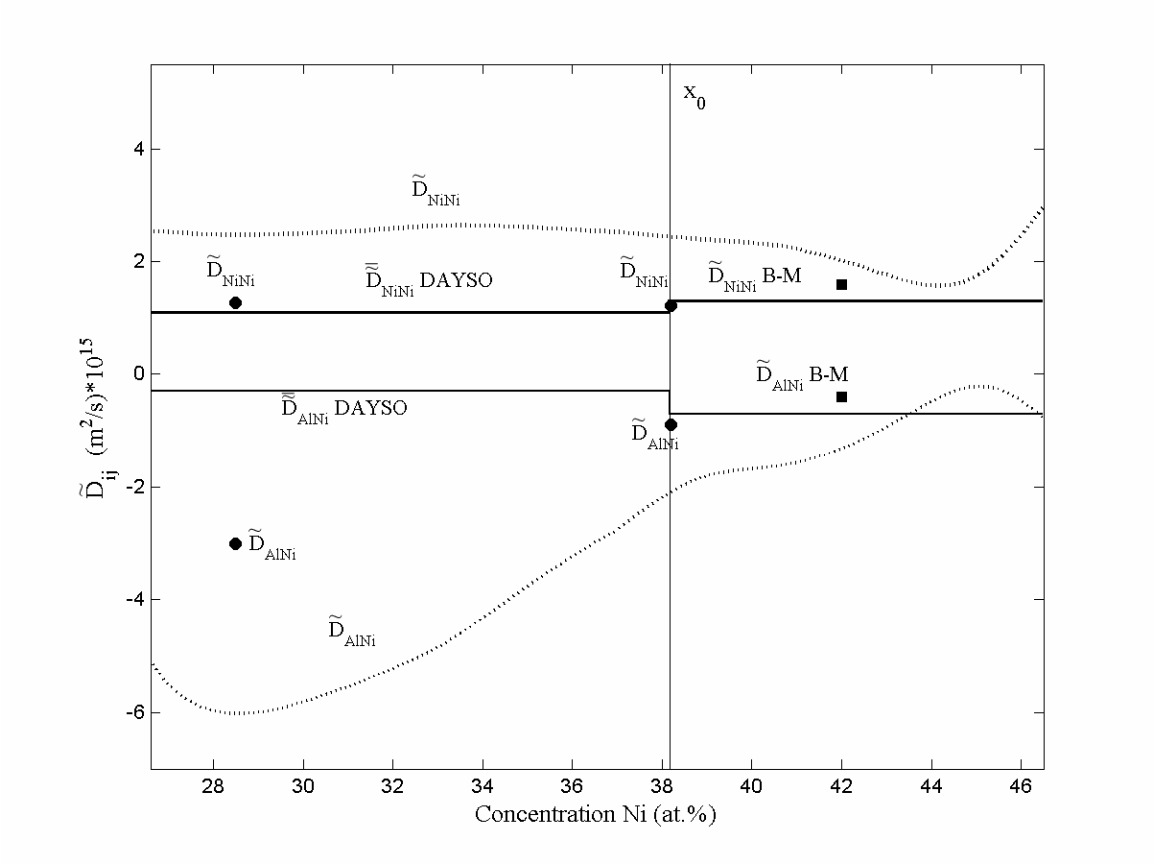

Figure 16. $\tilde{D}_{\mathrm{NiNi}}$ and $\tilde{D}_{\mathrm{AlNi}}$ vs. Ni Concentration for the Fe-Ni-Al diffusion couple β_5 vs. β_9. The interdiffusion coefficients from the new technique are compared with those reported by Dayananda and Sohn[4] and with Boltzmann-Matano analysis results.[34] The points illustrate the interdiffusion coefficients calculated where the Al concentration gradient is zero and the Ni is not.

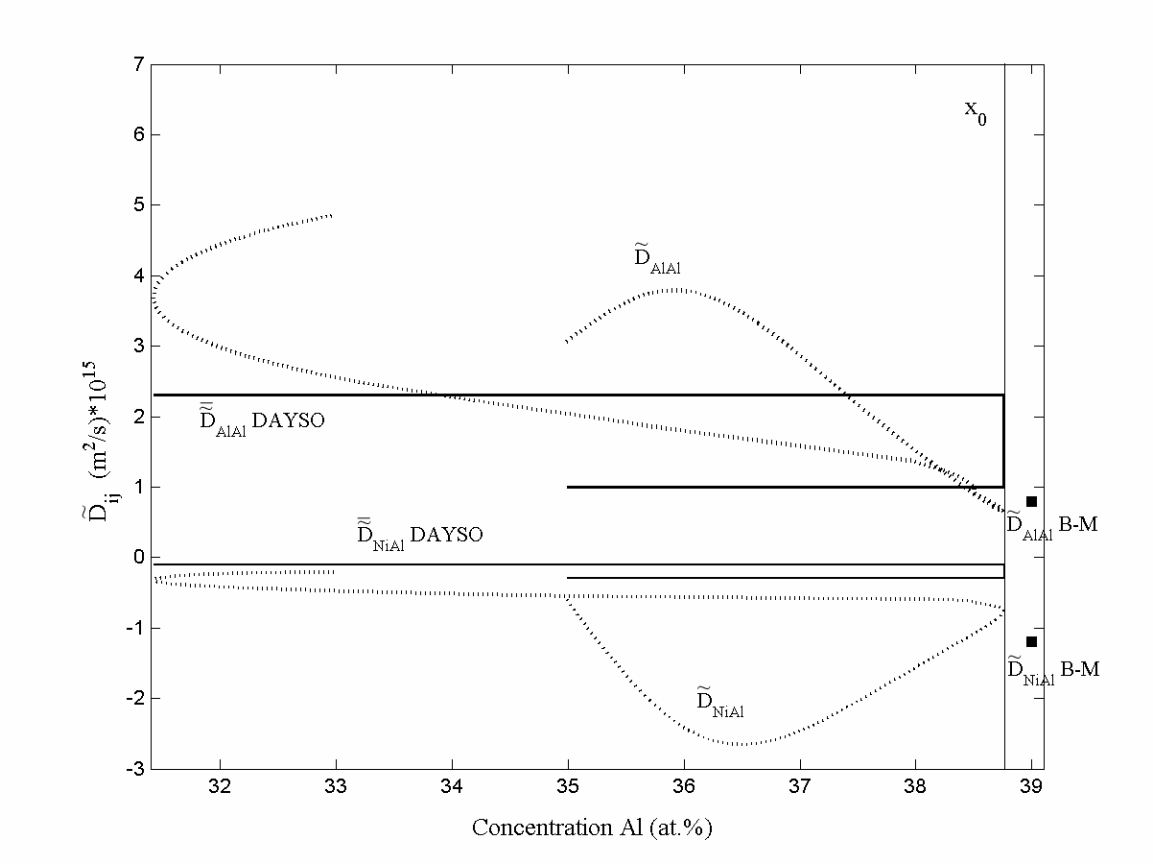

Figure 17. $\widetilde{D}_{NiAl}$ and $\widetilde{D}_{AlAl}$ vs. Al Concentration for the Fe-Ni-Al diffusion couple β_5 vs. β_9. The interdiffusion coefficients from the new technique are compared with those reported by Dayananda and Sohn[4] and with Boltzmann-Matano analysis results.[34]

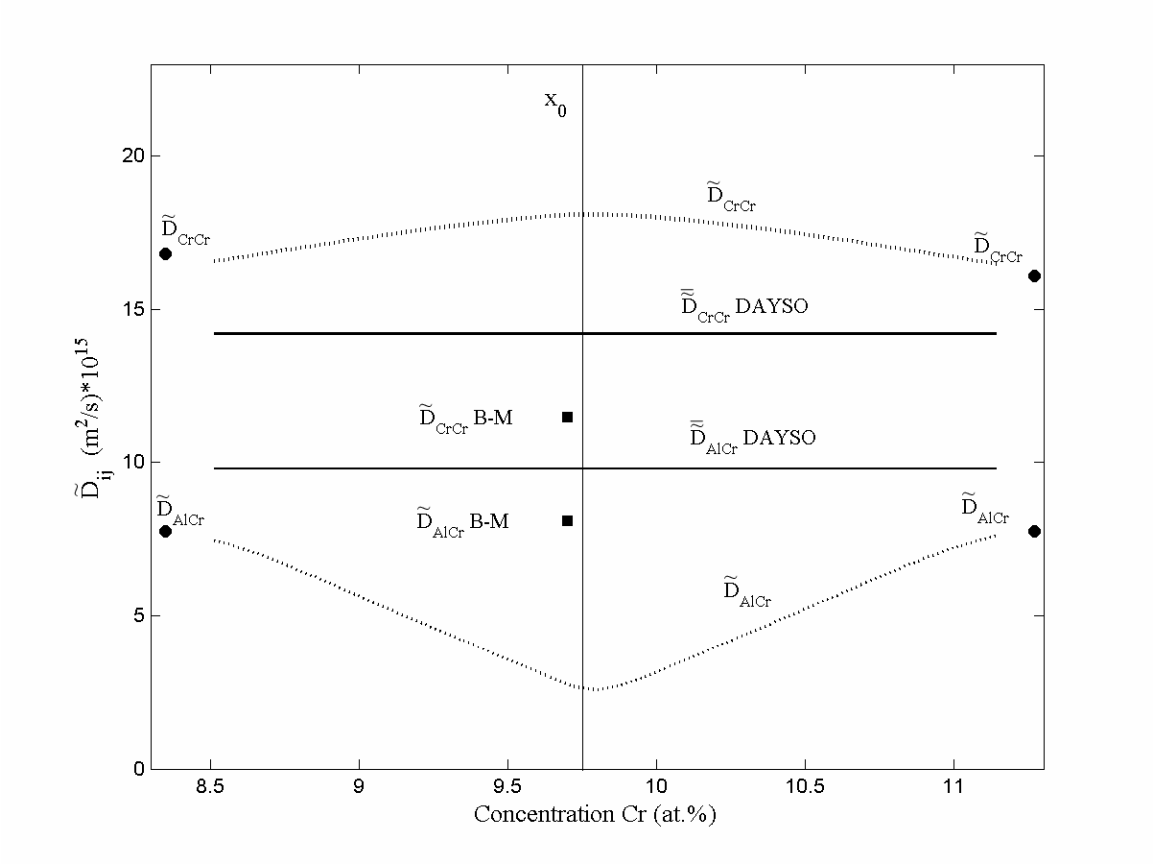

Figure 18. $\widetilde{D}_{CrCr}$ and $\widetilde{D}_{AlCr}$ vs. Cr Concentration for the Ni-Cr-Al diffusion couple 1vs.3. The interdiffusion coefficients from the new technique are compared with those reported by Dayananda and Sohn[4] and with Boltzmann-Matano analysis results. The points illustrate the interdiffusion coefficients calculated where the Al concentration gradient is zero and the Cr is not.

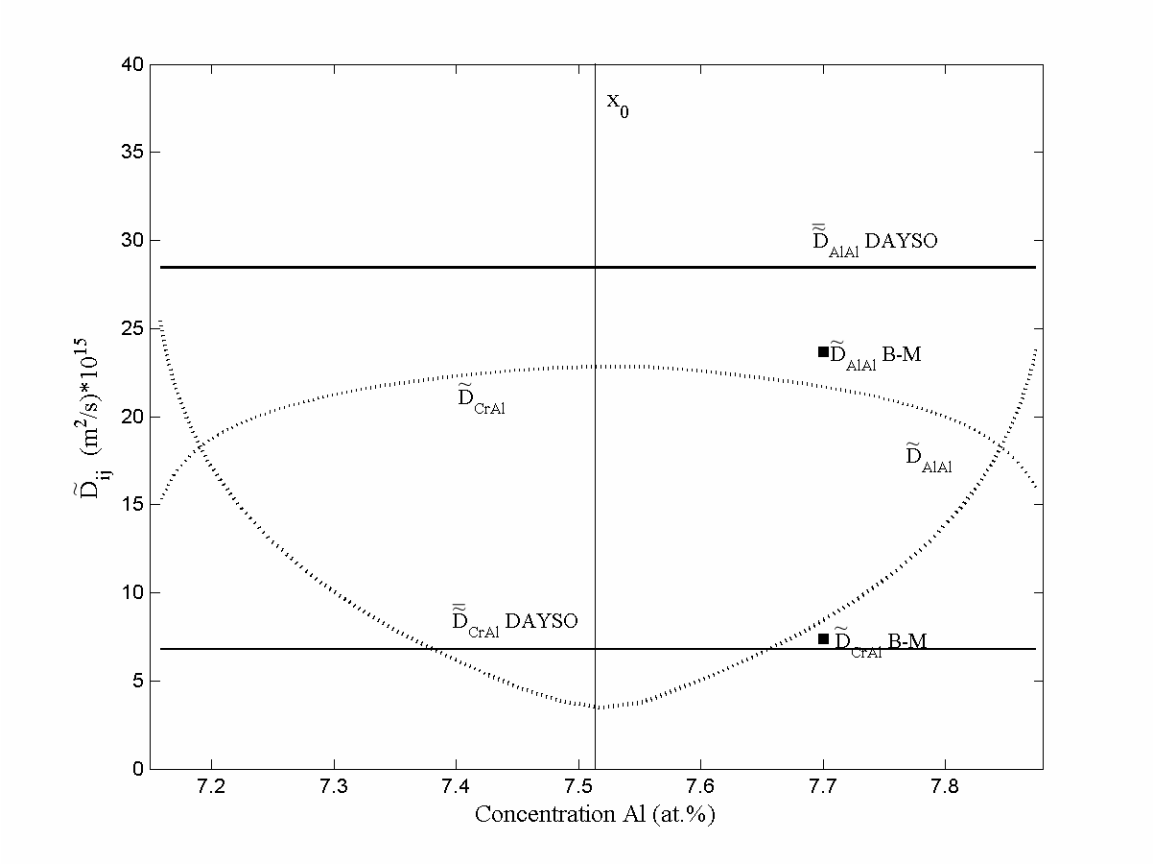

Figure 19. $\tilde{D}_{CrAl}$ and $\tilde{D}_{AlAl}$ vs. Al Concentration for the Ni-Cr-Al diffusion couple 1vs.3. The interdiffusion coefficients from the new technique are compared with those reported by Dayananda and Sohn[4] and with Boltzmann-Matano analysis results.

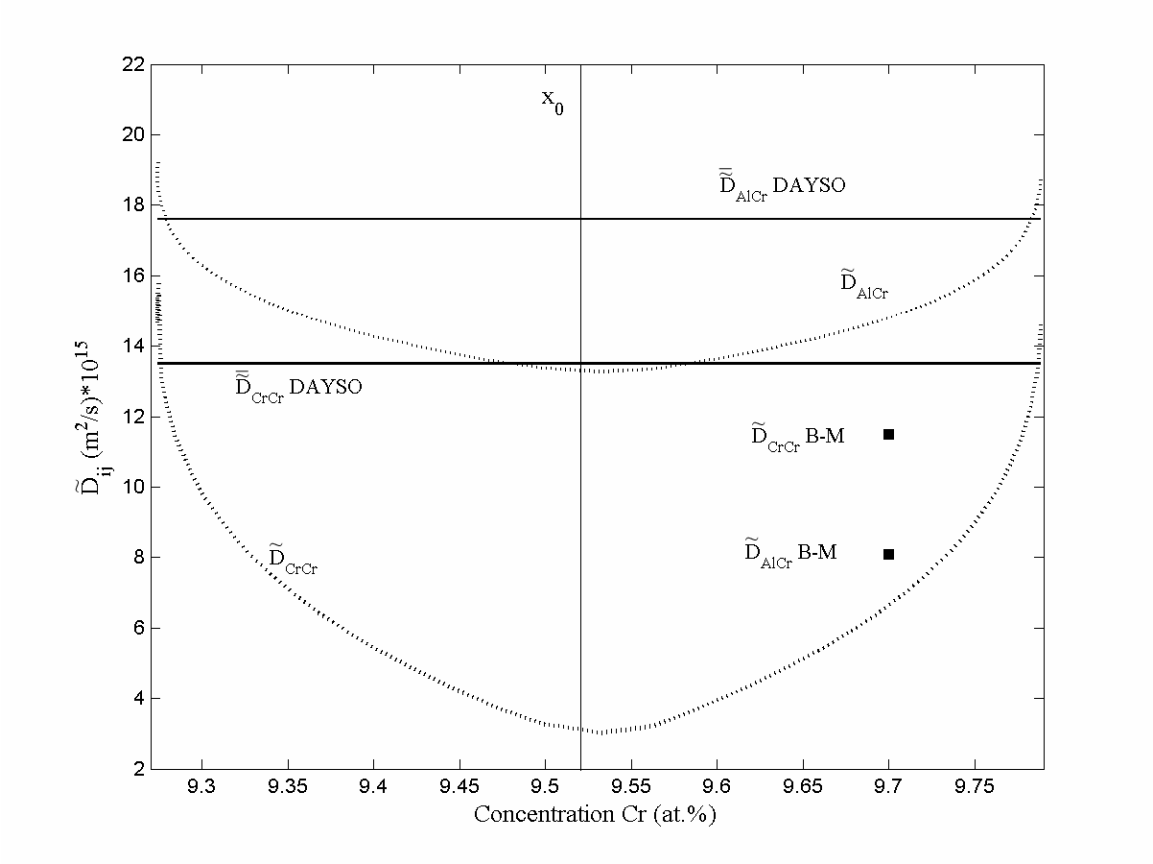

Figure 20. $\tilde{D}_{CrCr}$ and $\tilde{D}_{AlCr}$ vs. Cr Concentration for the Ni-Cr-Al diffusion couple 2vs.4. The interdiffusion coefficients from the new technique are compared with those reported by Dayananda and Sohn[4] and with Boltzmann-Matano analysis results.

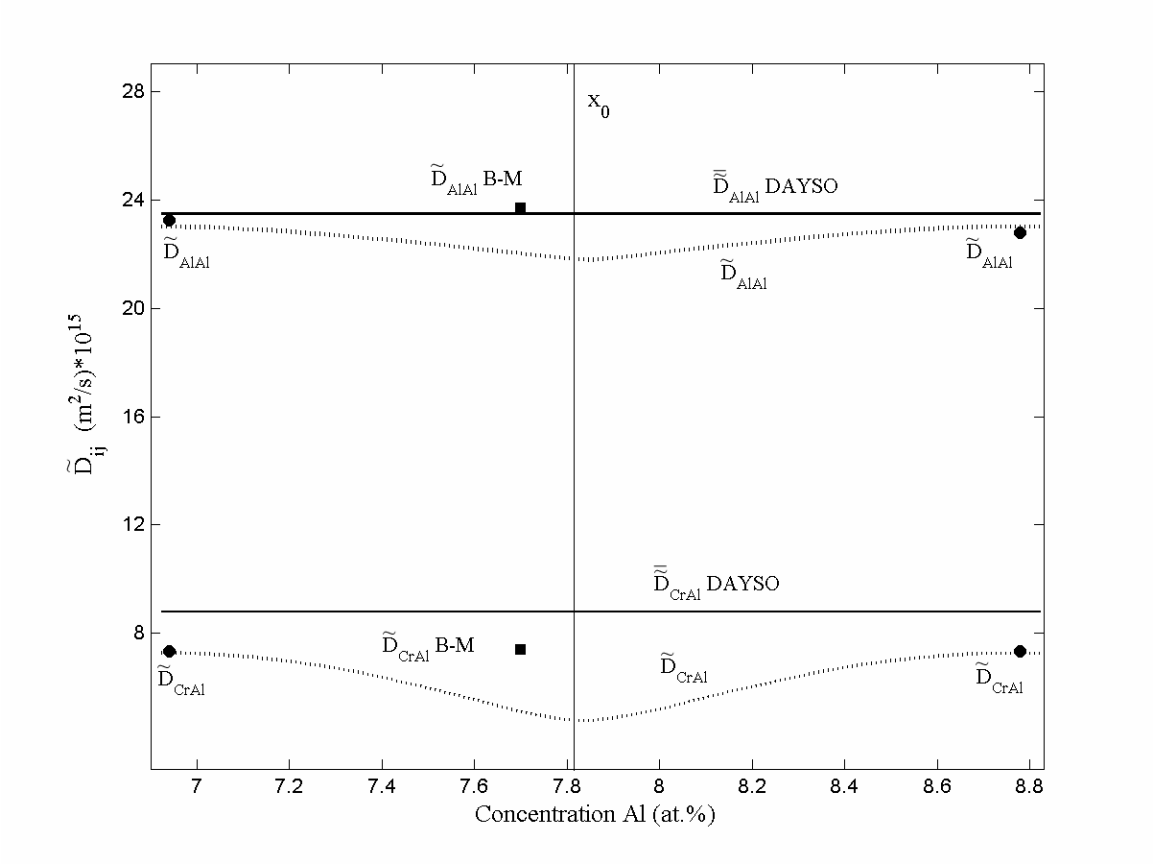

Figure 21. $\widetilde{D}_{CrAl}$ and $\widetilde{D}_{AlAl}$ vs. Al Concentration for the Ni-Cr-Al diffusion couple 2 vs.4. The interdiffusion coefficients from the new technique are compared with those reported by Dayananda and Sohn[4] and with Boltzmann-Matano analysis results. The points illustrate the interdiffusion coefficients calculated where the Cr concentration gradient is zero and the Al is not.

Table 3. Average interdiffusion coefficients for the DAYSO method and the for the new technique for couples α_5 vs. α_{12}, β_5 vs. β_9, Alloy 1 vs. Alloy 3, and Alloy 2 vs. Alloy 4.

Couple	**From C^- to C^0** $\overline{\tilde{D}}_{ij}\left(\times 10^{15}\,\mathrm{m}^2/\mathrm{sec}\right)$		**From C^0 to C^+**	
	New Technique	**DAYSO**	**New Technique**	**DAYSO**
α_5 vs. α_{12}	$\overline{\tilde{D}}^{Cu}_{NiNi} = 2.22$ $\overline{\tilde{D}}^{Cu}_{NiZn} = -4.90$ $\overline{\tilde{D}}^{Cu}_{ZnNi} = -2.78$ $\overline{\tilde{D}}^{Cu}_{ZnZn} = 19.6$	$\overline{\tilde{D}}^{Cu}_{NiNi} = 2.3$ $\overline{\tilde{D}}^{Cu}_{NiZn} = -6.1$ $\overline{\tilde{D}}^{Cu}_{ZnNi} = -1.2$ $\overline{\tilde{D}}^{Cu}_{ZnZn} = 12.5$	$\overline{\tilde{D}}^{Cu}_{NiNi} = 1.78$ $\overline{\tilde{D}}^{Cu}_{NiZn} = -1.66$ $\overline{\tilde{D}}^{Cu}_{ZnNi} = -0.83$ $\overline{\tilde{D}}^{Cu}_{ZnZn} = 9.07$	$\overline{\tilde{D}}^{Cu}_{NiNi} = 1.0$ $\overline{\tilde{D}}^{Cu}_{NiZn} = -0.01$ $\overline{\tilde{D}}^{Cu}_{ZnNi} = -2.5$ $\overline{\tilde{D}}^{Cu}_{ZnZn} = 6.4$
β_5 vs. β_9	$\overline{\tilde{D}}^{Fe}_{NiNi} = 2.07$ $\overline{\tilde{D}}^{Fe}_{NiAl} = -1.77$ $\overline{\tilde{D}}^{Fe}_{AlNi} = -0.92$ $\overline{\tilde{D}}^{Fe}_{AlAl} = 2.51$	$\overline{\tilde{D}}^{Fe}_{NiNi} = 1.3$ $\overline{\tilde{D}}^{Fe}_{NiAl} = -0.3$ $\overline{\tilde{D}}^{Fe}_{AlNi} = -0.7$ $\overline{\tilde{D}}^{Fe}_{AlAl} = 1.0$	$\overline{\tilde{D}}^{Fe}_{NiNi} = 2.53$ $\overline{\tilde{D}}^{Fe}_{NiAl} = -0.40$ $\overline{\tilde{D}}^{Fe}_{AlNi} = -5.05$ $\overline{\tilde{D}}^{Fe}_{AlAl} = 3.09$	$\overline{\tilde{D}}^{Fe}_{NiNi} = 1.1$ $\overline{\tilde{D}}^{Fe}_{NiAl} = -0.1$ $\overline{\tilde{D}}^{Fe}_{AlNi} = -0.3$ $\overline{\tilde{D}}^{Fe}_{AlAl} = 2.3$
Alloy 1 vs. Alloy 3	$\overline{\tilde{D}}^{Ni}_{CrCr} = 17.3$ $\overline{\tilde{D}}^{Cr}_{CrAl} = 19.9$ $\overline{\tilde{D}}^{Ni}_{AlCr} = 5.52$ $\overline{\tilde{D}}^{Ni}_{CrCr} = 13.6$	$\overline{\tilde{D}}^{Ni}_{CrCr} = 14.2$ $\overline{\tilde{D}}^{Cr}_{CrAl} = 6.8$ $\overline{\tilde{D}}^{Ni}_{AlCr} = 9.8$ $\overline{\tilde{D}}^{Ni}_{CrCr} = 28.5$	$\overline{\tilde{D}}^{Ni}_{CrCr} = 17.2$ $\overline{\tilde{D}}^{Cr}_{CrAl} = 19.2$ $\overline{\tilde{D}}^{Ni}_{AlCr} = 5.91$ $\overline{\tilde{D}}^{Ni}_{CrCr} = 15.3$	$\overline{\tilde{D}}^{Ni}_{CrCr} = 14.2$ $\overline{\tilde{D}}^{Cr}_{CrAl} = 6.8$ $\overline{\tilde{D}}^{Ni}_{AlCr} = 9.8$ $\overline{\tilde{D}}^{Ni}_{CrCr} = 28.5$
Alloy 2 vs. Alloy 4	$\overline{\tilde{D}}^{Ni}_{CrCr} = 10.3$ $\overline{\tilde{D}}^{Cr}_{CrAl} = 6.64$ $\overline{\tilde{D}}^{Ni}_{AlCr} = 16.6$ $\overline{\tilde{D}}^{Ni}_{CrCr} = 22.7$	$\overline{\tilde{D}}^{Ni}_{CrCr} = 13.5$ $\overline{\tilde{D}}^{Cr}_{CrAl} = 8.8$ $\overline{\tilde{D}}^{Ni}_{AlCr} = 17.6$ $\overline{\tilde{D}}^{Ni}_{CrCr} = 23.5$	$\overline{\tilde{D}}^{Ni}_{CrCr} = 10.1$ $\overline{\tilde{D}}^{Cr}_{CrAl} = 6.71$ $\overline{\tilde{D}}^{Ni}_{AlCr} = 16.5$ $\overline{\tilde{D}}^{Ni}_{CrCr} = 22.7$	$\overline{\tilde{D}}^{Ni}_{CrCr} = 13.5$ $\overline{\tilde{D}}^{Cr}_{CrAl} = 8.8$ $\overline{\tilde{D}}^{Ni}_{AlCr} = 17.6$ $\overline{\tilde{D}}^{Ni}_{CrCr} = 23.5$

In order to verify the consistency of the method outlined in this paper, selected interdiffusion coefficients were plugged into error function solutions to generate concentration profiles for a hypothetical A-B-C ternary couple whose interdiffusion coefficients were known. The profiles generated are shown in Figure 22. The error function solutions used to generate these profiles were Equations 6 and 7 and the interdiffusion coefficients were chosen so that they vary from

one side of the Matano plane to the other. The interdiffusion coefficients for the left-hand side of the Matano plane are $\overline{\widetilde{D}}_{AA}^{C} = 32 \times 10^{-15}\,\mathrm{m}^2/\mathrm{s}$, $\overline{\widetilde{D}}_{AB}^{C} = 7 \times 10^{-15}\,\mathrm{m}^2/\mathrm{s}$, $\overline{\widetilde{D}}_{BA}^{C} = -4 \times 10^{-15}\,\mathrm{m}^2/\mathrm{s}$, and $\overline{\widetilde{D}}_{BB}^{C} = 19 \times 10^{-15}\,\mathrm{m}^2/\mathrm{s}$. The interdiffusion coefficients for the right-hand side of the Matano plane are $\overline{\widetilde{D}}_{AA}^{C} = 15 \times 10^{-15}\,\mathrm{m}^2/\mathrm{s}$, $\overline{\widetilde{D}}_{AB}^{C} = 9 \times 10^{-15}\,\mathrm{m}^2/\mathrm{s}$, $\overline{\widetilde{D}}_{BA}^{C} = -3 \times 10^{-15}\,\mathrm{m}^2/\mathrm{s}$, and $\overline{\widetilde{D}}_{BB}^{C} = 28 \times 10^{-15}\,\mathrm{m}^2/\mathrm{s}$. Note that the left hand side of the Matano plane in Figure 22 corresponds to the right hand side of the Matano plane in Figure 24 because the concentration of B is decreasing. The new technique was then used on the generated profiles to back-calculate the interdiffusion coefficients and the results are shown in Figures 23 and 24. The figures reveal how the interdiffusion coefficient profiles tend to extreme towards the end of the profile where the concentration gradient becomes nominal. The calculated coefficients are in precise agreement with those originally plugged into the error function solutions (those labeled Actual in the figures), which attests to not only the consistency of the method but also the reliability of the calculations within the method. The interdiffusion coefficients originally plugged into the error functions were constant on either side of the Matano plane. The new technique accurately predicted the interdiffusion coefficients to be constant on either side of the Matano plane.

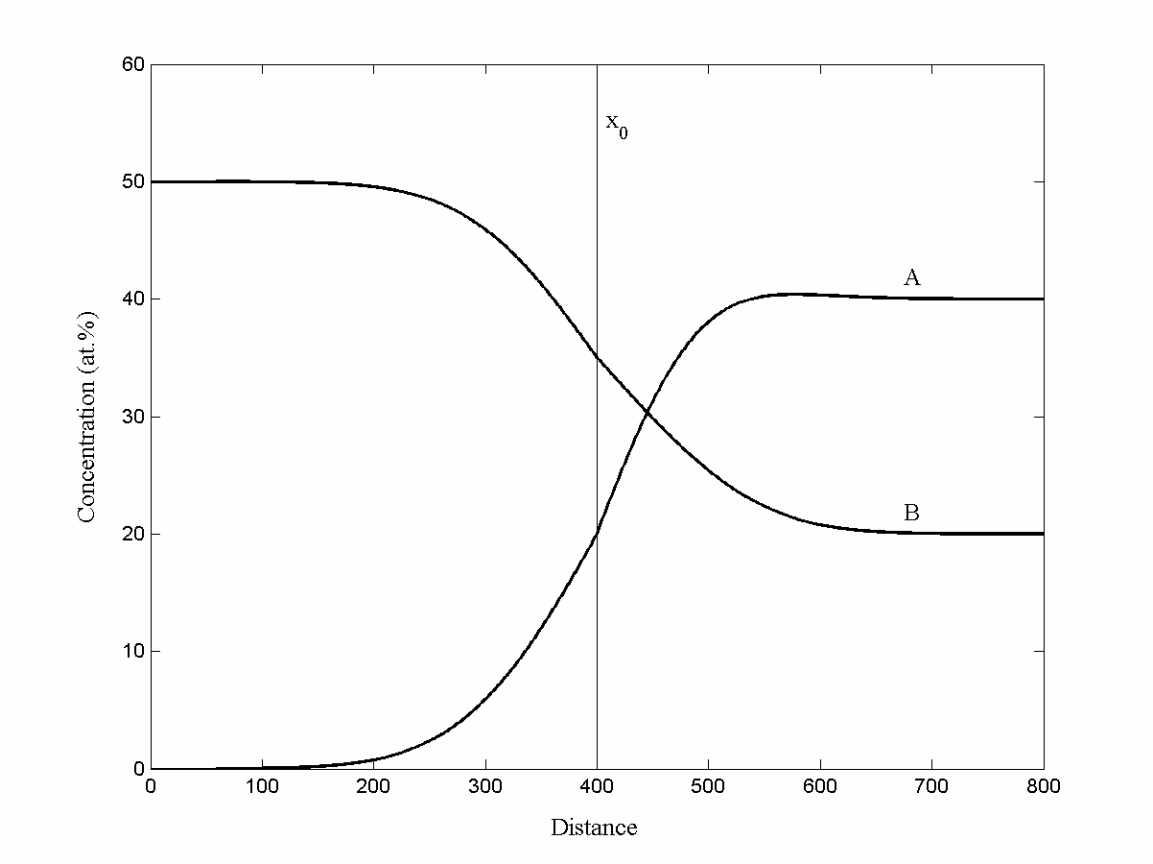

Figure 22. Concentration vs. Distance for a hypothetical A-B-C diffusion couple; x_0 denotes the Matano plane location.

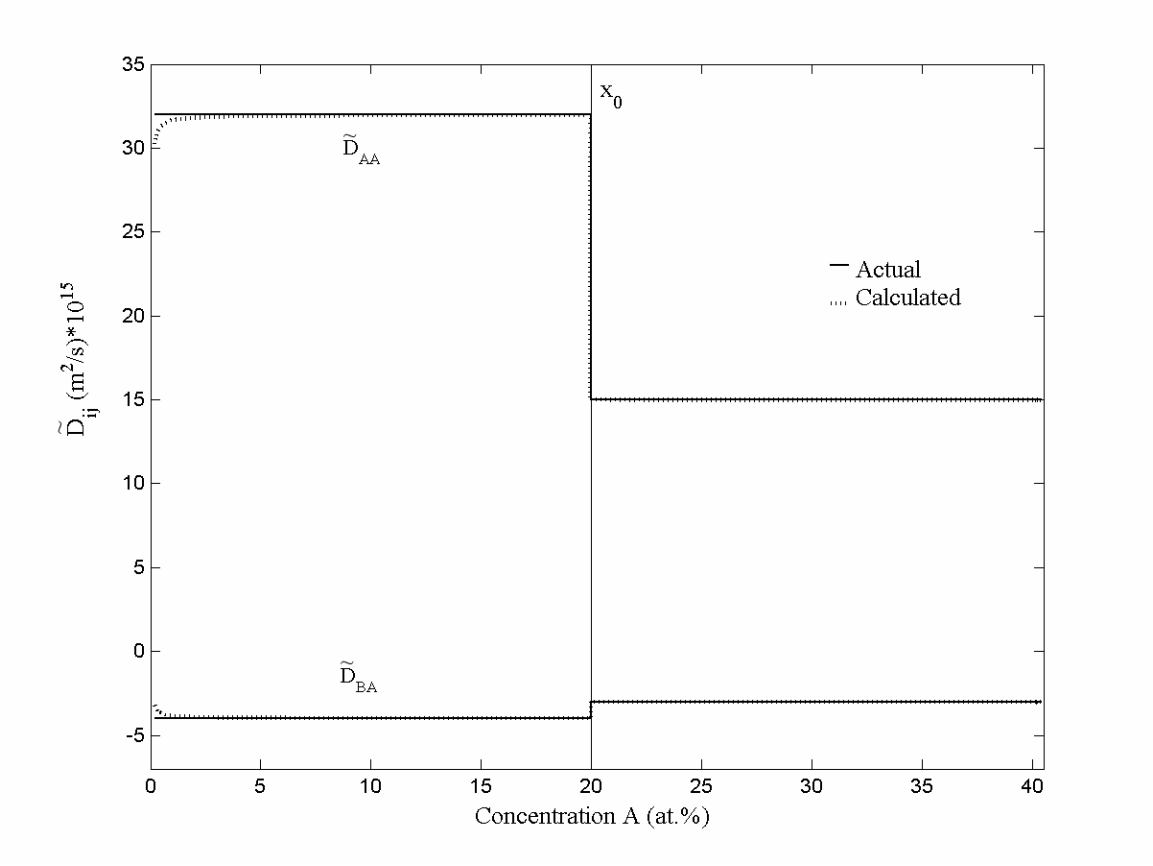

Figure 23. $\widetilde{D}_{AA}$ and $\widetilde{D}_{BA}$ vs. Concentration A for a hypothetical ternary diffusion couple. The values calculated from the new technique are observed to match the actual, initial input values.

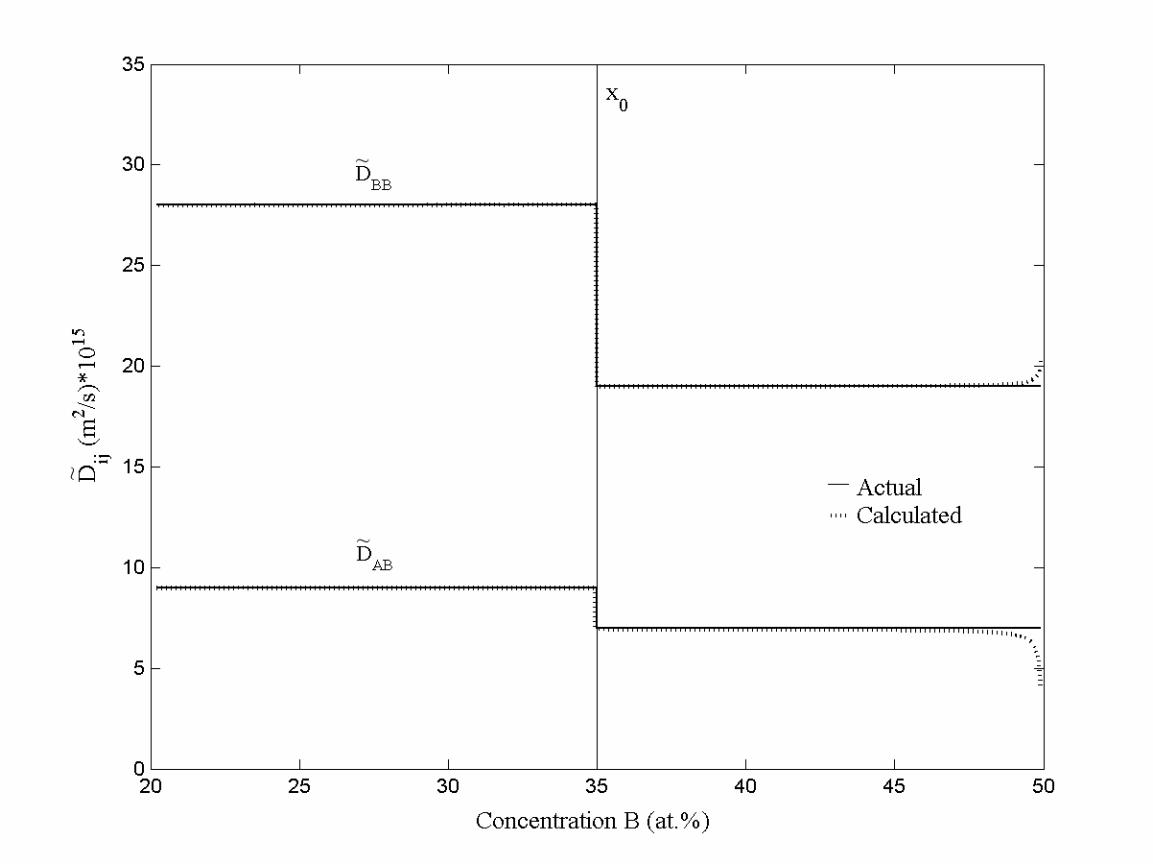

Figure 24. $\widetilde{D}_{AB}$ and $\widetilde{D}_{BB}$ vs. Concentration B for a hypothetical ternary diffusion couple. The values calculated from the new technique are observed to match the actual, initial input values.

6.2 Application of the New Technique to Previously Unexamined Ni-Pt-Al Couples

The prior section defends the validity of the new technique by applying it to diffusion couples whose previous analysis is quite exhaustive so that the new technique is fairly measured against the well-substantiated earlier findings. Now that the validity of the new technique is confirmed, it is applied to previously unexamined Ni-Pt-Al couples. The concentration data for these couples was given as raw microprobe data that was smoothed using Matlab; this smoothing process is crucial because it can lead to significant variations in the interdiffusion coefficients.

The new technique was applied to the smoothened profiles and the results are shown in Figures 25-33. There are no previously reported results on these couples; however, Boltzmann-Matano analysis can be used for comparison as shown in the Figures 30-33. Gleeson et. al[39] report two interdiffusion coefficients for this system at the composition 55.2Ni-2.3Pt-42.5Al at.%. Though this composition does not allow for a direct comparison with the results reported here, a generic comparison may be made. Gleeson reports $\widetilde{D}^{Ni}_{AlAl}$ = 17.3*10^{-10}cm^2/sec and $\widetilde{D}^{Ni}_{AlPt}$ =-3.0*10^{-10}cm^2/sec; that is, $\widetilde{D}^{Ni}_{AlAl}$ is quite large and the $\widetilde{D}^{Ni}_{AlPt}$ is negative. This is consistent with the findings in this study.

From Figures 28-29 and 31-33, the main interdiffusion coefficients $\widetilde{D}^{Ni}_{AlAl}$ and $\widetilde{D}^{Ni}_{PtPt}$ appear relatively constant. Figure 30 is the only exception to this rule, as $\widetilde{D}^{Ni}_{AlAl}$ shows significant variation from one side of the Matano plane to the other. The wavy interdiffusion coefficient profiles in Figures 32 and 33 are likely an anomaly of the spline curve fitting. The cross-coefficients $\widetilde{D}^{Ni}_{AlPt}$ and $\widetilde{D}^{Ni}_{PtAl}$ are shown to be negative. $\widetilde{D}^{Ni}_{AlPt}$ is very small for the couple 10 vs. 13, shown in Figure 29, yet it is quite large for couples 11 vs. 16 and 12 vs. 15 in Figures 31 and 33. The Pt composition range is almost the same for these couples but the Al content is much higher in the 10 vs. 3 couple than in the other two. This indicates that the effect of the Pt concentration gradient on the interdiffusion flux of Al becomes significant when the Al content falls below a certain range. This effect of Pt, because of the sign of the flux and the sign of the cross-coefficient, is an increasing contribution to Al, meaning it contributes an increase to the magnitude of the flux.

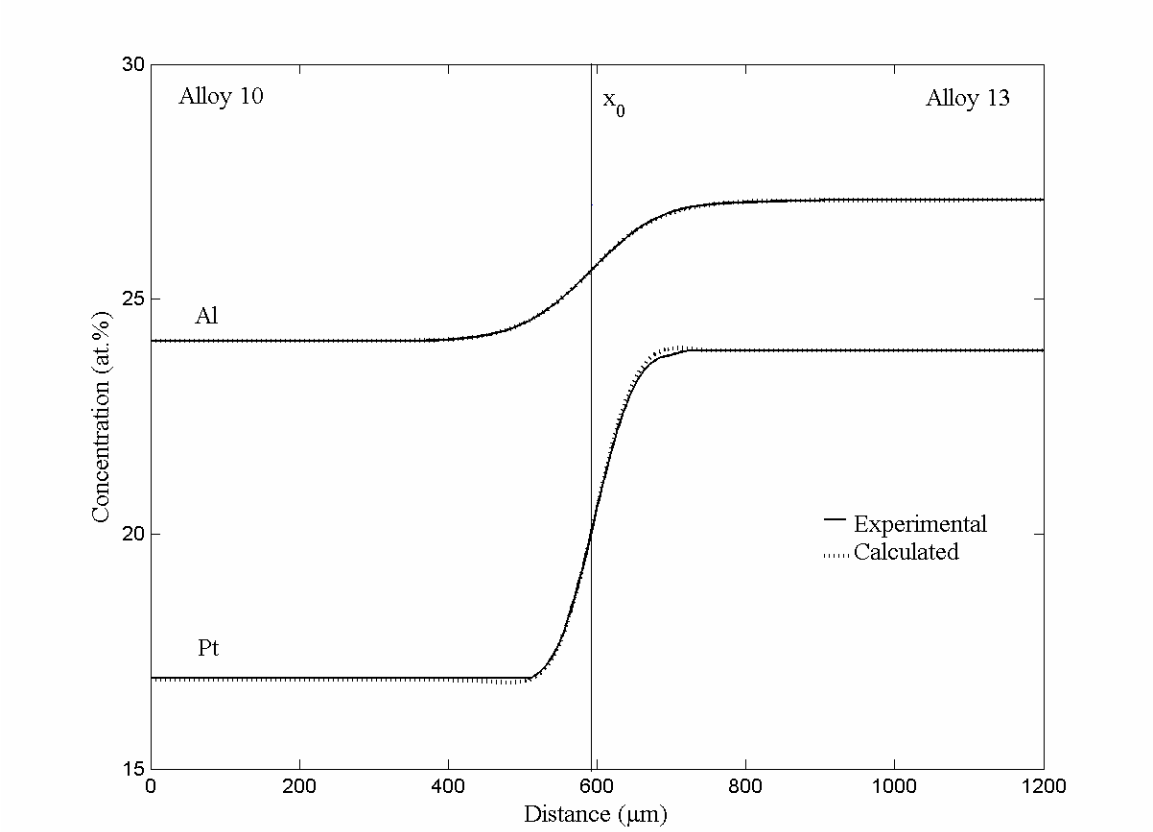

Figure 25. Concentration profiles of the diffusion couple Alloy 10 vs. Alloy 13. Calculated interdiffusion coefficients are plugged into error function solutions and compared with the original experimental data.

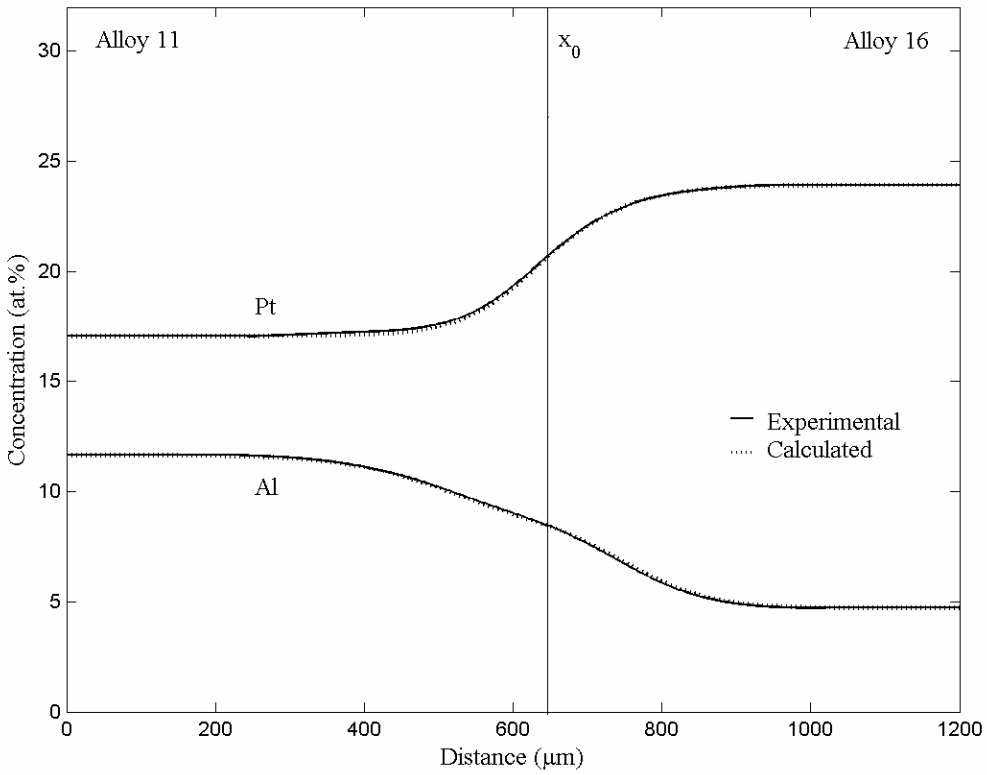

Figure 26. Concentration profiles of the diffusion couple Alloy 11 vs. Alloy 16. Calculated interdiffusion coefficients are plugged into error function solutions and compared with the original experimental data.

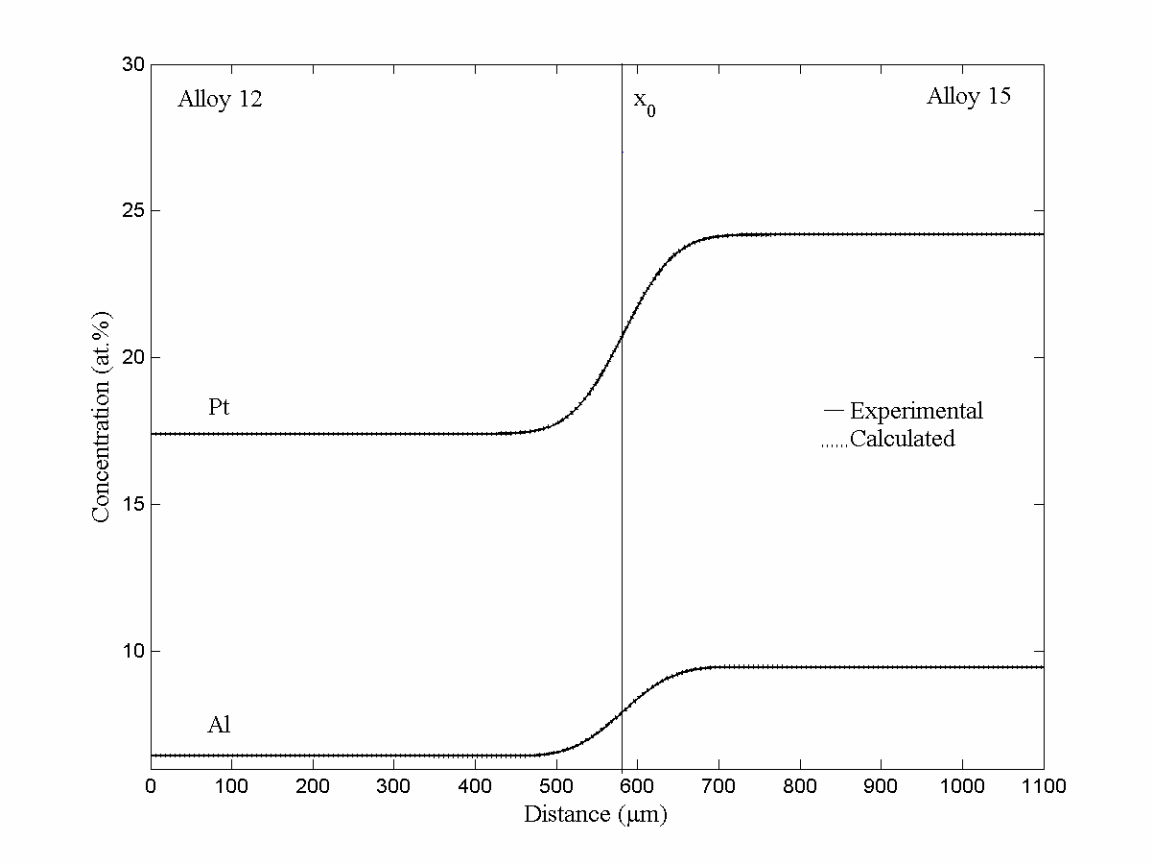

Figure 27. Concentration profiles of the diffusion couple Alloy 12 vs. Alloy 15. Calculated interdiffusion coefficients are plugged into error function solutions and compared with the original experimental data.

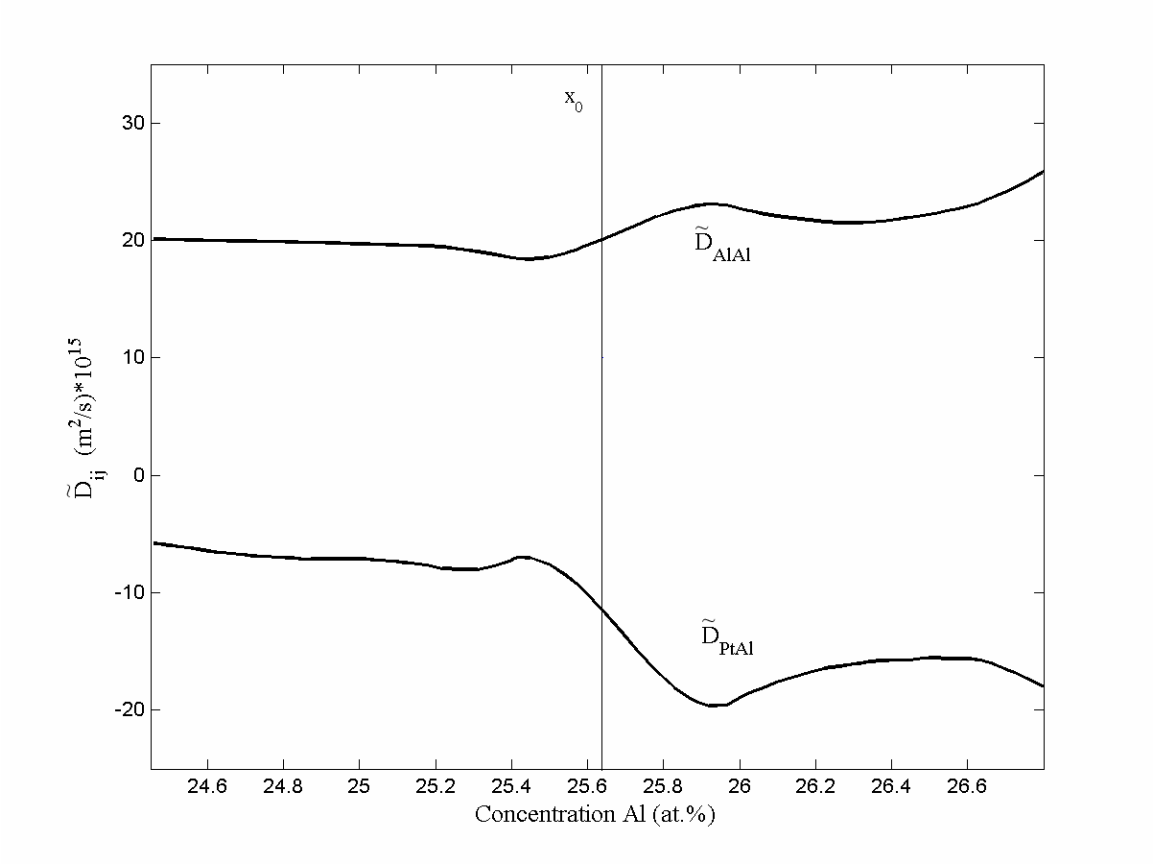

Figure 28. Interdiffusion coefficients $\widetilde{D}_{AlAl}$ and $\widetilde{D}_{PtAl}$ vs. Concentration Al for the couple Alloy 10 vs. Alloy 13.

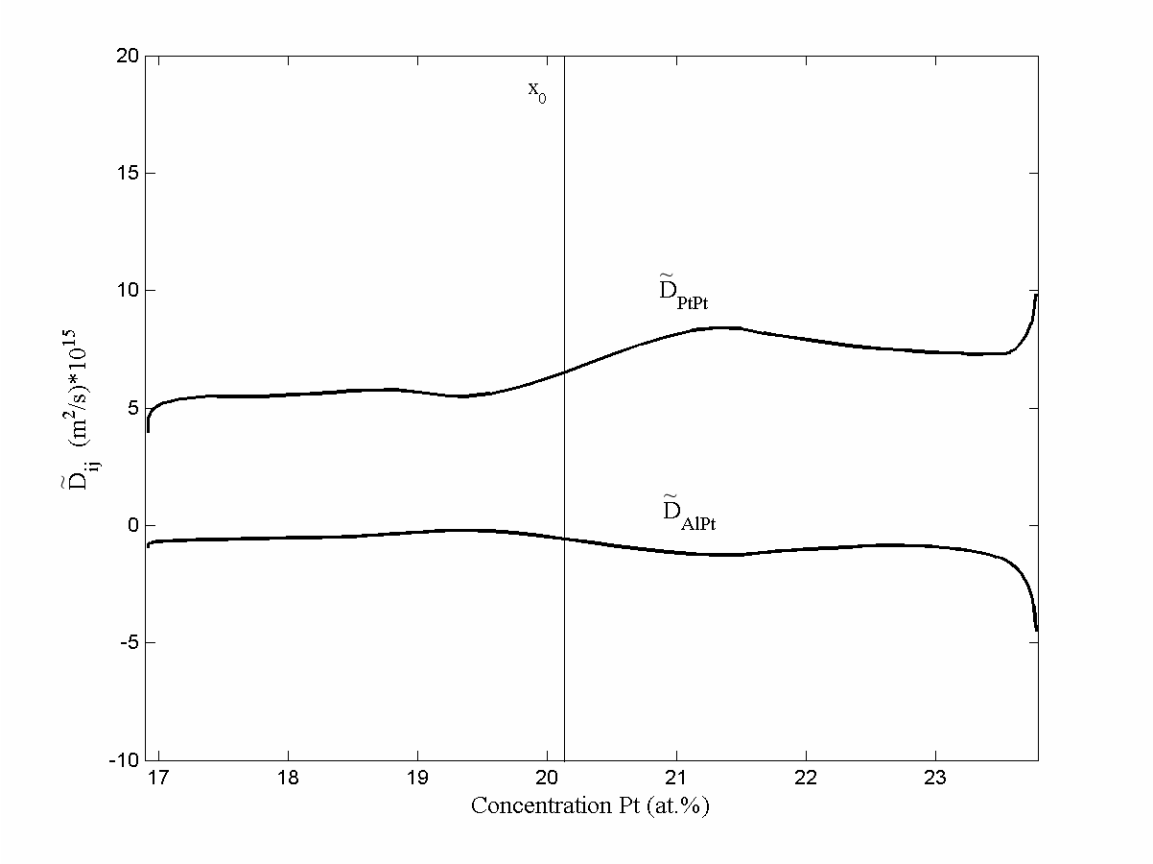

Figure 29. Interdiffusion coefficients $\widetilde{D}_{AlPt}$ and $\widetilde{D}_{PtPt}$ vs. Concentration Pt for the couple Alloy 10 vs. Alloy 13.

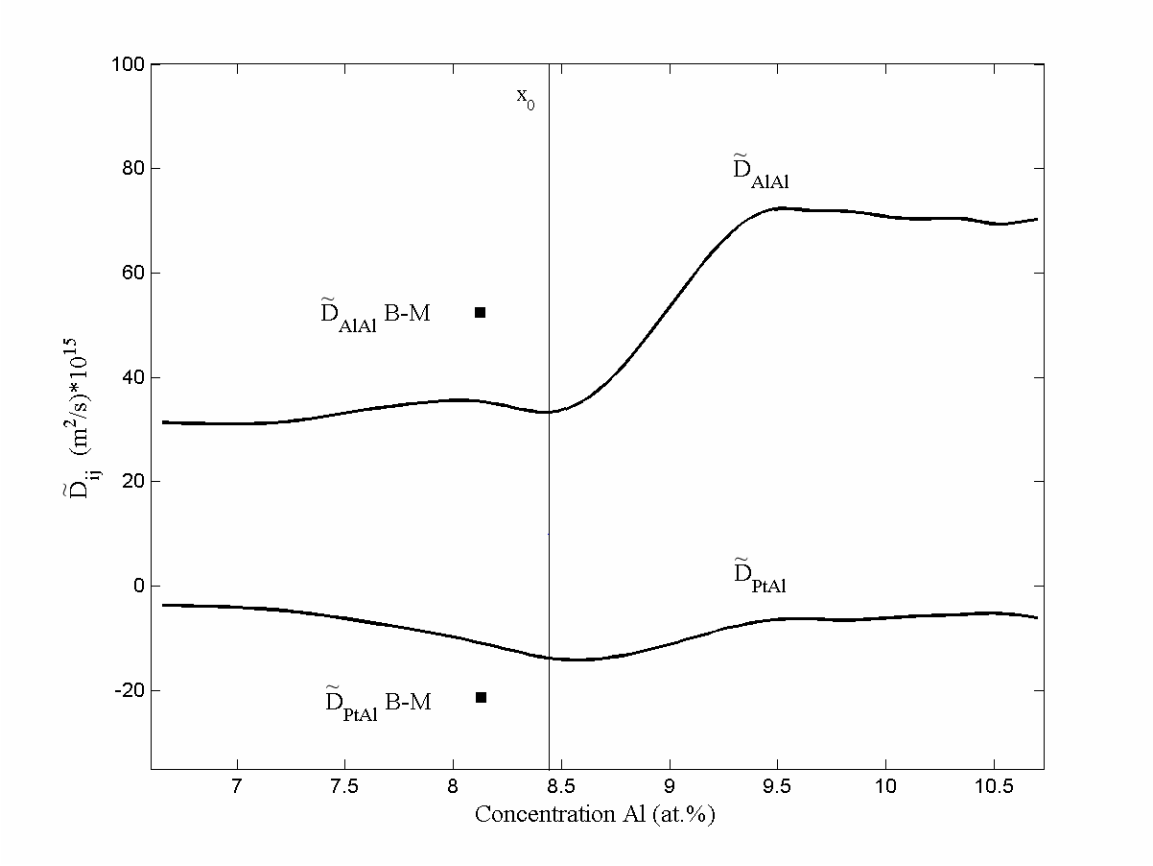

Figure 30. Interdiffusion coefficients $\widetilde{D}_{AlAl}$ and $\widetilde{D}_{PtAl}$ vs. Concentration Al for the couple Alloy 11 vs. Alloy 16.

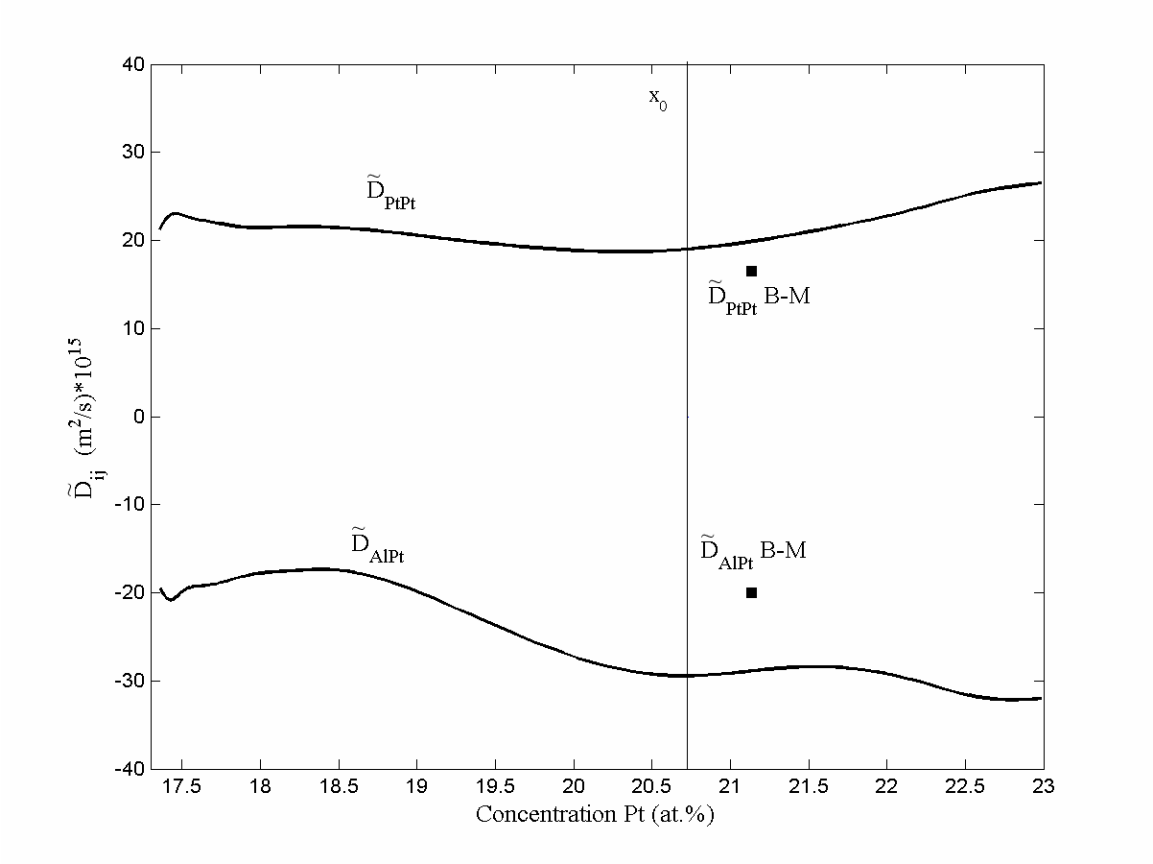

Figure 31. Interdiffusion coefficients $\widetilde{D}_{\mathrm{AlPt}}$ and $\widetilde{D}_{\mathrm{PtPt}}$ vs. Concentration Pt for the couple Alloy 11 vs. Alloy 16.

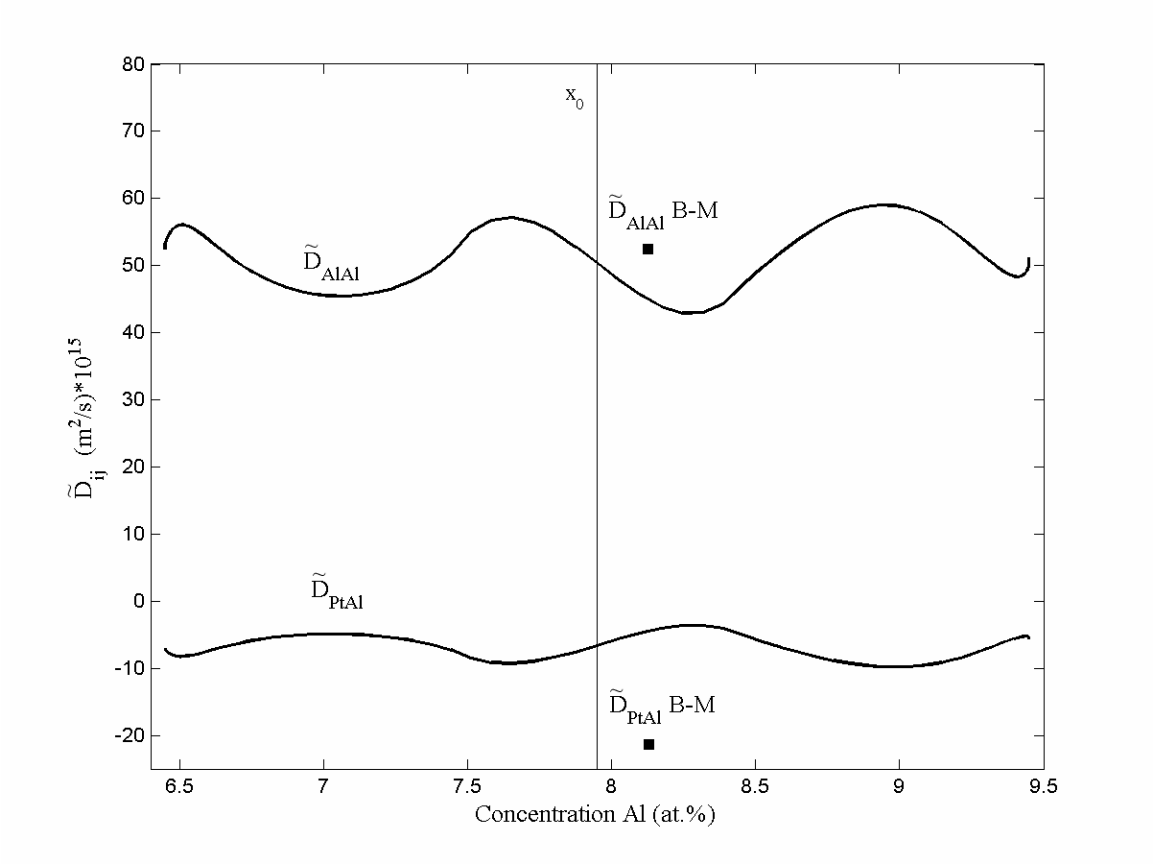

Figure 32. Interdiffusion coefficients $\widetilde{D}_{AlAl}$ and $\widetilde{D}_{PtAl}$ vs. Concentration Al for the couple Alloy 12 vs. Alloy 15.

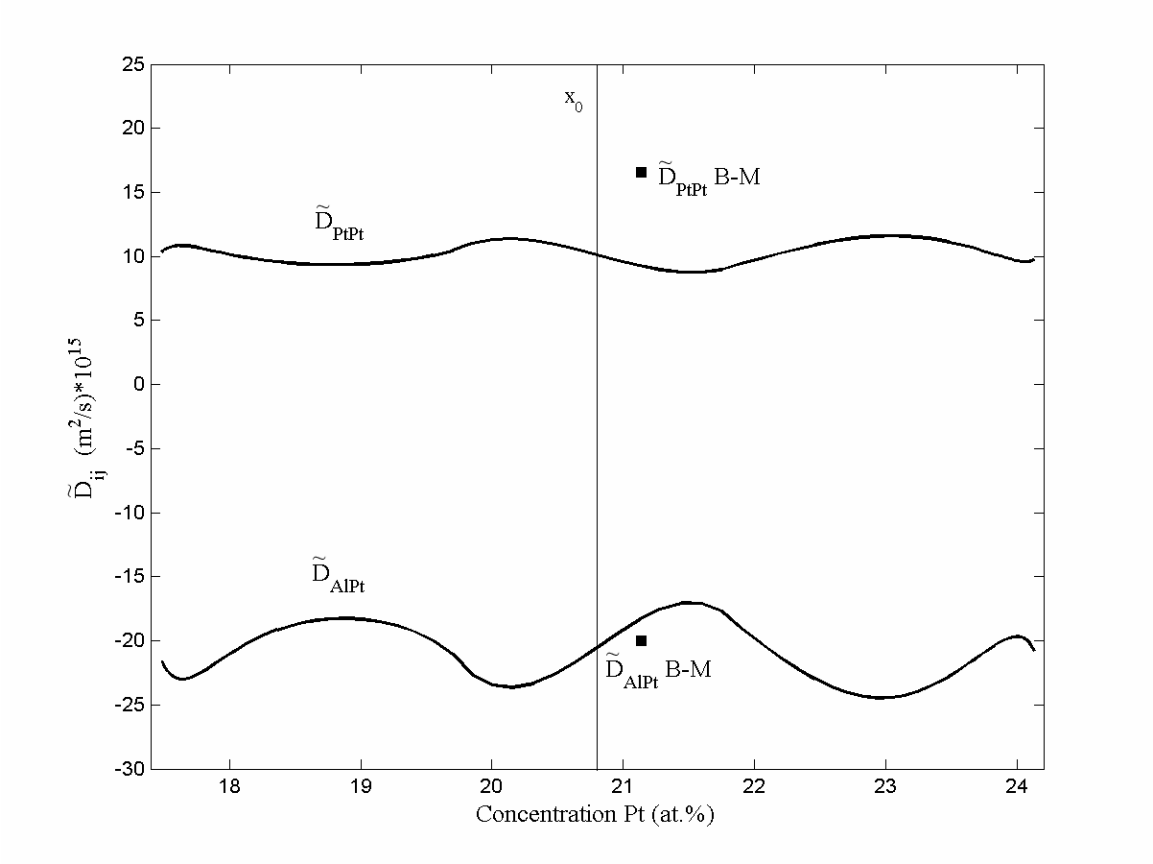

Figure 33. Interdiffusion coefficients $\tilde{D}_{AlPt}$ and $\tilde{D}_{PtPt}$ vs. Concentration Pt for the couple Alloy 12 vs. Alloy 15.

6.3 Experimental Evidence of a Category 2:1 Phase Boundary

The category 1:0 and 1:1 boundaries are commonly observed in binary and ternary systems. Cheng et al.[23] demonstrate planar and non-planar 1:0 boundaries for the Fe-Ni-Al system. Several micrographs of Cu-Ni-Zn couples with 1:0 and 1:1 boundaries are reported.[40,41] Here is presented experimental evidence of the unique category 2:1 boundary that exhibits three-phase equilibria, joining three phases at one boundary. Figure 34 displays micrographs of this boundary for the solid-to-solid diffusion couple in the Fe-Ni-Al system with two single-phase

terminal alloys. The concentration and interdiffusion flux data for this couple is given in Figures 35 and 36, respectively. The interdiffusion flux of Ni is shown to be much greater than that of Fe in the two-phase (β+β') region, but then in transitioning to the single-phase β region, the interdiffusion flux of Fe becomes higher than that of Ni. The diffusion path for this couple travels along the γ | γ+β phase boundary until it enters the vertex of the tie-triangle and then proceeds into the β+β' two-phase region as shown in Figure 37. That the diffusion path passes through the vertex of the tie-triangle to result in three-phase equilibria is rather surprising, and here is shown for the first time in Figures 34-37, experimental verification of this phenomenon.

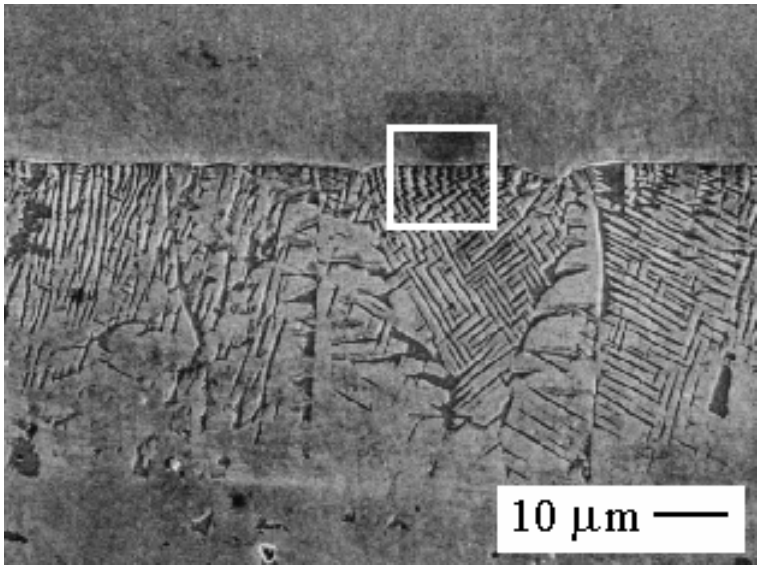

a.

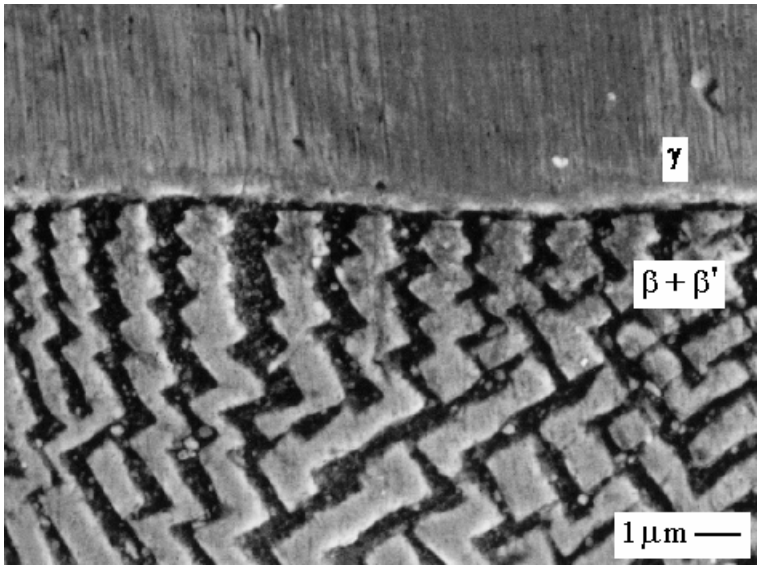

b.

Figure 34. a. Micrograph of the Fe-Ni-Al couple exhibiting a category 2:1 ternary phase boundary. b. Micrograph displaying the γ < > β+β' phase boundary as highlighted in a.

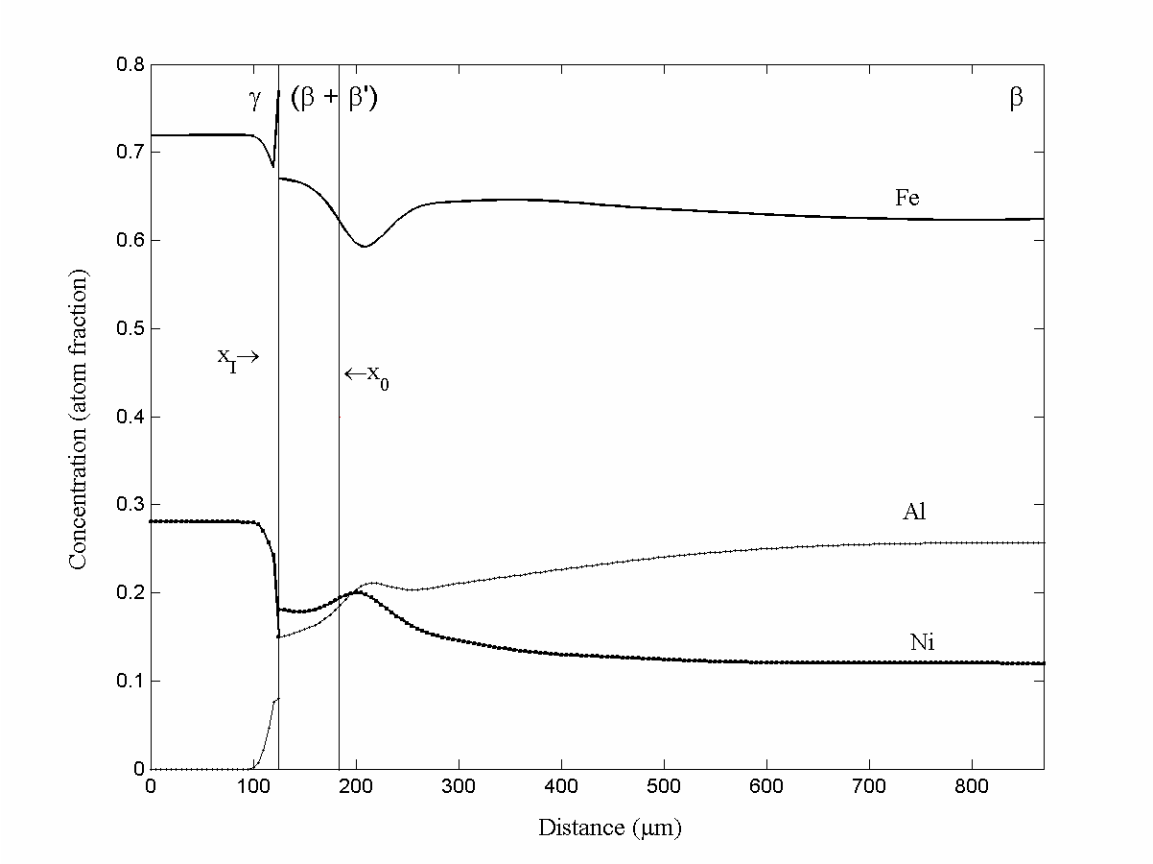

Figure 35. Concentration profiles for the Fe-Ni-Al couple exhibiting three-phase equilibria in a ternary system. x_I denotes the interphase boundary and x_0 denotes the Matano plane location.

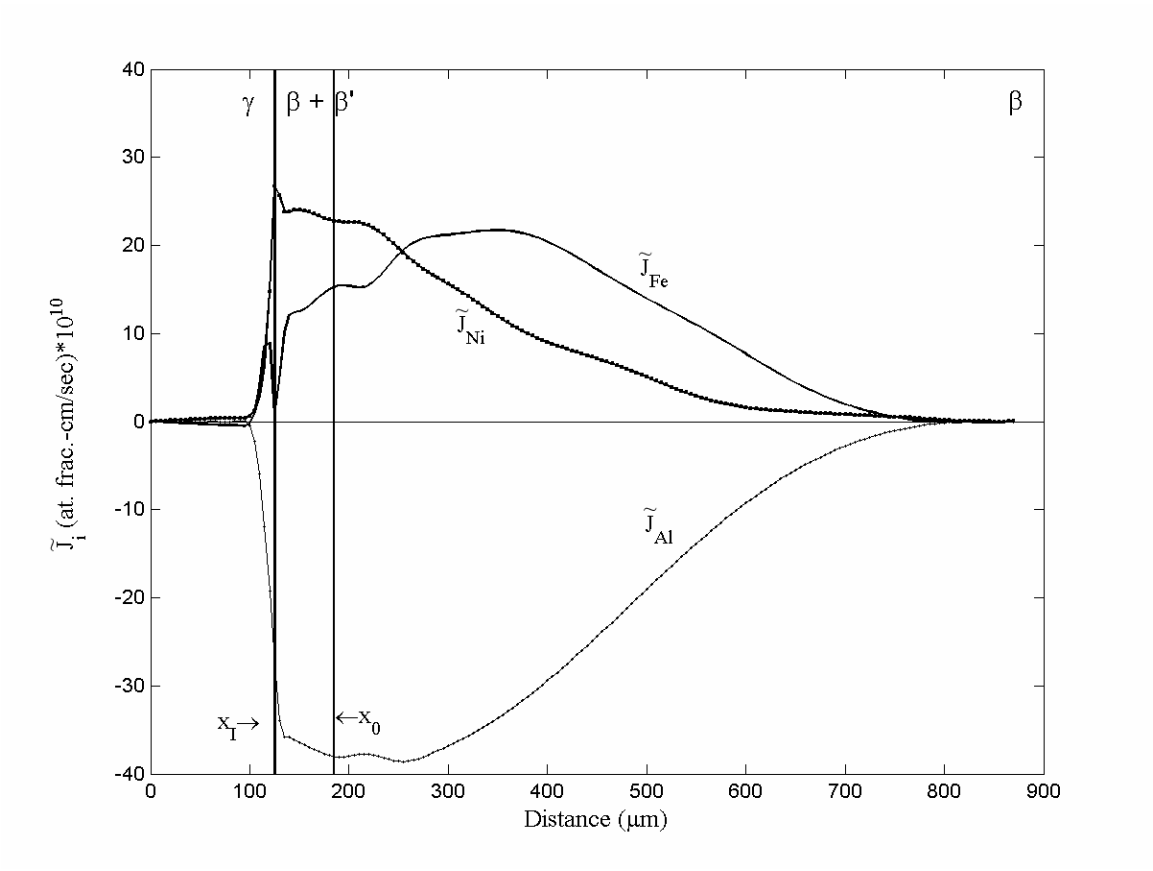

Figure 36. Interdiffusion flux data for the Fe-Ni-Al couple exhibiting three-phase equilibria in a ternary system. x_I denotes the interphase boundary and x_0 denotes the Matano plane location.

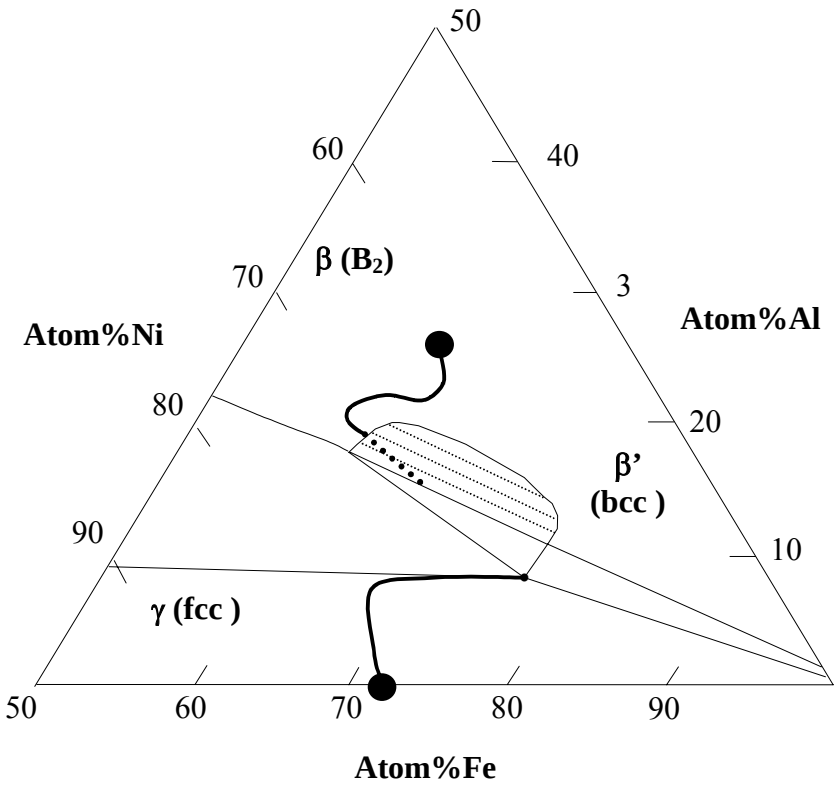

Figure 37. The diffusion path mapped out on the ternary isotherm at 1000°C of the for the Fe-Ni-Al couple exhibiting a category 2:1 boundary.

7 SUMMARY

Given Onsager's formalism of Fick's first law for an isothermal ternary diffusion couple, a system of two equations are had with four unknown interdiffusion coefficients. The Boltzmann-Matano method generates an additional two equations by using two couples whose paths intersect on the ternary isotherm yielding coefficients only at the one composition corresponding to that intersection point. The experimental investment for this method is great and the return is small. The DAYSO method yields average interdiffusion coefficients on either side of the Matano plane from one diffusion couple and assumes constant diffusivity over a wide range of concentrations. The experimental investment for this method is at least half and the return double as compared to the Boltzmann-Matano method.

The method presented in this paper builds on the ideas presented by Dayananda and Sohn by also using manipulations of Onsager's formalism along with direct calculations of the interdiffusion flux from the concentration profiles to generate the four equations necessary to solve for the four interdiffusion coefficients in a ternary system. The new method does not assume constant diffusivity over a wide range of compositions, as does the DAYSO method, but instead uses integration over short, discrete areas and differentiation to calculate a large discrete set of interdiffusion coefficients. The experimental investment is the same as that for the DAYSO method, but the return is much greater. Also, new equations that aid in the accuracy of the

calculations involved are also presented, such as an alternate interdiffusion flux equation and an alternate equation for the derivative of the interdiffusion flux.

The analysis is applied to selected single-phase, substitutional, isothermal diffusion couples in the Cu-Ni-Zn, Fe-Ni-Al, and Ni-Cr-Al systems and main and cross interdiffusion coefficients are calculated over regions of the profiles where the concentration gradient is significant. The calculated coefficients are shown to be in good agreement with both the Boltzmann-Matano method and the Dayananda and Sohn method. Concentration profiles generated from averages of the calculated coefficients using error function solutions match the experimental concentration profiles. Hypothetical concentration profiles are generated from given interdiffusion coefficients then back-calculated using the new method. The graphs of the interdiffusion coefficients calculated from the new technique not only match the input values, but also accurately detect that the coefficients are constants. After rigorous verification of the new technique, it was applied to previously unexamined Ni-Pt-Al couples. The new technique yielded very large $\widetilde{D}^{\mathrm{Ni}}_{\mathrm{AlAl}}$ values for this system as well as relatively constant $\widetilde{D}^{\mathrm{Ni}}_{\mathrm{AlAl}}$ and $\widetilde{D}^{\mathrm{Ni}}_{\mathrm{PtPt}}$ main coefficients. Both cross-coefficients $\widetilde{D}^{\mathrm{Ni}}_{\mathrm{AlPt}}$ and $\widetilde{D}^{\mathrm{Ni}}_{\mathrm{PtAl}}$ were found to be negative. The effect of Pt on the interdiffusion flux of Al becomes quite significant for relatively low Al concentrations.

The method demonstrated in this paper provides an effective way of calculating concentration dependent interdiffusion coefficients given a single diffusion couple and may be an effective tool for building a database of interdiffusion coefficients. In this manner the ternary isotherm may be mapped out in terms of interdiffusion coefficients, that one may be able to predict coefficients given an unexamined couple.

A new system for classifying boundary types for an *n*-component system has been established. The movement of the phase boundaries has been discussed in terms of degrees of freedom via Gibb's phase rule. Experimental evidence of a category 2:1 boundary is presented with a solid-solid diffusion couple in the Fe-Ni-Al system with two single-phase terminal alloys. The diffusion path for this couple surprisingly passes through the vertex of the equilibrium tie triangle on the phase diagram to exhibit three phase equilibria in a ternary system. Experimental verification of this phenomenon was shown here for the first time.

APPENDIX

SMOOTHING OF EXPERIMENTAL PROFILES

The extraction of experimental concentration data from diffusion couples as explained in Chapter 5 results in rough profiles that need to be smoothed. The data from the Cu-Ni-Zn, Fe-Ni-Al, and Ni-Cr-Al couples reported in Section 6.1 were previously smoothed.[6-9] The concentration profiles from the Ni-Pt-Al system reported in Section 6.2 and from the Fe-Ni-Al system reported in Section 6.3 were initially raw microprobe data that needed to be smoothed. The rough data was imported into Matlab and the smoothing spline function within the spline toolbox was employed. The error tolerance was manually increased until the second derivative of the concentration profile was smooth. The following figures show how the as-received microprobe data was smoothed for use in this thesis.

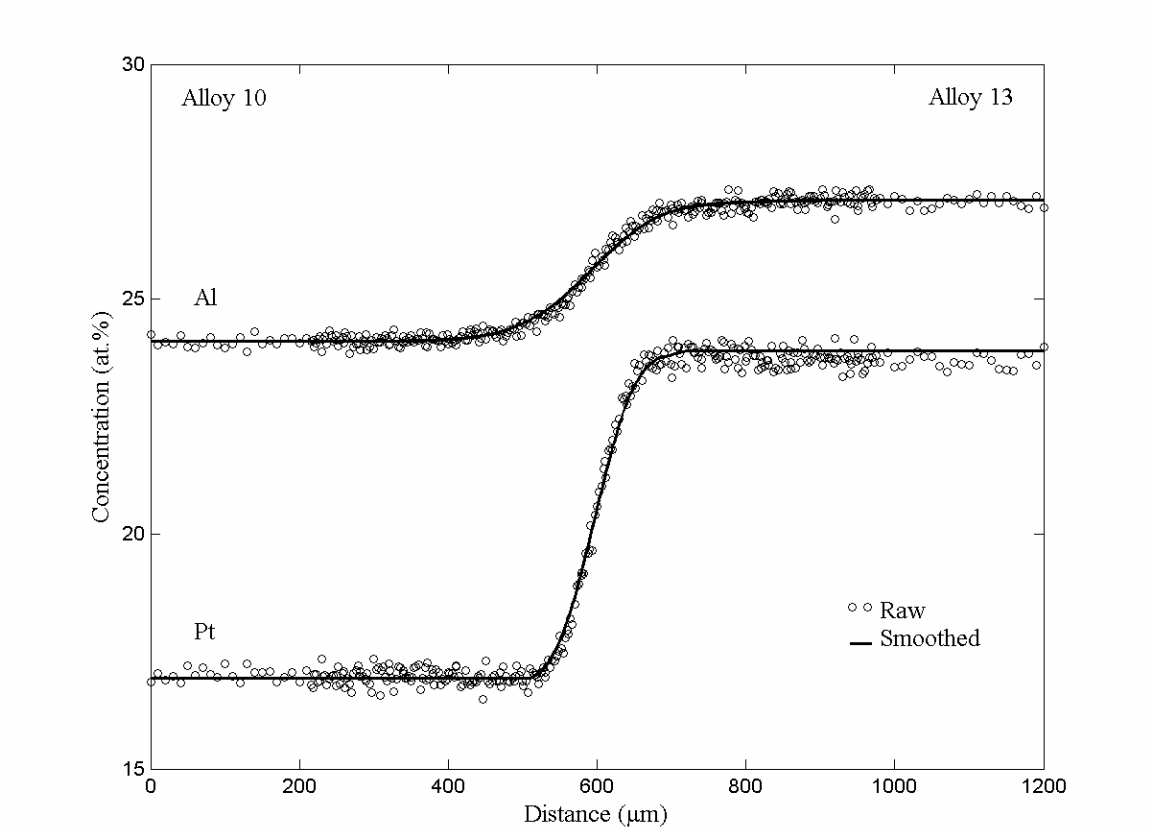

Figure 38. Smoothing of the raw data for the Ni-Pt-Al couple Alloy 10 vs. Alloy 13.

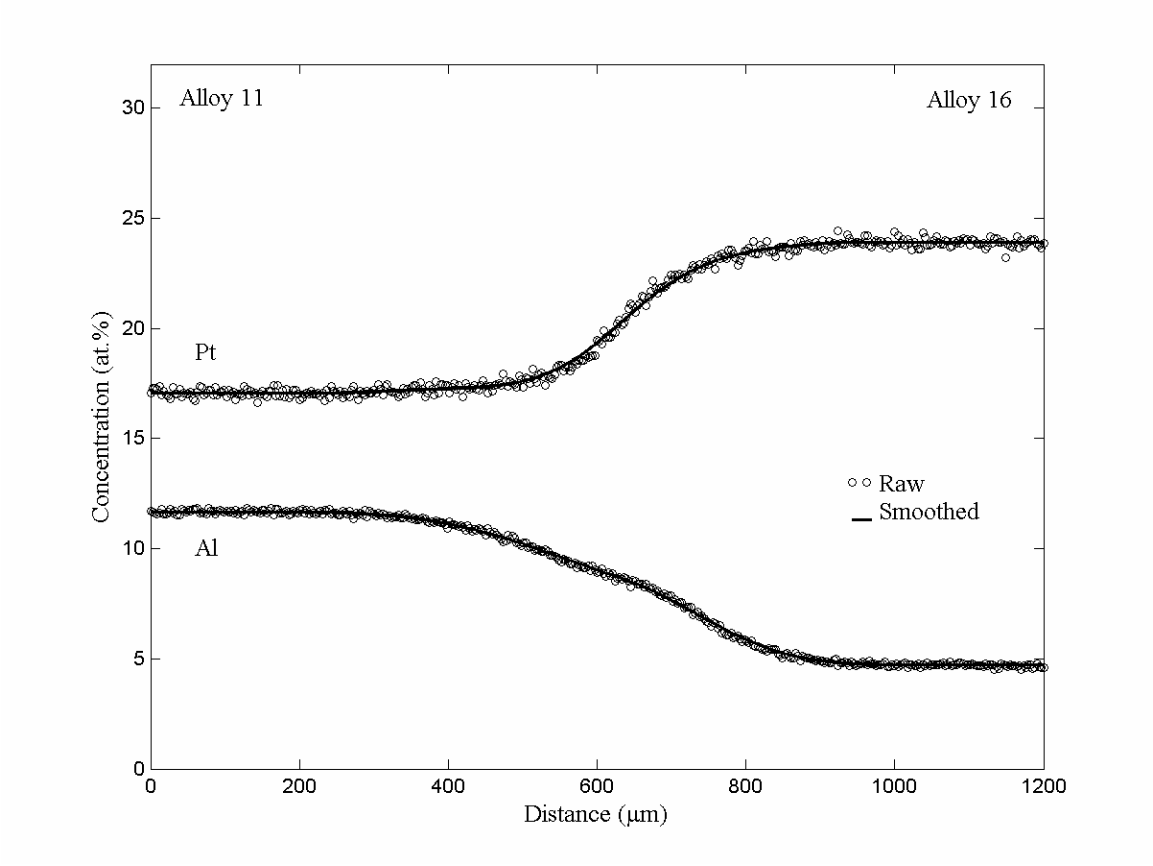

Figure 39. Smoothing of the raw data for the Ni-Pt-Al couple Alloy 11 vs. Alloy 16.

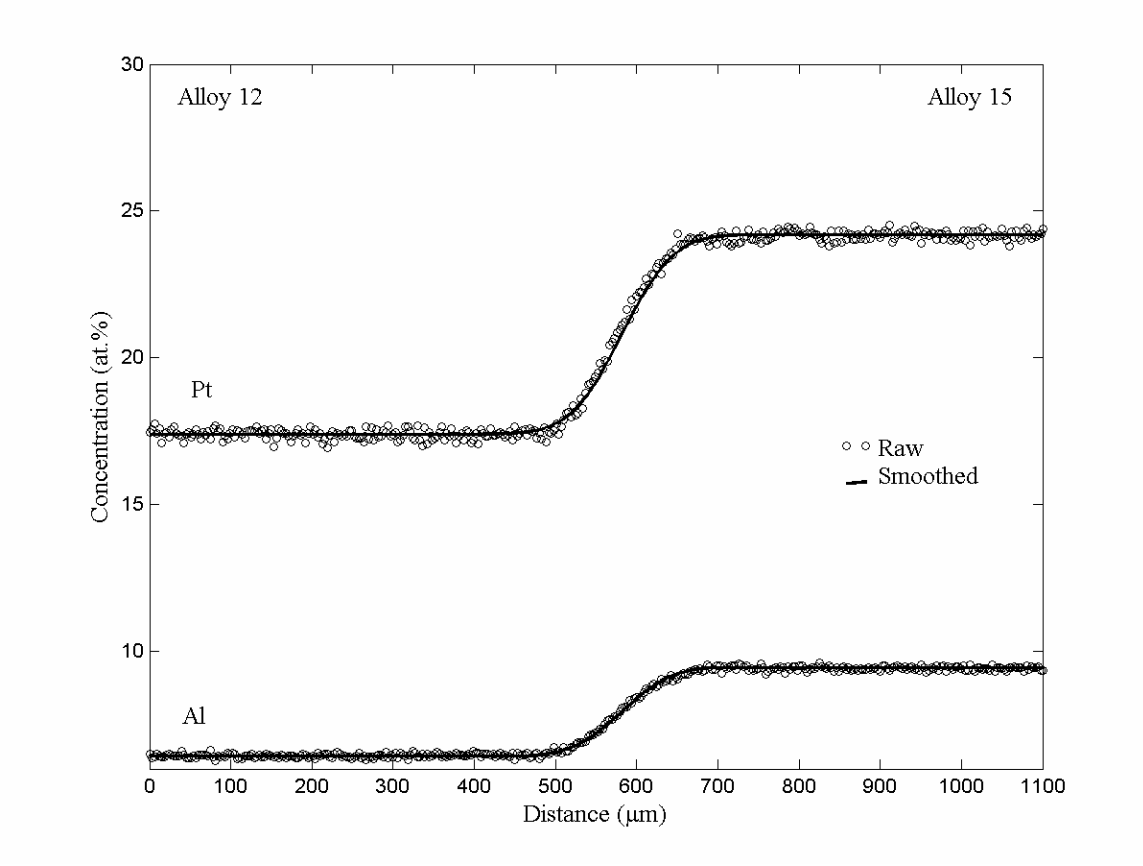

Figure 40. Smoothing of the raw data for the Ni-Pt-Al couple Alloy 12 vs. Alloy 15.

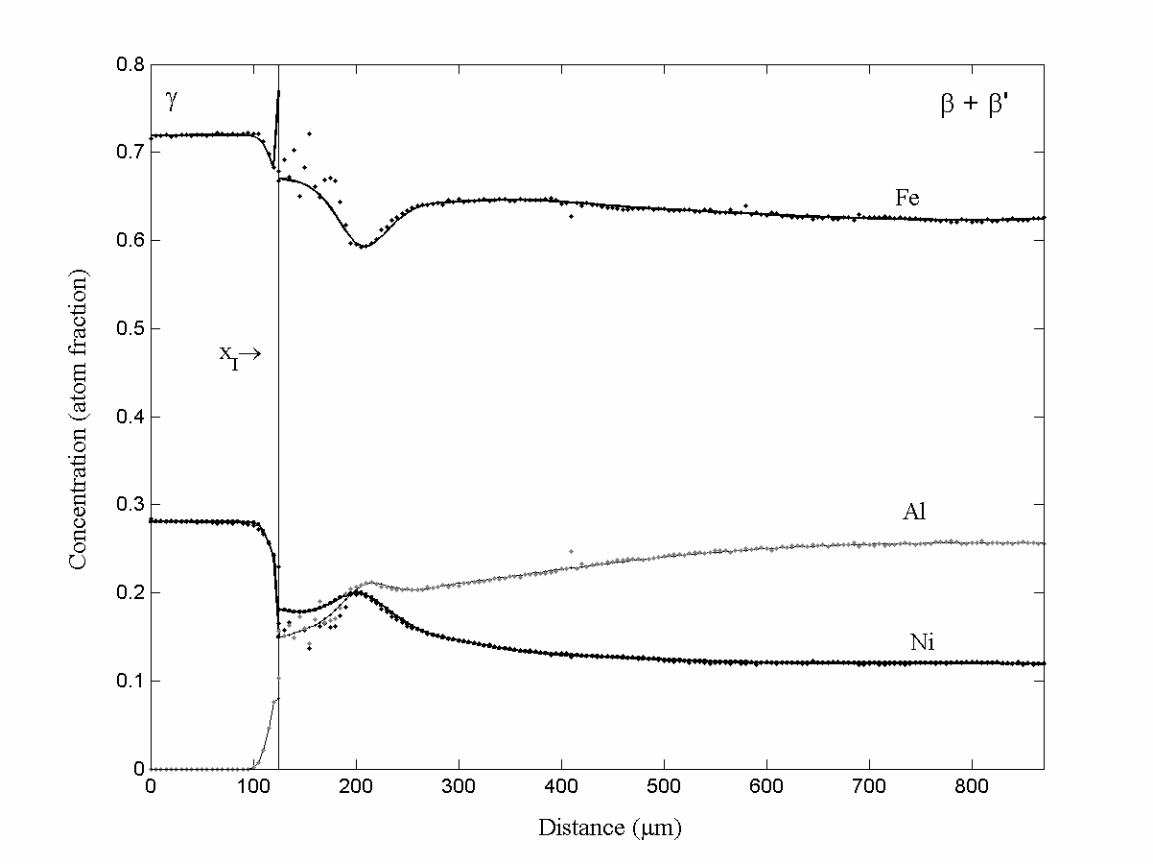

Figure 41. Smoothing of the raw data for the Fe-Ni-Al couple exhibiting three-phase equilibria.

LIST OF REFERENCES

1. L. Onsager: *Phys. Rev.*, 1931, vol. 37, pp. 405-26.
2. L. Onsager: *Phys. Rev.*, 1931, vol. 38, pp. 2265-79.
3. L. Onsager: *Ann. NY Acad. Sci.*, 1965, vol. 46, pp. 241-65.
4. M.A. Dayananda and Y.H. Sohn: *Metall. Mater. Trans.,* 1999, vol. 30A, pp. 535-43.
5. R. Bouchet and R. Mevrel: *Acta Metall.*, 2002, vol. 50, pp. 4887-4900.
6. C.W. Kim and M.A. Dayananda: *Metall. Trans. A*, 1984, vol. 15A, pp. 649-59.
7. T.D. Moyer and M.A. Dayananda: *Metall. Trans. A*, 1976, vol. 7A,pp. 1035-40.
8. M.S. Thompson and J.E. Morral, and A.D. Romig, Jr.: *Metall. Trans. A*, 1990, vol. 21A, pp. 2679-85.
9. J.E. Morral, Y.H. Son, and A.D. Romig, Jr.: *Fundamentals and Applications of Ternary Diffusion*, G.R. Purdy, ed., Pergamon Press, New York, NY, 1990, pp. 119-26.
10. J.E. Morral, C. Jin, A. Engström, and J. Ågren: *Scripta Mat.*, 1996, vol. 34, pp. 1661-66.
11. A. Fick: *Progg. Ann.*, 1855, vol. 94, pp. 59.
12. M.E. Glicksman: *Diffusion in Solids*, John Wiley & Sons, New York, NY, 2000.
13. P. Shewmon: *Diffusion in Solids*, The Minerals, Metals & Materials Society, Warrendale, PA, 1989.
14. Philibert: *Atom Movements*, les éditions de physique Les Ulis Cedex A, France, 1991.
15. H. Fujita and L. J. Gosting, *J. Am. Chem. Soc.* 1956, vol. 78, pp. 1099-1106.
16. A. G. Guy, V. Leroy, and T. B. Lindemer: *Trans. of the ASM*, 1966, vol. 59, pp. 517-534.

17. L. S. Castleman and H. A. Froot: *Acta Metall.*, 1964, vol. 12, pp. 15-19.

18. J. S. Kirkaldy: *Can. J. Phys*, 1958, vol. 36, pp.899-906.

19. M. A. Dayananda: *Defect and Diffusion Forum*, 1992, vol. 83, pp. 73-86.

20. T. O. Ziebold and R. E. Ogilvie: *Trans TMS-AIME*, 1967, vol. 239, pp. 942-53.

21. J. S. Kirkaldy, J. E. Lane, and G. R. Mason: *Can. J. Phys.*, 1963, vol. 41, pp. 2175-2186.

22. J.S. Kirkaldy and D.J. Young: *Diffusion in the Condensed State*, The Institute of Metals, London, 1987.

23. G. H. Cheng and M. A. Dayananda: *Metall. Trans. A*, 1979, vol. 10A, pp. 1415-1419.

24. J.S. Kirkaldy: *Can. J. Phys.*, 1958, vol. 36, pp. 899-906.

25. G.W. Roper and D.P. Whittle: *Scr. Metall*, 1974, vol. 8, pp. 1357-1362.

26. M.A. Dayananda and C. W. Kim: *Metall. Trans. A*, 1979, vol. 10A, pp. 1333-39.

27. M.A. Dayananda: *Metall. Trans. A*, 1983, vol. 14A, pp. 1851-58.

28. M. S. Thompson and J. E. Morral: *Acta Metall.*, 1986, vol. 34, pp. 339-46.

29. M.A. Dayananda and Y.H. Sohn: *Scr. Metall*, 1996, vol. 35, pp. 683-88.

30. L. S. Castleman and G. Wo: *Metall. Trans. A.*, 1984, vol. 15A, pp. 1359-66.

31. C. Matano: *Jap. J. Phys.*, 1933, vol. 8, pp. 109-13.

32. S.K. Kailasam, J. C. Lacombe, and M. E. Glicksman: *Metall. Trans. A*, 1999, vol. 30A, pp. 2605-10.

33. R. T. Dehoff and N. Kulkarni: *Materials Research*, 2002, vol. 5, pp.1-21.

34. M.A. Dayananda: in *Diffusion in Metals and Alloys, Landoldt and Bornstein*, H. Mehrer, ed., Springer-Verlag, Berlin, 1991, Ser. III, vol. 26, pp. 372-436.

35. C.W. Kim and M.A. Dayananda: *Metall. Trans. A*, 1983, vol. 14A, pp. 857-64.

36. M.A. Dayananda: *Diffusion in Solids: Recent Development*, Proc. TMS-AIME Fall Meeting, Detroit, MI, 1984, M. A. Dayananda and G. E. Murch, eds., TMS-AIME, Warrendale, PA, 1984, pp. 195-230.

37. R.D. Sisson, Jr. and M.A. Dayananda: *Metall. Trans. A*, 1977, vol. 8A, pp. 1849-56.

38. R.T. DeHoff, K.J. Anusavice, and C.C. Wan: *Metall. Trans*., 1974, vol. 5, pp. 1113-26.

39. B. Gleeson, W. Wang, S. Hayashi, and D. Sordelet: *unpublished research*.

40. R.D. Sisson, Jr., M.A. Dayananda: *Metall. Trans.*, 1972, vol. 3, pp. 647-52.

41. L.E. Wirtz, M.A. Dayananda: *Metall. Trans. A*, 1977, vol. 8A, pp. 567-75.